# ABSTRACT

Title of Dissertation: FACTORS INFLUENCING REMOTE SENSING MEASUREMENTS OF WINTER COVER CROPS

Kusuma Prabhakara, Doctor of Philosophy, 2016

Dissertation directed by: Chair, Dr. Christopher Justice, Department of Geographical Sciences

Winter cover crops are an essential part of managing nutrient and sediment losses from agricultural lands. Cover crops lessen sedimentation by reducing erosion, and the accumulation of nitrogen in aboveground biomass results in reduced nutrient runoff. Winter cover crops are planted in the fall and are usually terminated in early spring, making them susceptible to senescence, frost burn, and leaf yellowing due to wintertime conditions. In addition to remote sensing imagery, advances have been made in the use of proximal sensors integrated with GPS for on-field measurements, and the comparability of such measurements between platforms, as well as based on processing level is important. Cover crop growth on six fields planted to barley, rye, ryegrass, triticale or wheat was measured over the 2012-2013 winter growing season. There was a strong relationship between the Normalized Difference Vegetation Index (NDVI) and percent groundcover ($r^2$ =0.93) suggesting that date restrictions effectively eliminate yellowing vegetation from analysis. The Triangular Vegetation

Index (TVI) was most accurate in estimating high ranges of biomass ($r^2$=0.86), while NDVI did not experience a clustering of values in the low and medium biomass ranges but saturated in the higher range (>1500 kg/ha). Accounting for index saturation, senescence, and frost burn on leaves can greatly increase the accuracy of estimates of percent groundcover and biomass for winter cover crops. Surface reflectance measurements were more correlated with proximal sensors compared to top of atmosphere, with intercepts closer to zero, regression slopes nearer to the 1 to 1 line, and less variance between measured values. NDVI was highly correlated with percent vegetative groundcover, though surface reflectance products did not necessarily improve the relationships. When the Scattering for Arbitrarily Inclined Leaves (SAIL) model was used with measured field variables reflective of realistic winter cover crop scenarios, there were not large differences between NDVI despite differences in residue cover and moisture. At low LAI, NDVI is not capable of differentiating between residue and vegetative cover.

# FACTORS INFLUENCING REMOTE SENSING MEASUREMENTS OF WINTER COVER CROPS

by

Kusuma Prabhakara

Dissertation submitted to the Faculty of the Graduate School of the
University of Maryland, College Park, in partial fulfillment
of the requirements for the degree of
Doctor of Philosophy
2016

Advisory Committee:
Dr. Christopher O. Justice, Chair
Dr. Ralph O. Dubayah
Dr. Samuel N. Goward
Dr. W. Dean Hively
Dr. Richard A. Weismiller

# Dedication

I dedicate this dissertation to my parents, Madanapalli & Padmaja, who have supported me unconditionally throughout my life; and to my daughter, Veda, for whom I hope to do the same.

# Acknowledgements

First, I'd like to thank my advisor, Dr. Chris Justice, for his time and commitment in seeing me through this complex dissertation process. I would also like to extend a warm thanks to my committee members, especially Drs. Goward and Dubayah, for their patience and imparting their scientific knowledge. Dr. W. Dean Hively has been a valued mentor who has extended numerous research opportunities to me through the years, and for that, I am grateful. I'd also like to thank Dr. Richard Weismiller for accepting the important role of my dean's representative.

I'd like to acknowledge Dr. Greg McCarty at the United States Department of Agriculture Hydrology and Remote Sensing Lab for providing me support, tools, and a place where I could carry out my research. I'd like to thank Drs. Craig Daughtry and Miguel Quemada for sharing their data, equipment, and knowledge. The countless scientists, colleagues, interns, and students at the United States Department of Agriculture (USDA) who helped me collect field data, run laboratory samples, and kept me company have been invaluable to me, especially Dr. Bryan Vinyard who greatly helped me through his knowledge of statistics. Dr. Julie Silva has acted as a teaching mentor and shoulder to lean on when I needed it most, and I'd like to thank her for that.

This research was made possible through support from the United States Department of Agriculture – Agricultural Research Service (ARS) Hydrology and Remote Sensing Laboratory (HRSL), the United States Geological Survey (USGS) Eastern Geographic Science Center (EGSC), and the University of Maryland, College Park. Funding was provided by the USDA Choptank River Conservation Effects

Assessment Project (CEAP), the USGS Land Change Science Program, and the National Fish and Wildlife Foundation.

Last but absolutely not least, I'd like to thank my friends and family for their unconditional love and support over the last six years. My husband, Dan, has stuck with me through thick and thin, and I couldn't ask for more. I'd like to thank my daughter, Veda, for being a breathing reminder of why life is worth living every single second of every single day. I'd like to thank my best friend, Priti, who has always been there for moral support, my parents who have never wavered in their support for me, and my sisters, especially Ranjani who has counseled me during tough times. I will always remember my time here for the intellectual endeavor, but perhaps the friendships I have made in Graduate School will be with me forever – you know who you are. Thank you.

# Table of Contents

# List of Tables

# List of Figures

# List of Abbreviations

**AERONET:** Aerosol Robotic Network is a network of sun photometer and radiometer sites.

**ARS:** Agricultural Research Service, the research part of the United States Department of Agriculture

**AVHRR:** Advanced Very High Resolution Radiometer is a remote sensing instrument that has bands in the visible, near-infrared and thermal regions

**BARC:** Beltsville Agricultural Research Center is a large complex located in Beltsville, Maryland

**CEAP:** The Conservation Assessment Effects Project was launched by the Natural Resources Conservation Service to develop science in the evaluation of conservation practices and programs used to manage agricultural and environmental quality programs.

**DSLR:** Digital single-lens reflex camera used to take red-green-blue photos

**EGSC:** Eastern Geographic Science Center

**EROS:** Earth Resources Observation and Science

**ESPA:** Earth Resources Observation and Science Center Science Processing Architecture

**EVI:** Enhanced Vegetation Index

**FC:** Field capacity of a soil, which here is the water content after 24 hours of air drying

**FSA:** Farm Services Agency, a part of the United States Department of Agriculture

**GDD:** Growing Degree Days are a measure use temperature data to indicate the rate of growth and are related to phenological development of plants.

**GIS:** Geographic Information Systems are a way to analyze and display data. One ubiquitous example is ArcGIS.

**GNDVI:** Green Normalized Difference Vegetation Index

**GPS:** Global Positioning Systems locate and record coordinate positions on the earth's surface and can interface with other software.

**HRSL:** Hydrology and Remote Sensing Lab

**LAI:** Leaf Area Index is a dimensionless measure that is the one-sided leaf area per unit ground surface.

**MACS:** Maryland Agricultural Cost-Share Program

**MDA:** Maryland Department of Agriculture

**MODIS:** Moderate Resolution Imaging Spectroradiometer which is a coarse-resolution instrument that is widely used due to its frequent overpasses and wide range of spectral bands

**MODTRAN:** MODerate resolution atmospheric TRANsmission is a computer code used to compensate for atmospheric effects in satellite data and other applications
**NAIP:** National Aerial Imagery Program provides high-resolution aerial photography, both leaf-on and leaf-off.

**NCDC:** National Climatic Data Center

**NDREI:** Normalized Difference Red Edge Index

**NDVI:** Normalized Difference Vegetation Index ratios wavelengths in the red and near-infrared portions of the electromagnetic spectrum to product a vegetation index that measures plant vigor.

**NFWF:** National Fish and Wildlife Foundation

**NGRDI:** Normalized Green Red Difference Index

**NIR:** Near-infrared refers to the portion of the electromagnetic spectrum between 700 – 1000 nm

**NOAA:** National Atmospheric and Oceanic Administration

**RGB:** Red-green-blue photographs

**RWC:** Relative water content, which is water content of the sample divided by the water content of the sample at saturation

**SAIL:** Scattering by Arbitrarily Inclined Leaves is a radiative transfer model with four streams

**SAVI:** The soil-adjusted vegetation index uses a linear soil adjustment factor

**SPOT:** Satellite Probatoire d'Observation de la Terre is a French Satellite. SPOT-5 has a 10-m resolution in the visible and near-infrared bands

**SR:** Simple Ratio

**SR:** Surface Reflectance is the reflectance that has been corrected for atmospheric attenuation

**TDML:** Total Daily Maximum Load was established by the United States Environmental Protection Agency to specify the maximum amount of pollution allowed and reductions in pollution for a water body.

**TOA:** Top of atmosphere reflectance has not been corrected for atmospheric attenuation

**TVI:** Triangular vegetation index has no upper bound

**USDA:** United States Department of Agriculture

**USEPA:** United States Environmental Protection Agency

**VARI:** Visible Atmospherically Resistant Index

# Chapter 1: Introduction

## *1.1 Research Context, Questions & Objectives*

The increase of global population requires intensification of agricultural systems required to sustain growing numbers of people and without compromising environmental and human health (Tilman et al., 2002). Use of nutrient fertilizers is a necessary part of being able to increase yields, but needs to be managed properly to prevent negative consequences for soil fertility and water quality (Mueller et al., 2012; Tilman et al., 2011). Increases in fertilizer application are often necessary to increase yield, but excessive or poorly-managed fertilization of lands can cause nutrient leaching into nearby waterways, with potentially hazardous consequences for aquatic ecosystems, water quality, and humans alike (Beman, Arrigo & Matson, 2005; Doran, 2002; Foley et al., 2009). Soil erosion can lead to permanent soil loss, lessened agricultural productivity, and reduction of water clarity that can impact sensitive species (Kling, et al. 2014; Pimental et al., 2004). Preventing soil loss is a pivotal piece of agricultural sustainability and is a major priority in many regions across the globe (Panagos et al., 2015; Smith, et al., 2015). Balancing agricultural needs, water quality, and soil quality is a problem that needs to be addressed at the present and well into the future, and the scale at which these issues are addressed is important (Tong & Chen, 2002; Verhoeven et al., 2006). CEAP was launched by the United States Department of Agriculture (USDA) to support research on conservation within sensitive watersheds on regional and watershed scales (Arnold et al., 2014).

The Mid-Atlantic Region and especially the Chesapeake Bay are areas of intense research focused on the balance between reducing environmental degradation while maintaining agricultural output (Boesch, Brinsfield & Magnien, 2001). The Chesapeake Bay Watershed includes the largest estuary in the United States and is comprised of several states, including Delaware, Maryland, New York, Pennsylvania, Virginia, West Virginia and the District of Columbia (Cooper, 1995). It is an economically important resource in terms of its use for recreation and its extensive and productive fisheries, as well as for transportation. Land use in the Chesapeake Bay watershed is 24% agricultural (Shenk & Linker, 2013). A consequence is that it has suffered extensively from nutrient and sediment runoff into its waters, as such these pollutants have had grievous consequences for water quality in sensitive estuarine ecosystems (Anderson, Gilbert & Burkholder, 2002; Hagy et al., 2004).

Farming operations are found throughout the Chesapeake Bay Watershed, and Maryland's Eastern Shore has the most concentrated poultry production in the watershed and a higher ratio of agricultural land (Staver and Brinsfield, 2001). Fertilizer nitrogen in the form of nitrate ($NO_3$), is readily exported from croplands and its fate is difficult to manage in sensitive watersheds (Meisinger et al., 1991). Residual nitrate in the soil profile after crop harvest is particularly subject to leaching from agricultural areas and into adjacent tributaries. Pollution from such fertilizers has negative consequences for waterways, including eutrophication, reduced stocks of fish, and declining habitats through destruction of submerged aquatic vegetation (Dauer et al., 2000). These conditions have worsened in the Chesapeake Bay over time, largely due to increased fertilizer application on agricultural lands (Jordan et al.,

1997). In addition to nutrient pollution, sediments are also problematic as they can increase turbidity in the water and negatively impact submerged aquatic vegetation (Fisher et al., 2006). Additionally, sediments often bond with other pollutants, such as nutrients and toxins, and heavy metals, and transport them (Yu et al., 2001). The Eastern Shore has relatively low-relief, but increased sedimentation from it and from surrounding areas has impaired the Bay (Shenk & Linker, 2013).

Agreements to reduce nutrient runoff into the Chesapeake Bay have been in place for several decades. Research on nutrient and sediment pollution in the Chesapeake Bay was already taking place by the late 1970s and early 1980s, resulting in The Chesapeake Bay Agreement of 1983 (CBP, 1983; Nixon, 1987). In 1987, the Chesapeake Bay Agreement set a goal for a 40 percent reduction in nutrient pollution (USEPA, 2003). Five years later, this general nutrient goal was split into basin allocations of nitrogen and phosphorus for Maryland, Pennsylvania and Virginia (Linker et al., 2013). Controls on sediments were added in the Chesapeake 2000 Agreement, and additional agreements were put into place for the following decade, including President Obama's Executive Order on the Chesapeake Bay, which prioritized cooperative involvement by federal and state agencies to achieve water quality goals (Executive Order, 2009). However, the goals put forth in the Chesapeake 2000 Agreement were not reached, leading the United States Environmental Protection Agency (USEPA) to devise the 2010 Chesapeake Bay Total Daily Maximum Load (TDML). The TDML sets limits on the amount of nutrients and sediments that can be released to adequately meet water quality standards (Batiuk et al., 2013). Despite these advancements, the nation's largest

estuary continues to suffer from water pollution and poor overall health (Chesapeake Bay Program, 2015; Leight et al., 2015).

Planting cover crops is widely considered to be an effective method to reduce both nitrogen leaching and sedimentation into waterways (Meisinger et al., 1991). Winter cover crops are planted post-harvest on corn and soybean fields to scavenge residual nitrogen that remains in the soil, and to meet soil erosion guidelines, providing positive water quality benefits (Dabney, 1998; Delgado et al., 2007). Typical winter cover crops can include legumes, grasses and brassicas (Dabney et al., 2001). Traditional cover crops are often not harvested and are commonly killed by use of herbicides or through mechanical methods such as chopping, rolling, slicing, mowing, or roller-crimping (Ashford & Reeves, 2003). Though traditional cover crops are not allowed to be harvested, they can have other beneficial uses for famers, such as chopping for silage. Additionally, cover crops provide many environmental benefits to waterways and fields including: nutrient cycling efficiency, weed suppression, and soil fertility enhancement (Reicosky and Forcella, 1998; Snapp et al., 2005; Teasdale, 1996; Unger & Vigil, 1998).

Maryland and Virginia, the states closest in proximity to the Chesapeake Bay, have agricultural cost-share programs to incentivize farmers to implement best management practices, including cover crops. To help farmers overcome economic obstacles and encourage planting of cover crops, the Maryland Department of Agriculture (MDA) offers grants for farmers with the Maryland Agricultural Water Quality Cost-Share (MACS) program, through which farmers can either plant traditional non-harvested cover crops or commodity cover crops that can be

harvested. Though there is a commodity cover crop program in place for farmers who wish to harvest, cash incentives are significantly less than with the traditional cover crop program. The amount of grant money given to farmers is greater for those who plant traditional non-harvest cover crops compared with commodity cover crops. Through MACS, Maryland has allocated $22 million in grants for the 2015-2016 winter cover cropping season and a record number of cover crop acres are set to be planted (MDA, 2015; MDA 2016). Subsidized crops include barley, canola, rapeseed, kale, rye, ryegrass, spring oats, triticale, forage radish and wheat.

Although MDA requires fields enrolled in their traditional cover crop program to be planted by November 5, there are economic incentives for earlier planting. The planting date cutoff varies slightly year to year, but always occurs during the first week of November (MDA, 2015). These include bonuses for planting by October 15, and larger bonuses for planting by October 1. Such incentives are intended to create maximum water quality benefits, as cover crops with early planting dates generally have greater yields (Richards et al., 1996). Cover crops typically do not reach the reproductive stage, as cold weather during the winter months inhibits growth and they are killed off in the spring before they reach maturity. Because production of aboveground biomass in cover crops is related to nutrient sequestration post-harvest, cover crop planting date has serious implications for accumulation of biomass. For example, early-planted rye has been shown to be more effective at nitrate sequestration than other species or later planting dates due to more days of favorable growing weather (Hively et al, 2009). Winter cover crops can experience a period in the spring when climate conditions are more favorable for growth before kill-down,

allowing for additional uptake if there is residual nitrogen left in the soil (Dabney et al., 2001). Availability of soil nitrogen also plays a role in the accumulation of biomass. The initial availability of soil nitrogen on different fields can vary based on the previous crop and any fertilization that has taken place.

Remote sensing and derived vegetation indices are widely used in agricultural applications as a method to measure plant productivity (Baret & Guyot, 1991; Moran, Inoue & Barnes, 1997; Wiegand et al., 1991). One method to gauge greenness of vegetation uses ratios and other indices that utilize reflectance in visible, red edge, and near-infrared (NIR) portions of the Electromagnetic Spectrum. One ubiquitous example is the Normalized Difference Vegetation Index, (NDVI) (Tucker, 1979). Such data can be gathered through remote sensing instruments such as Earth-orbiting satellites, aerial photos, proximal sensors, or other means. A majority of solar radiation in the visible spectrum is absorbed by pigments in the leaves, resulting in low transmittance and reflectance, especially in the red portion of the spectrum, with slightly higher reflectance in the green wavelengths. This is coupled with brightness in the near-infrared region of the spectrum, where there is low absorption and high transmittance and reflectance (Tucker and Sellers, 1986). Ratios of low reflecting red and high reflecting infrared measurements allow for unit-less measures of the chlorophyll absorption peak in green vegetation.

While Maryland and Virginia record cover crop extent and agronomic data as part of cost-share program management, the extent of information gathered varies from state to state. However, readily available remote sensing data can be used to monitor the amount and extent of vegetation in cover cropped landscapes (Hively et

al., 2009). Because high biomass is important for nutrient sequestration and percent groundcover is vital to prevent sedimentation and soil loss, vegetation index measurements can be used to gauge the rigor or overall growth of cover crops. As winter cover crops are not planted during the normal growing season, and are subject to different climatic and growing conditions than other spring-planted crops, is vital to understand where the relationship between indices and biomass (for nutrient uptake) or percent groundcover (for erosion control benefits) is accurate and where it is not, as well as factors that may be confounding this relationship. Some factors that can affect remote sensing measurements of winter cover crops include chlorosis, frost burn, yellowing of leaves from nutrient deficiency and senescence (Prabhakara, 2015). Low temperatures and unfavorable growing conditions during the winter season may be partially to blame. Nutrient deficiency occurs because cover crops are not fertilized over the winter to permit maximum uptake of residual soil nitrate (MDA, 2015). Although crops will not grow during freezing conditions, frost burn can occur on leaves, yellowing them and complicating directly relationships with vegetation indices. Chlorosis, or lack of chlorophyll in leaves can have the same effect, as can leaf senescence. With senescence, older, higher leaves will yellow first and lower, green leaves can reemerge in the spring. With frost burn, tips of leaves are often first to yellow and green-up may not occur so readily.

Because of the importance of remote sensing in measuring cover crop efficiency, Objectives 1 and 2 of this dissertation focus on understanding special considerations that need to be accounted for when taking spectral measurements of groundcover and biomass of winter cover crops, respectively. Winter conditions can

result in chlorosis, senescence and frost damage that can result in leaf damage and reduced NDVI reflectance. Measurements taken before the onset of winter weather may be more accurate than those taken in the spring, after such damage has occurred.

In addition to agronomic, nutrient and weather-related issues that can affect reflectance measurements from winter cover crops, the comparability of sensors used to measure reflectance and the level to which the data are processed are also worth exploring. Though there may be a generalized understanding of the process of soil erosion and nutrient leaching at global scales, field-scale measurements are required for precise application and measurement of crops (Gebbers, 2010). Although fields are generally homogenous areas with the same crop and management regime, there are, in actuality, differences in vegetation across the field. These differences can be due to subtle or large variations in topography, soil moisture, soil type, field edge effects, and nutrient availability (Godwin & Miller, 2003; Stafford, 2000; Taylor et al., 2003). Technology such as geographical information systems (GIS), geographic positioning systems (GPS), as well as high spatial resolution sensors integrated with these systems, can be utilized to achieve the goal of field-scale measurements to provide economic, human, and environmental benefits. Hence, ground-based proximal sensors are become more widely used for agricultural monitoring and precision agriculture applications (Hedley, 2014; Mulla, 2012). The sensors used in these studies are unique in the way they collect data. They are handheld and "on the go", meaning they do not have any specified pixel size but instead take reflectance readings every few seconds as they cross the landscape. The sensors are integrated with GPS technology that connects each individual reading to a unique location on

the Earth's surface. The constant readings taken by such proximal sensors are a major benefit for remote sensing of agricultural areas.

Although satellite platforms cannot capture this within-field variability as well as "on the go" sensors because of their spatial resolution, it is worth seeing whether measurements are comparable when aggregated to the same pixel size. Freely-available Landsat data have a spatial resolution in the visible and near-infrared of 30 meters. Satellite Probatoire d'Observation de la Terre 5 (SPOT-5) and WorldView-2 data need to be purchased and have higher spatial resolutions of 10- and 2-meters respectively. When dealing with small agricultural fields, coarse-resolution data with larger pixel sizes (e.g. 250m - 1km) can have sub-pixel variability, especially in areas where there is low fractional groundcover, a greater amount of background reflectance, and the vegetation signal is not pure. Therefore, while fine-and medium-resolution satellite imagery is useful in this context, coarser resolution data are not (Li et al., 2015). Although coarse resolution satellite data are available on a daily basis, instruments with high or medium resolution imagery often have infrequent overpass times. For instance, in general Landsat 7 images the same area every 16 days (NASA, 2011). The low temporal resolution of these sensors can pose a number of problems. First, with such a long duration between overpasses combined with cloud interference can pose major problems in being able to monitor crops effectively (Moran, Inoue & Barnes, 1997). Despite lack of growth in the coldest part of the winter, vegetation could be sustaining damage during this period, and growth that occurs in late fall and early spring can also be missed.

Atmospheric effects are also present in satellite data as particles in the atmosphere, including water vapor, can cause scatter of incoming and outgoing radiation. The greater the length of the path taken from the source of radiance (the sun) to the ground and back to the remote sensing instrument, the greater the magnitude of this potential atmospheric interference (Fraser & Kaufman, 1985; Vermote et al., 1997). Although Landsat always takes its images at nadir, SPOT-5 and WorldView-2 are pointable sensors. Increases in off-nadir acquisition angles increase the length of the path through the atmosphere and any effects could be increased under these circumstances. Converting satellite products to surface reflectance theoretically reduces such effects, and the results after processing are more comparable to ground-based sensors (Maiersperger et al., 2013; Mulla, 2013).

Fine spatial resolution and temporal flexibility in data collection, paired with the data being unadulterated by atmospheric effects, clouds and other sensor artifacts, are all benefits of on-the-go, GPS-enabled, ground-based proximal sensors. However, it is time- and labor-intensive to collect in-situ information using proximal sensors, making moderate- and fine-spatial resolution satellite imagery an attractive option for field-scale vegetation studies. Previous studies have compared reflectance measurements from satellite-to-satellite, and ground-based sensors to ground-based sensors (Deery et al., 2013; Yao et al., 2013). Additionally, there are studies comparing surface reflectance products between sensors (Feng, 2013). Studies were carried out using coarse resolution satellite data, such as the Moderate Resolution Imaging Spectroradiometer (MODIS) or the Advanced Very High Resolution Radiometer (AVHRR), that are not appropriate for fine-scale field study. Research

comparing ground-based sensors to satellite platforms often use proximal sensors that take snapshot readings instead of continuous field measurements (Maiersperger et al, 2013; Hmimina, 2013; Wagner & Hank, 2013; Li et al., 2015).

Objective 3 of this study will consider different sensors and processing levels to determine how well-correlated reflectance measurements are among them. Specifically, ground-based proximal sensors that record continuous measurements will be compared against two moderate resolution satellite platforms, Landsat 7 and SPOT-5, and fine-resolution WorldView-2 data. These satellite products have all been downloaded in surface reflectance or converted to surface reflectance using the MODerate resolution atmospheric TRANsmission code (MODTRAN5).

Because cover crops are unique, based on their comparatively slow growth, satellite remote sensing methods for measuring cover crop biomass are challenged by effects of soil reflectance in areas with low percent groundcover, as well as variability in soil wetness (Huete 1998). The percentage of vegetative cover in winter cover crops can be low (< 20%) compared to harvest crops due to poor growing weather, especially if they are planted late. Leaf area index (LAI) of full-canopy crops start saturating the NDVI at 2 to 5 and issues remain in relating indices to LAI (Haboudane, 2004; Baret & Guyot, 1991). Much like percent groundcover, LAI can be significantly lower in winter cover crops. Additionally, sun angles are lower during the winter months resulting in greater shadowing (Curran & Steven, 1983). As solar zenith angle changes relative to viewing angle, shadowing of canopies can increase (Li & Strahler, 1992; Roy et al., 2016). As some of the moderate to high

spatial resolution data might be acquired from pointable sensors, differences in off-nadir measurements may also have an effect on reflectance measurements.

Another interesting and relevant problem when studying winter cover crops is the issue of residue. As part of conservation tillage, large amounts of corn and soybean residue are found in fields post-harvest (Daughtry et al., 2005). They provide benefits such as reduced soil erosion, increased soil organic matter, and reduced nutrient runoff (Quemada & Daughtry, 2016). With large amounts of residue interacting with background soils under variable moisture conditions, the soil surface background spectrum can be quite variable. Radiative transfer models can be used to help interpret reflectances based on the scattering, absorption, refraction and transmittance of incident light on vegetative canopies (Jacquemoud, 2000; Verhoef, 1984). They are particularly useful for understanding the sensitivity of the signal based on multiplicative scattering between the background and vegetative canopy under a variety of conditions based on the geometry of individual leaves, and Sun and sensor directions (Jacquemoud, 2009).

The Scattering by Arbitrarily Inclined Leaves (SAIL) model is a 4-stream model that describes downward specular and diffuse fluxes and upward diffuse flux (Goward & Huemmrich., 1992; Verhoef, 1984). Additionally, SAIL allows variations in the inclinations of individual leaves (Verhoef et al., 2007). This model is particularly well suited for cover crops, as it assumes a homogeneous canopy and winter cover crops at early growth stages that do not generally exhibit multilayer, complex canopies. Though there may be within-field variation, field management and crop type are homogenous. SAIL also incorporates background reflectance and

output LAI can be controlled within the model. Objective 4 involves using the SAIL model to see how varying background spectra for maize, wheat, and soybean residue interact with soil reflectance at varying moisture. Objective 5 will look at how shadows cast within the canopy due to low sun angle, present during winter, affect reflectance measurements. Lastly, it will look at differences in viewing angle between sensors under the above conditions.

The research contained herein was carried out at the Beltsville Agricultural Research Center in Beltsville, MD. The fields chosen for study include those that had been planted to winter cover of barley, rye, ryegrass, wheat or triticale. These crops are the most commonly planted for winter groundcover in the mid-Atlantic region.

This research is the product of collaboration between the USDA-Agricultural Research Service Hydrology and Remote Sensing Lab, the United States Geological Survey (USGS) Eastern Geographic Science Center (EGSC), Maryland Department of Agriculture, and the University of Maryland, College Park. Funding is provided by the Choptank CEAP and the National Fish and Wildlife Foundation (NFWF).

### *1.2 Dissertation Organization*

The dissertation is composed of three individual research papers that address the objectives presented above. Figure 1 shows schematically how the chapters work toward informing an operational cover crop performance monitoring system (Figure 1).

**Figure 1:** The five objectives laid out in the dissertation as arranged by chapter.

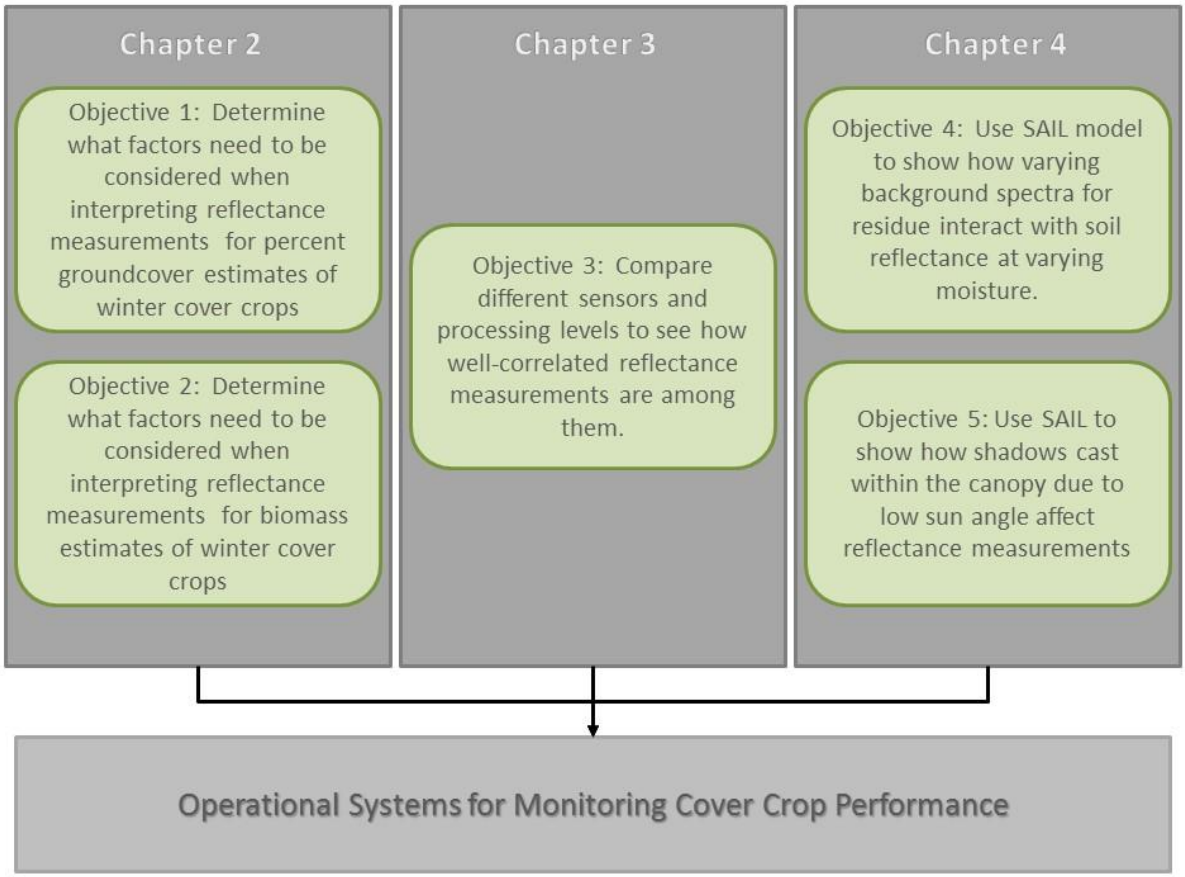


Chapter 2 encompasses Objectives 1 & 2, involving considerations that need to be accounted for when taking spectral measurements of groundcover and biomass of winter cover crops and the effects of chlorosis, senescence and frost damage that can result in leaf damage and reduced NDVI reflectance under winter conditions. Chapter 2 has been published in the International Journal of Applied Earth Observation and Geoinformation.

Chapter 3 addresses Objective 3 and presents a comparison of different sensor measurements and processing levels. The first portion of the chapter looks at how comparable absolute reflectance measurements are across a variety of sensors and processing levels, while the second part focuses on how much these differences

matter when they are used to calibrate satellite data to ground measurement data. The research presented in Chapter 3 has been submitted as a paper to Remote Sensing of Environment and is currently under review.

Chapter 4 focuses on modeling cover crop reflectance for low LAI, based on shadow due to low Sun angle, and background reflectance, as described above in Objectives 4 and 5. Chapter 4 will be combined with related research as a paper and submitted for peer-review.

# Chapter 2: Evaluating the relationship between biomass, percent groundcover and remote sensing indices across six winter cover crop fields in Maryland, United States

## *2.1 Introduction*

The Chesapeake Bay watershed is located in the mid-Atlantic on the East Coast of the United States. The Chesapeake Bay is the largest estuary in the United States, with the watershed comprising portions of six states and the District of Columbia (Goetz et al., 2004). Nutrient runoff from farmland has negative effects on water quality in the Chesapeake Bay. Residual nitrate in the soil profile after crop harvest is subject to leaching from agricultural areas into groundwater and adjacent tributaries. Pollution from nutrients and sediment has negative consequences for waterways, including eutrophication, reduced stocks of fish, and declining habitats through destruction of submerged aquatic vegetation (Dauer et al., 2000). These conditions have worsened in the Chesapeake Bay over time, in part due to fertilizer and manure application on agricultural lands (Jordan et al., 1997).

### 2.1.1 Cover Crops

Planting cover crops is an effective method to reduce both nitrogen leaching and sedimentation from agricultural lands (Meisinger et al., 1991). Winter cover crops are planted post-harvest on corn and soybean fields to scavenge residual nitrogen that remains in the soil, and to meet soil groundcover conservation guidelines, providing substantial water quality benefits (Dabney, 1998; Delgado et al., 2007). Cover crops accumulate biomass during the fall, with growth slowing through the winter, and typically green up again in the spring. Earlier planted cover crops are able to

accumulate more biomass prior to the onset of cold weather (Hively et al., 2009), leading to increased water quality benefits. In addition to planting date, a variety of factors, including species, planting method, and the amount of residual nitrogen available in soils, can lead to a large range of biomass and groundcover outcomes on cover cropped fields. Because increased biomass is related to increased groundcover and nutrient uptake, it is important to be able to accurately estimate cover crop biomass.

A majority of the Chesapeake Bay estuary is located in Maryland. MDA offers cover crop subsidies to farmers with the MACS program, through which farmers can either plant traditional non-harvested cover crops or commodity cover crops for harvest. Table 1 shows the breakdown of Maryland subsidized cover crops that were planted during the 2012-2013 cover cropping season.

**Table 1.** Extent of winter cover crops enrolled in the Maryland Agricultural Cost Share program during the winter of 2012-2013. Data were provided by the Maryland Agricultural Cost Share program.

| Species | Hectares (% of total) | Hectares | Fields (% of total) | Number of Fields |
|---|---|---|---|---|
| Wheat | 67 | 112061 | 62 | 7981 |
| Barley | 15 | 24491 | 14 | 1795 |
| Rye | 12 | 20182 | 17 | 2246 |
| Forage Radish | 3 | 5369 | 2 | 320 |
| Triticale | 2 | 3201 | 2 | 288 |
| Spring Oats | 1 | 2117 | 2 | 228 |
| Ryegrass | <1 | 468 | <1 | 29 |
| Canola/Rapeseed | <1 | 196 | <1 | 14 |
| Clover/Wheat | <1 | 152 | <1 | 5 |

During 2012-2013, wheat was the most common cover crop in terms of both acreage and percent of enrolled fields. Together, barley, rye and wheat contributed 96 percent

of the cover crop acreage in Maryland. Triticale and ryegrass covered over 3,500 hectares combined.

Following winter dormancy, cover crops typically experience a spring green-up when warm temperatures return, allowing for additional nitrogen uptake before kill-down, if residual nitrogen is left in the soil (Dabney et al., 2001). Availability of soil nitrogen also plays a role in the accumulation of biomass, with some cover crops growing poorly due to nitrogen limitation. The amount of fall residual soil nitrogen found in different fields can vary based on the previous crop's performance relative to fertilization, temperature, and rainfall.

In addition to reducing nutrient runoff, cover crop groundcover provides protection from raindrop impact and increases soil aggregate stability, decreasing erosion by wind and water (Dabney et al., 2001). If plants can reach their tiller stage (formation of side shoots) before winter dormancy, they are able to cover a greater amount of soil, resulting in better erosion control and environmental outcomes (De Baets, et al., 2011; Fisher et al., 2011). Along with high residue tillage practices, cover crops are often used to meet groundcover requirements on highly erodible lands (Mirsky et al., 2012).

### 2.1.2 Phenology and spectral indices

Remote sensing indices that measure plant greenness based on reflectance in the near-infrared and visible wavelengths are often used to estimate aboveground biomass (Gitelson, 2004), and can also be used for measuring percent vegetative groundcover (Purevdorj, et al., 1998; Wiegand et al., 1991). Such data can be gathered through remote sensing instruments such as Earth-orbiting satellites, aerial photos, proximal

sensors, or other means. The atmosphere can create differences in the relationship between surface reflectance and radiance detected at the sensor, and ground-based proximal sensors can be utilized to minimize atmospheric effects. A majority of solar radiation in the visible spectrum is absorbed by pigments in the leaves, resulting in low transmittance and reflectance, and the chlorophyll adsorption feature maximally reduces reflectance in the red portion of the spectrum (around 660 nm) with slightly less adsorption in the green wavelengths (around 550 nm). Low reflectance in the red is coupled with increased brightness in the near-infrared region of the spectrum, where there is low absorption and high transmittance and reflectance (Tucker and Sellers, 1986). Ratios of low-reflecting red and high-reflecting infrared measurements allow for unit-less measures of the chlorophyll absorption peak in green vegetation. A myriad of vegetation indices have been developed and researched over the years, 10 of which are shown in Table 2.

**Table 2.** Definition of spectral indices. Bands are designated in the formulas as R (red), B (blue), G (green), RE (red-edge), NIR (near-infrared), and L (soil line).

| Index | Name | Citation | Formula |
|---|---|---|---|
| NDVI | Normalized difference vegetation index | Tucker, 1979 | (NIR - R)/(NIR + R) |
| GNDVI | Green normalized difference vegetation index | Moges et al., 2004 | (NIR - G)/(NIR + G) |
| SR | Simple Ratio | Tucker and Sellers, 1986 | NIR/R |
| SAVI | Soil-adjusted vegetation index (L =0.5) | Huete, 1988 | [(NIR - R)/(NIR + R + L)](1 + L) |
| G-R | Green minus red | | G - R |
| EVI | Enhanced vegetation index | Huete, 2002 | 2.5(NIR - R)/(NIR + 6·R - 7.5·B + 1) |
| TVI | Triangular vegetation index | Broge and Leblanc, 2001 | 0.5[120(NIR - G) - 200(R - G)] |
| NGRDI | Normalized green red difference index | Tucker, 1979 | (G - R)/(G + R) |
| VARI | Visible atmospherically resistant index | Gitelson et al., 2002 | (G - R)(G + R - B) |
| NDREI | Normalized difference red edge index | Gitelson and Merzlyak, 1994 | (RE - R)/(RE + R) |

Testing multiple indices is useful, because at low fractional vegetated groundcover factors such as soil reflectance may interfere with the vegetation signal, and different indices are more sensitive in different ranges of biomass and

groundcover. In cover crop fields there may be little growth by the beginning of the winter season due to low temperatures and late planting dates, leading to limited horizontal layering of plants and a reduced impact on reflectance from canopy structure. On one hand, this limited horizontal layering can reduce complexity in the relationship between remote sensing observations and surface conditions. However, low levels of canopy cover may cause inaccuracies due to background reflectance of soils and crop residues interfering with the vegetation signal (Huete, 1988). At higher biomass, plants can have a complicated relationship with biomass due to their canopy structures. At higher biomass, especially in plants with planophile leaf structure, the sensitivity of NDVI and other indices saturates as the canopy closes, and additional increases in biomass do not result in increased reflectance (Myneni & Williams, 1994).

Winter cover crops are unique because they experience a variety of wintertime conditions that can lead to reduced leaf greenness. Very cold temperatures can cause leaf burn and frost damage that is not recoverable, unlike spring-planted crops that would not experience such low temperatures. Certain species, such as barley, are more susceptible to damage caused by low temperatures (Andrews, 1987). Cover crops also are susceptible to nutrient deficiency over wintertime, in soils with low soil nitrogen and low nitrogen mineralization potential. Once plants have used the residual nitrogen remaining in the soil, chlorosis or yellowing of leaves may occur (Broge & Mortensen, 2002). Lastly, cold temperatures and reduced day length during wintertime can also initiate senescence and dormancy (Gregersen, et al., 2008). During this process, the plant partitions resources away from the leaves toward other

tissues and chloroplasts begin to degrade (Gan & Amasino, 1997). Unlike frost burn, yellowing leaves can recover during springtime green-up, with the onset of warmer temperatures and increased springtime nitrogen availability. Index saturation, chlorosis, and frost damage may lead to inaccurate estimates of aboveground biomass when using vegetation indices to measure greenness of crops, regardless of species.

Cover crops impact water quality by decreasing erosion and leaching of residual soil nitrogen into waterways. Therefore, it is important to understand what factors influence remote sensing measurements of percent groundcover and biomass when considering cover crops on a landscape scale. Problems persist in methodologies to accurately correlate biomass to greenness, including relating biomass to vegetation indices through various growth stages, accounting for differences in phenology among species, and accounting for wintertime conditions that can cause reduced leaf greenness. As winter cover crops become more popular as a best management practice to prevent nutrient and sediment pollution in waterways, knowledge of factors that influence the relationship between remote sensing measurements and plant groundcover and biomass is necessary.

### 2.1.3 Study objectives

The primary objective of this study was to determine to what extent remote sensing indices are capable of accurately estimating the percent groundcover and biomass of winter cover crops. A second objective involved analyzing under what critical ranges these relationships are strong and under which conditions they break down.

*2.2 Materials and Methods*

2.2.1 Study site and experimental design

Six field locations at the USDA-ARS, Beltsville Agricultural Research Center (BARC) were selected for this study. Figure 2 shows the study location, the six fields and the sampling points.

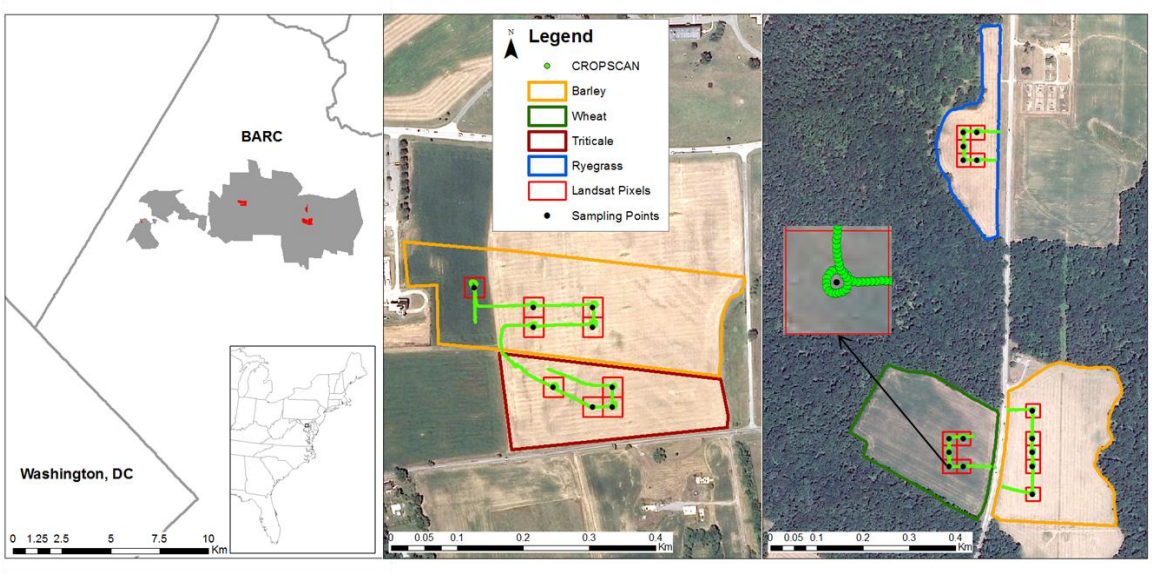


**Figure 2:** Red areas in the large area map (left panel) represent the six sampled fields. Field sampling occurred near flagged locations at the centroids (black points) of Landsat pixels (red boxes) falling within the center of each sampled field. Green points indicate the walking track of GPS-enabled CROPSCAN instrument (rye not shown). All fields were located on the USDA-BARC near Beltsville, Maryland.

The study sites were planted to cover crops in the fall of 2012 at various planting dates, following the harvest of summer row crops, and were not fertilized prior to March 1, 2013. The fields were planted to cover crops as a part of good field management practices but did not follow a specific experimental design, and therefore represented conditions found within the local farm landscape. The species of cover crop included barley (*Hordeum vulgare L.*), ryegrass (*Lolium multiflorum* Lam.), triticale (*Triticale hexaploide Lart.*), 'Aroostook' rye (*Secale cereale*), and

wheat (*Triticum aestivum L.*). Information regarding management practices on these fields can be found in Table 3.

**Table 3:** Agronomic data for the six sampled fields, including fertilization schedules, previous crop, weed treatment, planting, and spring harvest/kill dates.

| | **Triticale** | **Wheat** | **Ryegrass** |
|---|---|---|---|
| Planting Date | 10/11/2012 | 10/25/2012 | 9/26/2012 |
| Size (Hectares) | 3.6 | 6.6 | 3.5 |
| Previous Crop | Corn silage | Double crop soybean | Corn |
| Fall Fertilizer (% N) | 16.5 | 16.5 | 16.5 |
| Fall Fertilizer UAN (gal) | 5 | 5 | 5 |
| Weed Treatment | na | Harmony Xtra | na |
| First Spring Fertilizer Date | 3/1/2013 | 3/1/2013 | 3/1/2013 |
| Second Spring Fertilizer Date | 4/1/2013 | 4/1/2013 | 4/1/2013 |
| Spring Fertilzer Type | Nitrogen/Sulfur | Nitrogen | Nitrogen/Sulfur |
| Spring Fertilizer Amount (lb) | 60/5 | 80 | 60/5 |
| Spring Harvest Date | 5/13/2013 | 6/30/2013 | 5/4/2013 |
| Spring Harvest Type | Silage | Straw and grain | Silage |
| Spring Harvest Yield (kg/ha) | 10,088 | 3,699 | 8,967 |
| | **Rye** | **Barley1** | **Barley2** |
| Planting Date | 9/25/2012 | 9/24/2012 | 9/20/2012 |
| Size (Hectares) | na | 7.0 | 7.6 |
| Previous Crop | Soybean | Soybean | Soybean |
| Fall Fertilizer (% N) | 0 | 16.5 | 16.5 |
| Fall Fertilizer UAN (gal) | na | 5 | 5 |
| Weed Treatment | na | Harmony Xtra | Harmony Xtra |
| First Spring Fertilizer Date | na | 3/1/2013 | 3/1/2013 |
| Second Spring Fertilizer Date | na | 4/1/2013 | 4/1/2013 |
| Spring Fertilzer Type | na | Nitrogen | Nitrogen |
| Spring Fertilizer Amount (lb) | na | 65 | 65 |
| Spring Harvest Date | na | 6/18/2013 | 6/10/2013 |
| Spring Harvest Type | na | Grain | Straw and grain |
| Spring Harvest Yield (kg/ha) | na | na | 3,497 |

ArcGIS 10.2 was used for geospatial processing of field locations and sampling points (Esri, 2013). Field boundaries were digitized by hand, using a "leaf-on" aerial photograph downloaded through the USDA's Farm Services Agency's (FSA) National Agricultural Imagery Program (NAIP) as a base layer.

For all species except rye, sampling locations were established at the centroid points of Landsat satellite imagery pixels. Landsat pixels were used as a basis for selection of sampling points to allow for future comparisons between ground-based proximal sensor readings and satellite images, but satellite imagery analysis is not reported in this manuscript. Up to five pixels were chosen near the middle of fields to eliminate field border effects, and selected pixels were buffered by 5 m to eliminate edge effects between pixels. A centroid was calculated for each selected pixel, the coordinates of these pixels were loaded into a Trimble GeoXH GPS receiver with sub-meter horizontal accuracy, and flags were placed in the fields at each centroid location.

Unlike other fields, rye measurements were obtained from a plot-scale replicated trial maintained by Beltsville scientists, and rye sampling locations were therefore not based on Landsat pixels. Field sampling in all locations took place at multiple dates between October 12, 2013, and April 26, 2013 (Figure 3).

2.2.2 CROPSCAN

Reflectance spectra at each sampling location were measured using the CROPSCAN MSR16R hand-held multispectral radiometer (CROPSCAN, Inc.). The CROPSCAN gathers data across 16 distinct wavebands between 460 and 1640 nm, based on specific filter characteristics. It utilizes a two-way sensor to measure incident irradiation upon the top of the instrument, as well as reflected irradiation from the ground, and uses these two measurements to calculate percent reflectance for each waveband. The unit was linked to a Trimble GPS unit that recorded geographic coordinates of each data point. The handheld sensor recorded a

reflectance reading approximately every 3 seconds as the sensor was walked in a circle within a 3 m radius of each sampling point (Figure 2). The CROPSCAN was held at a height of approximately 1.8 m directly above the canopy, and the diameter of the field of view was 0.9 m. CROPSCAN relies on skylight illumination, and sun angles far from nadir can contribute to insufficient radiation reaching the sensor. Data were only collected during mid-day times with adequate sun angle and minimal cloud cover. Additionally, all data values that were collected with irradiance measurements below 300 $w/m^2$ were deleted from the analysis. Readings below this level may be inaccurate due to cloud cover and insufficient signal to noise ratio. Transects of collected data were converted into point shapefiles and were loaded into ArcGIS. To find the average for each sampling location, CROPSCAN points falling within each buffered Landsat pixel were averaged for each band. These averages were later used in calculation of vegetation indices. Multiple vegetation indices (Table 2) were calculated using the following CROPSCAN filter bands: blue (435-521 nm), green (556-566 nm), red (629-687 nm), red-edge (727-737 nm), and NIR (844-856 nm).

### 2.2.3 Red Green Blue (RGB) Photographs

Vertical, downward-looking (nadir) RGB photographs were taken from shoulder height (approximately 1.5 m) using a Nikon D5100 digital single-lens reflex (DSLR) camera in the red, green and blue channels of the visible spectrum. Three photos were taken within 3 m of every flag location on each sampling date. Photos were processed to determine percent vegetative groundcover using SamplePoint software (Booth et al. 2006). This software was used to generate 200 random points

over the photo and the user determined the type of groundcover under each crosshair point based on specified categories, including: green vegetation, bare soil, crop residue, frost damaged/yellowed vegetation, dark vegetation, dark bare soil, dark crop residue, dark frost damaged/yellowed vegetation, bright vegetation, bright bare soil, bright crop residue and bright frost damaged/yellowed vegetation. Categories were combined to quantify all vegetation, green vegetation, yellowed vegetation, crop residue, and exposed soil.

2.2.4 Plant and soil samples

Field samples of aboveground biomass were gathered within 3 m of each flagged sampling location using a destructive quadrat sampling (0.5 $m^2$) technique where three adjacent 1 m rows of cover crop were cut at ground height. The field study sites for barley1, barley2, wheat, and ryegrass had five flagged sampling points per field; triticale had four sampling points; and rye had three sampling points. Plant samples were dried overnight at 60$^o$ C and weighed. Dry weights and sampling area were extrapolated to estimate cover crop biomass at the field scale (kg/ha). Three 30-cm deep, 4-cm diameter soil cores collected near each flag location were combined into one bulk sample, dried at 50$^o$ C, extracted with 2M KCl, and analyzed for nitrate/nitrite content using colorimetric Lachat flow injection analysis in the laboratory.

2.2.5 Growing degree days

Calculation of growing degree days (GDD) predicts the timing of phenological milestones and normalizes for planting date by incorporating accumulated temperature, which is often a better predictor of plant growth than

calendar date (McMaster and Wilhelm, 1997). The calculation assumes a base temperature below which plants are unable to grow, and although this base temperature can vary based on species, for winter small grains it is often calculated with base temperatures of either 0° or 4° C. Daily GDD were calculating using the following formula (McMaster and Wilhelm, 1997):

$$GDD = [Tmax + Tmin)/2] - Tbase$$

where Tmax and Tmin were daily maximum and minimum temperatures, and Tbase was set to 4° C on advice of local agronomists. Mean temperatures below Tbase were set to Tbase, and then base temperature was subtracted from this value. The results were then used to calculate a cumulative sum of GDD between the planting date and the sampling date. For cover crops with planting dates in early fall, a larger number of GDD will elapse before spring termination, and the plants tend to produce higher biomass compared to late-planted species. This reaction to planting date and GDD has been widely documented in other research (Dabney et al., 2001; Hively et al., 2009).

#### 2.2.6 Climate data

Daily weather data for Beltsville were gathered from the National Atmospheric and Ocean Administration (NOAA) National Climatic Data Center (NCDC) for the Beltsville, Maryland, weather station. Long-term (30-year) climate daily normals (averages) were obtained for the same climate station.

*2.3 Results and Discussion*

Planting dates for each field ranged from September 20, 2012, to October 25, 2012 (Table 3), and field sampling dates ranged from October 12, 2012, to April 26, 2013. Figure 3 shows sampling dates and cumulative GDD for each field over time.

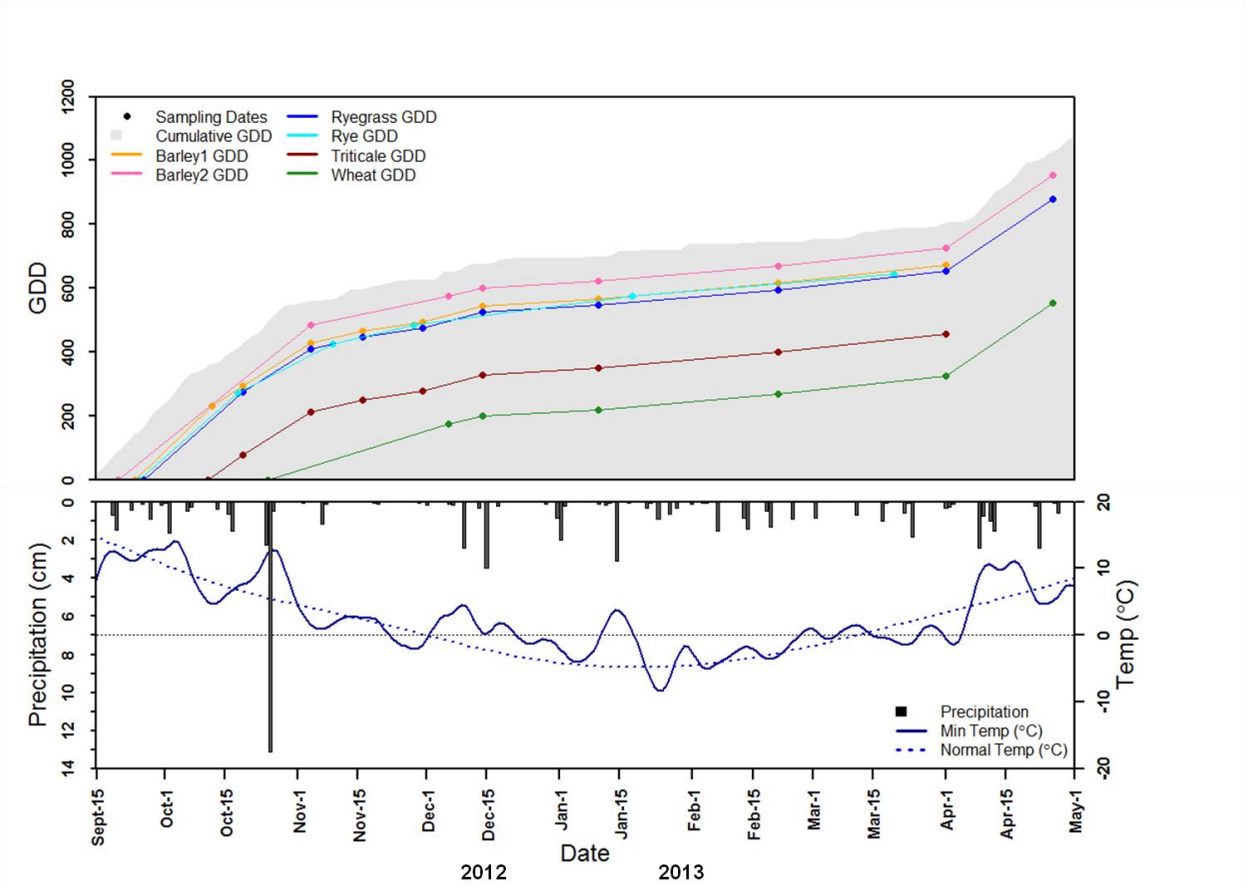


**Figure 3:** Accumulated GDD after planting for each sampled field with sampling dates (points), along with daily precipitation (black bars), 30-year daily normal minimum temperature (dashed blue line), and the observed daily minimum temperature (solid blue line) for 2012-2013 (NOAA-NCDC). The horizontal dotted black line represents 0° C.

Precipitation in 2012-2013 was well-distributed (Fig 2) and sufficient for cover crop growth. Subzero weather, during which plant tissue damage might be expected, occurred in four distinct periods: November 22 to December 1; December 23 to January 10; January 19 to March 5; and March 10 to April 4. The two periods

from December 23 through January 10, and from January 19 through March 5, were the coldest and most prolonged periods of subzero weather.

### 2.3.1 Species-specific crop growth

The USDA Natural Resources Conservation Service has established a minimum threshold for conservation tillage at 30 percent groundcover (ASAE, 2005), which will control approximately 50 percent of soil erosion resulting from raindrop impact. A threshold of 60 percent groundcover will reduce erosion by approximately 80 percent, depending on soil texture (Daniel et al., 1999). The Chesapeake Bay Program currently defines residue management classes as: high intensity tillage (0-30 percent groundcover); low intensity tillage (30-60 percent groundcover); and high residue management practices (>60 percent groundcover) (Chesapeake Bay Program, 2013). Groundcover thresholds can be achieved using either crop residue or vegetative materials such as winter cover crops. For nitrogen conservation, achieving a wintertime cover crop biomass threshold of at least 1000 kg/ha has been shown to substantially reduce soil nitrate concentrations (Hively et al., 2009), accounting for approximately 20 kg/ha N if a 2-percent tissue N content is assumed. Reaching these conservation goals can lead to increased water quality benefits by cover crops.
All sampled cover crops except for the late-planted wheat field eventually reached 60 percent groundcover (Figures 4b, 5). Barley1 and rye accumulated groundcover quickly and had 60 percent groundcover by November 4 and November 9, 2012, respectively. Barley2 reached 60 percent groundcover by November 4, fell below the threshold during mid-winter, and recovered by April 1, 2013. Triticale, although planted late, achieved 60 percent groundcover by December 14, 2012. Ryegrass,

although planted in early fall on September 26, did not uniformly reach 60 percent groundcover until very late in the spring, on April 26, 2013.

For biomass, barley1 and rye exceeded 1000 kg/ha by early November (Figure 4a). Ryegrass and barley2 reached 1000 kg/ha by early December, and triticale slightly later, in early January. Wheat did not reach the 1000-kg/ha threshold until early April, much later than the other fields.

The growth differences between the two barley fields, which had similar planting dates, could be explained by initial soil nitrogen. On November 4, 2012, barley1 had high residual soil nitrogen content (50 N kg/ha) due to long-term historical manure application on that field, whereas barley2 was more nitrogen limited with a residual soil nitrogen content of 6 N kg/ha. Although barley2 was planted slightly earlier, barley1 exhibited faster growth and earlier achievement of environmental thresholds. Despite these differences, both fields reached the critical thresholds before the onset of winter temperatures.

a) b)

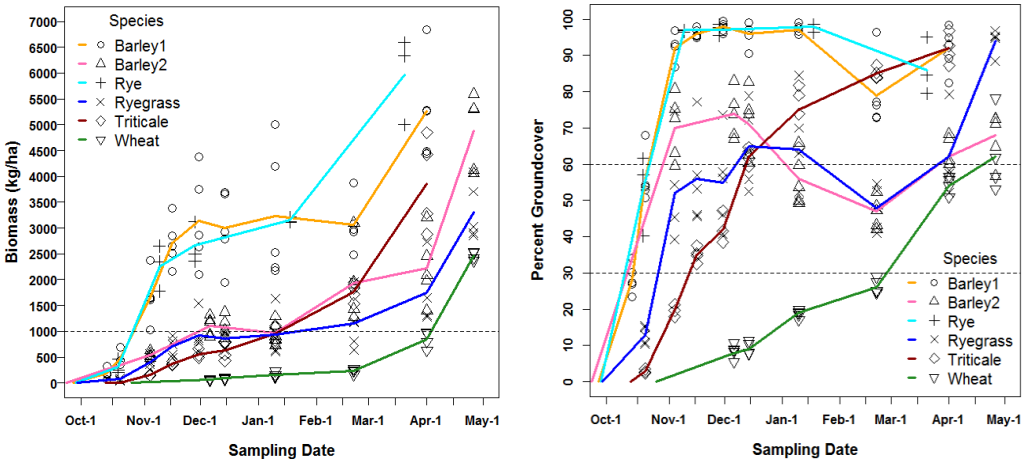


**Figure 4a-b:** a) Biomass accumulation and b) percent groundcover on sampled fields

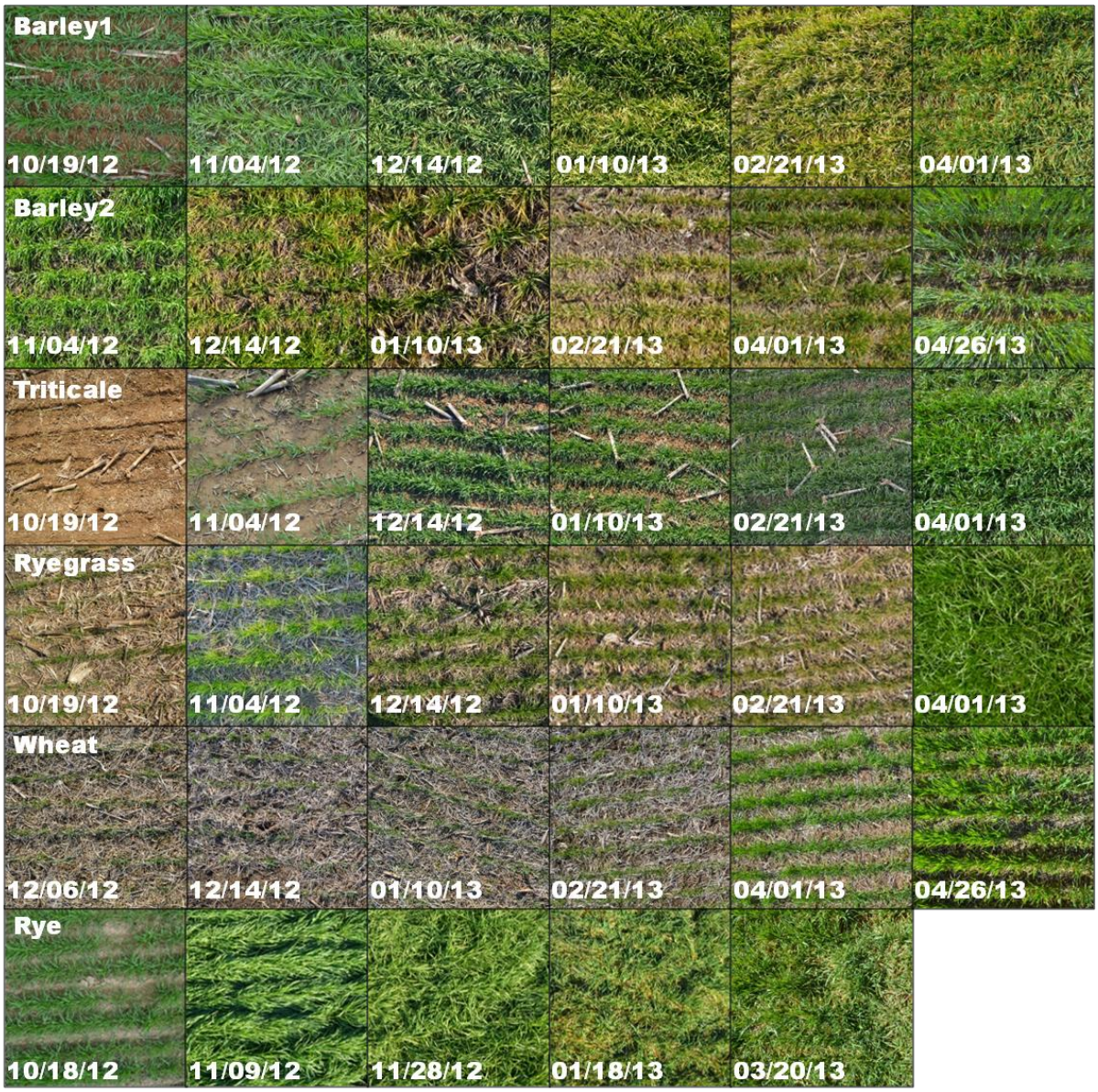


**Figure 5:** Shoulder-height photos of the measured cover crop species at various sampling dates throughout the winter of 2012-2013. Leaf yellowing can be noted in the January and February images.

2.3.2 Greenness over time

The amount of leaf yellowing varied considerably among species over the sampling period. Triticale and wheat, which had later planting dates (October 11, 2012, and October 25, 2012, respectively) exhibited negligible yellowing of leaves (Figure 5) with a continuous rise in NDVI values from 0.3 in the fall to greater than

0.8 in the spring (Figure 6a, b). Ryegrass and rye had earlier planting dates (September 26, 2012, and September 25, 2012, respectively), and exhibited yellowing of up to 20 percent of leaves during winter (Figure 5) with a corresponding slight dip in NDVI (Figure 6c, d), and by the spring had greened up to less than 10 percent yellowed leaves, The two barley fields, planted on September 23 and 24, experienced more yellowing than all other fields during the sampling period, with over 40 percent of leaves affected by February (Figure 5). Although the barley fields also greened up in springtime, there was still a large amount of yellowing in spring. Mid-winter NDVI values decreased significantly on both barley fields due to frost damage and leaf yellowing (Figure 6e-f). These results indicate that early planted cover crops experienced more frost damage, perhaps because they achieve a later growth stage by the onset of cold weather, with particular susceptibility of barley. Leaf yellowing and frost damage reduced reflectance in the NIR and increased reflectance in the red wavelengths, resulting in reduced NDVI values.

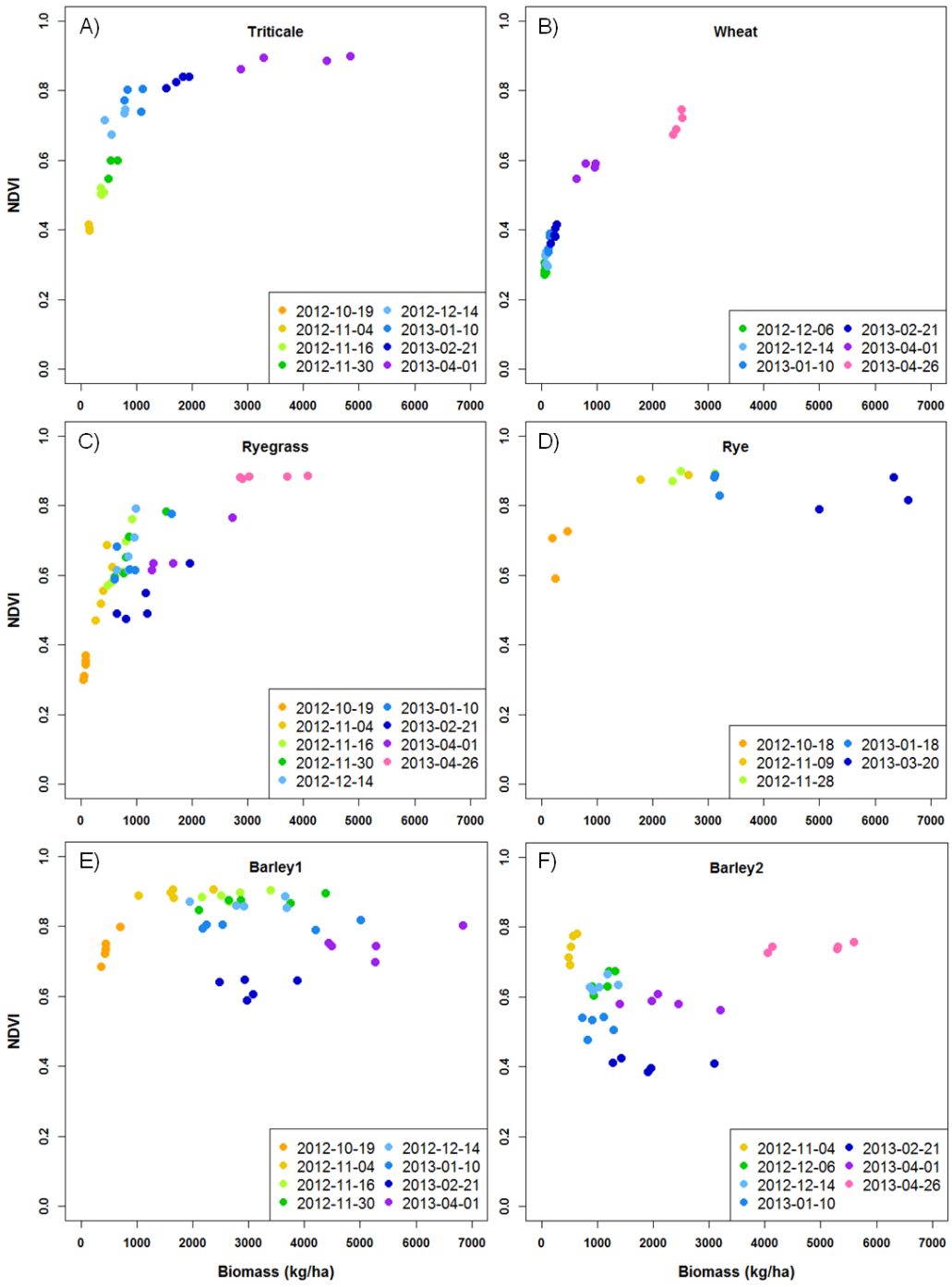


**Figure 6:** Aboveground biomass for the six sampled fields versus NDVI associated with each sampling date.

### 2.3.3 Biomass over time

Biomass increased on all fields over time, although some fields experienced a slight decrease in biomass over the mid-winter months. Triticale, wheat, and rye rose steadily with no decrease in biomass or NDVI. Although rye did not experience a reduction in NDVI, it reached NDVI saturation earlier than triticale or wheat. Due to some yellowing on ryegrass, NDVI dipped during the wintertime, though not as severely as barley1 and barley2, both of which reached NDVI saturation and experienced yellowing that resulted in a drop in NDVI during the winter months (Fig 5c, e-f). Barley2 followed a similar pattern as barley1, accumulating biomass before it experienced a drop by January 10, 2013. Barley2 experienced greening up by the last sampling date.

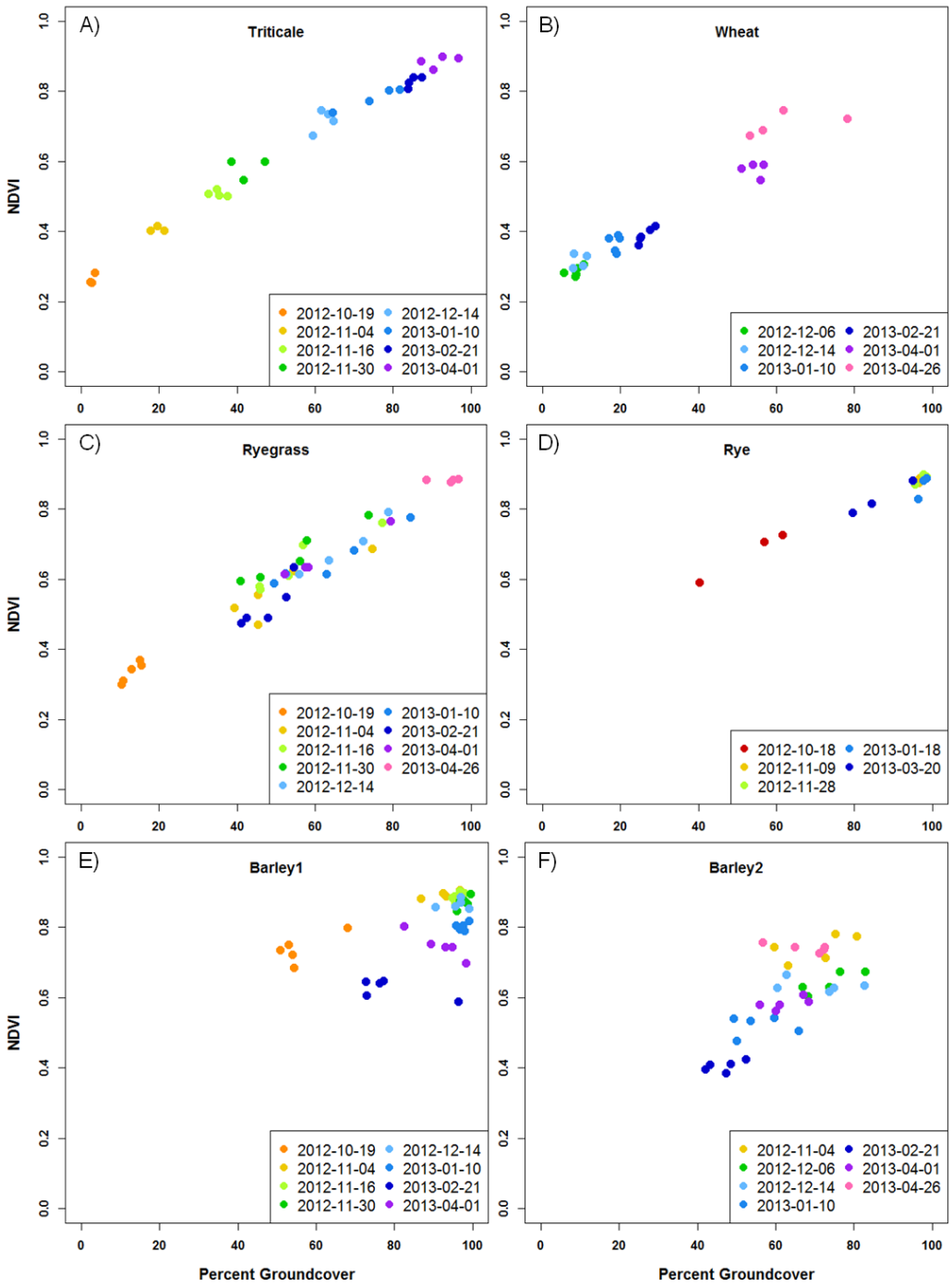


**Figure 7:** Percent groundcover for the six sampled fields versus NDVI associated with each sampling date.

### 2.3.4 Percent groundcover over time

All fields except for wheat and barley2 reached near 100 percent groundcover by the end of the sampling period. Triticale and wheat had steady rises in both percent groundcover and NDVI (Figure 7a-b). Ryegrass generally followed the same trend but did experience some yellowing and had a drop in NDVI corresponding to percent groundcover (Figure 7c). Rye also rose steadily but reached 100 percent cover earlier than all fields except for barley1 (Figure 7d). Both barley fields experienced a drop in percent groundcover from significant mid-winter yellowing, with a corresponding drop in NDVI, although barley1 achieved higher overall groundcover (Figure 7e-f).

### 2.3.5 Spectral indices and percent groundcover

Preventing erosion by achieving high percent groundcover on agricultural fields is a goal of planting winter cover crops. Vegetative groundcover prevents erosion from both wind and water, regardless of whether it is green or yellowing, and accurately estimating percent groundcover is important for assessing cover crop success.

There was considerable yellowing and damage to leaves after January 1, 2013, on all fields except for triticale and wheat. Groundcover assessment of shoulder-height photos showed that frost damage occurred during three periods of sub-zero temperatures between January 1, 2013, and mid-March (Figure 3), particularly in barley and ryegrass fields (Figure 7). Spectral vegetation indices are most sensitive to healthy green vegetation and do not detect yellowed and browned leaves, although this plant material continues to reduce erosion and nutrient loss. A higher percentage

of leaves with yellowing or damage will reduce the correlation between remote sensing indices and percent groundcover. Such winter effects varied widely across the fields (Figure 7). The percent groundcover measurements that were determined from RGB shoulder-height photos were split into two categories: green plus yellowed and frost damaged groundcover, and green groundcover only. Regressing the spectral indices with groundcover data collected prior to January 1, 2013, before the onset of reduced leaf greenness, resulted in higher correlations than using the entire date range, and were comparable to those made using green vegetation only (Table 4).

**Table 4:** Linear model goodness of fit ($r^2$) values between spectral indices and percent groundcover for all vegetation (green plus yellowed and frost damaged) versus green-only vegetation, for all sampling dates and for early sampling dates (October 18, 2012, through December 14, 2012). For definitions of indices see Table 2.

| All Sampling Dates | NDVI | GNDVI | SR | SAVI (L = 0.5) | G-R | EVI | TVI | NGRD | VARI | NDREI |
|---|---|---|---|---|---|---|---|---|---|---|
| All Vegetation | 0.87 | 0.84 | 0.64 | 0.88 | 0.78 | 0.79 | 0.85 | 0.73 | 0.73 | 0.83 |
| Green Vegetation | 0.94 | 0.90 | 0.74 | 0.94 | 0.86 | 0.90 | 0.87 | 0.83 | 0.83 | 0.90 |
| **Early Sampling Dates** | | | | | | | | | | |
| All Vegetation | 0.93 | 0.88 | 0.72 | 0.93 | 0.94 | 0.88 | 0.89 | 0.88 | 0.88 | 0.89 |
| Green Vegetation | 0.95 | 0.91 | 0.75 | 0.95 | 0.93 | 0.91 | 0.89 | 0.89 | 0.89 | 0.92 |

Although vegetation indices performed relatively well ($r^2$ = 0.64 to 0.88) in predicting the groundcover of all vegetation (green, yellowed, and frost damaged) for all sampling dates, goodness of fit increased across all indices ($r^2$ = 0.74 to 0.94) when groundcover was restricted to green-only vegetation (Table 4). Regression using restricted dates, prior to January 1, yielded similar values to green-only ($r^2$ = 0.75 to 0.95) and can be used as a proxy for green vegetation. This is evidenced by small differences of less than 0.08 in $r^2$ values between all vegetation and restricted dates versus green-only and unrestricted dates. The highest correlations were for

green-only and restricted dates, as this eliminated yellowing and frost damaged vegetation.

For prediction of green groundcover, NDVI, SAVI, and G-R performed better than other indices. SAVI was calculated setting L = 0.5, a typical value for medium amounts of vegetative cover, creating an upper limit of 1.5 (Huete, 1988). However, setting the optimal value for L requires some existing knowledge on amount of groundcover, whereas NDVI does not require such knowledge. G-R yielded good results for percent groundcover. As green reflectance is high in healthy vegetation and red reflectance is low, while the opposite is generally true with soils, positive values can be associated with vegetative groundcover while negative values are associated with soil. Further discussion regarding measurement of groundcover using spectral indices is limited to NDVI, as this index always outperformed or performed equally to the other indices when assessing percent groundcover.

There was a strong linear relationship between percent groundcover (green, yellowed, and frost damaged) and NDVI, regardless of species, and across all levels of groundcover, with an $r^2$ value of 0.87. Restricting the analysis to dates before reductions in leaf greenness occurred increased this correlation and resulted in an $r^2$ value of 0.93, making it nearly as effective as the correlation with green-only vegetation (0.94). This demonstrates that improvements can be made in the relationship between NDVI and percent groundcover by using climate data to assess when freezing may have occurred and modeling data separately before and after freezing temperatures. This method is especially useful where information about amounts of green versus yellowed or frost-burned vegetation is not readily available.

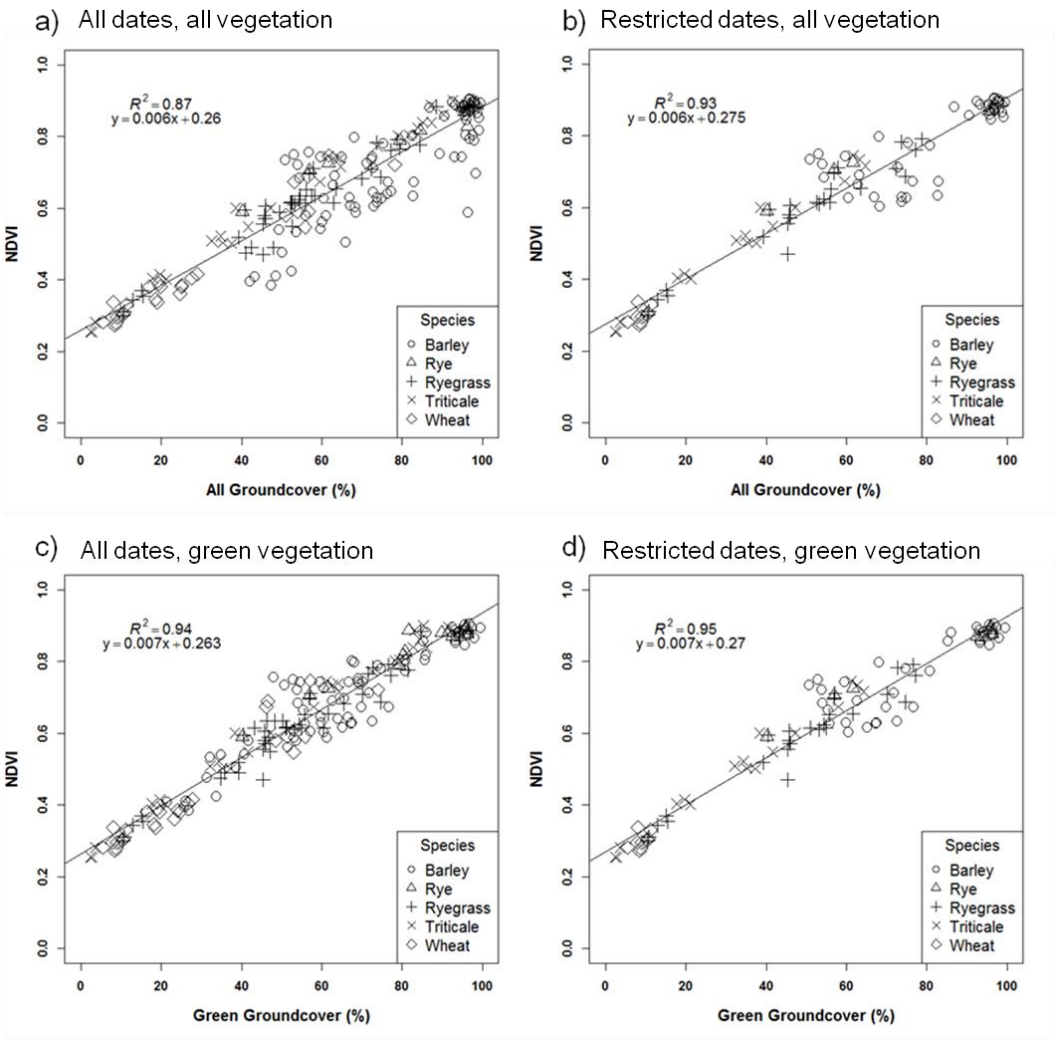


**Figure 8a-d:** Linear model goodness of fit ($r^2$) values from a linear regression between NDVI and vegetative cover, for all dates on the left (a and c) and early dates on the right (b and d). The two top graphs represent all groundcover (a and b), while the two bottom graphs represent green groundcover only (c and d).

As previously noted, vegetative cover, whether green, yellowed or frost damaged, is useful in preventing sediment erosion into waterways. NDVI performed well when assessing percent groundcover but, like other indices designed to measure vegetation vigor, it underestimated total vegetative cover because NDVI is not sensitive to senesced vegetation. Early-planted cover crops, including barley and

ryegrass, had more leaves at the onset of prolonged freezing temperature and suffered increased frost damage to leaves. Wheat had the latest planting date and while it did not yellow or experience frost burn, it also did not achieve maximum groundcover or biomass (Figure 5, 6b, 7b). Although late planted crops may experience less leaf damage and may have a better correlation to vegetation indices, they are not more successful than cover crops that suffered extensive leaf damage but exhibited high biomass and percent groundcover due to robust growth in the early winter period. Because of the effects of leaf yellowing and frost burn on vegetation indices, remote sensing tends to underestimate the groundcover of winter cover crops.

As seen in Figure 8, saturation in both NDVI and percent groundcover measurements results in a clustering of points near 100 percent groundcover and 0.9 NDVI. Removing these points from analysis yields an $r^2$ of 0.89 for all vegetation across restricted dates. This demonstrates that NDVI and other indices can successfully measure percent groundcover resulting from cover crop establishment through critical thresholds, from 0-80 percent groundcover, with considerable accuracy.

2.3.6 Spectral indices and biomass

Wintertime assessments of cover crop biomass are unique in that the plant tissues are subject to freezing temperatures that can result in significant leaf yellowing and frost burn. As a result, the utility of vegetation indices to estimate total plant biomass may become limited. Results for the 10 vegetation indices that were correlated with biomass using linear regression and log-linear regression (ln Biomass) are shown in Table 5.

**Table 5:** Goodness of fit ($r^2$) values between vegetation indices and biomass for both date unrestricted and date restricted (prior to January 1, 2013) values. Values are also included for date restricted regressions.

| No transformation | NDVI | GNDVI | SR | SAVI (L = 0.5) | G-R | EVI | TVI | NGRD | VARI | NDREI |
|---|---|---|---|---|---|---|---|---|---|---|
| All Sampling Dates | 0.37 | 0.39 | 0.32 | 0.37 | 0.26 | 0.33 | 0.37 | 0.28 | 0.28 | 0.40 |
| Early Sampling Dates | 0.59 | 0.60 | 0.74 | 0.60 | 0.64 | 0.65 | 0.84 | 0.70 | 0.69 | 0.65 |
| **Log transformation** | **NDVI** | **GNDVI** | **SR** | **SAVI (L = 0.5)** | **G-R** | **EVI** | **TVI** | **NGRD** | **VARI** | **NDREI** |
| All Sampling Dates | 0.61 | 0.63 | 0.38 | 0.61 | 0.44 | 0.50 | 0.57 | 0.40 | 0.40 | 0.58 |
| Early Sampling Dates | 0.86 | 0.84 | 0.63 | 0.86 | 0.84 | 0.78 | 0.86 | 0.74 | 0.74 | 0.80 |

Spectral indices are most sensitive to green living vegetation, whereas field sampled biomass included both living and dead plant material. Therefore, index performance for all sampling dates was poor with $r^2$ ranging from 0.26 to 0.40 (Table 5). When evaluation was limited to early sampling dates prior to January 1, 2013, to avoid the effects of leaf yellowing and frost damage, correlations improved substantially with $r^2$ ranging from 0.59 to 0.84.

When linear regression was limited to early sampling dates, SR, EVI, NGRD, VARI and NDREI all demonstrated a limited ability to detect meaningful differences at low biomass and also saturated at high biomass (figures not shown) leading to low overall goodness of fit (Table 5, early sampling dates with log transformation). While NDVI, GNDVI, SAVI and G-R where more accurate at lower biomass, they also saturated at high biomass. The problem of index saturation has been widely documented in the literature, especially for agricultural landscapes (Mutanga and Skidmore, 2004; Thenkabail, 2000). As an example, Figure 9 shows the relationship between measured biomass and NDVI for all species. In Figure 9b, the NDVI index saturates above approximately 0.8, associated with a biomass of approximately 1500 kg/ha, beyond which further increases in biomass do not result in corresponding increases in NDVI.

a) b)

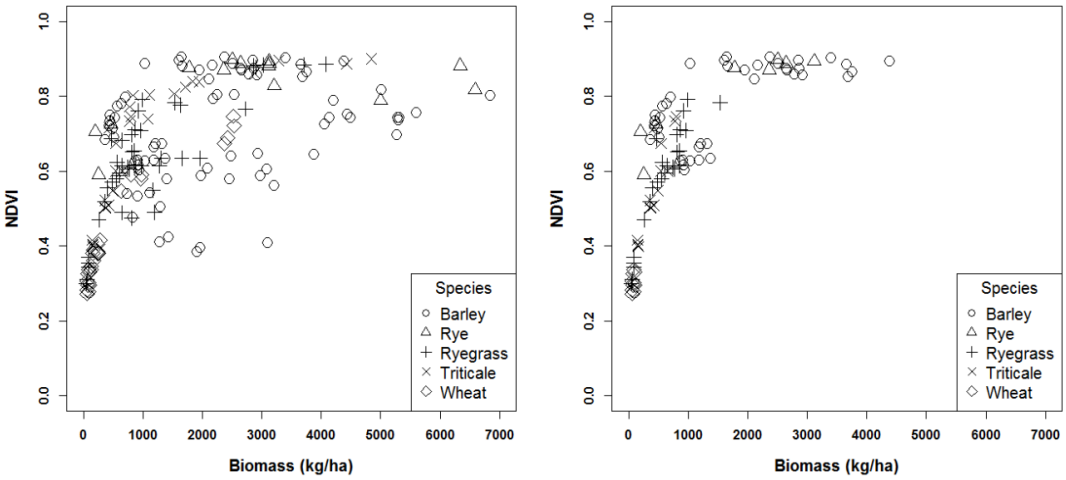


**Figure 9a-b:** a) NDVI versus measured biomass (kg/ha) for all species and sampling dates, and b) restricted to early sampling dates prior to January 1, 2013. This date falls before the onset of the frost period that occurred between December 14, 2012, and January 10, 2013.

Once data were limited to early dates, the linear regression fit between indices and biomass was further improved by calculating the natural log of biomass data. For NDVI, doing so resulted in an $r^2$ value of 0.86.

While restricting sampling dates before January 1, 2013, eliminates all high biomass points with yellowing leaves, eliminating saturation from the data also was necessary to achieve high correlation. The barley and rye fields in this study all reached 1000 kg/ha earlier than other fields and before the onset of cold temperatures, and comprise the saturated values shown in Figure 9. Although fast accumulation of biomass is desirable from an environmental perspective, it causes index saturation and complicates estimation of biomass.

While it seems that a natural log transformation can be used to account for saturation, in reality it is not possible to derive a proportional relationship between indices and biomass as biomass increases in the saturated range. Transforming data

prior to removing saturated values can therefore mask real issues within the data. A superior method is to eliminate saturated values and then apply a natural log transformation to the remaining data. Overall, saturation, yellowing, and frost damage will result in underestimation of cover crop biomass by remote sensing indices.

a) b)

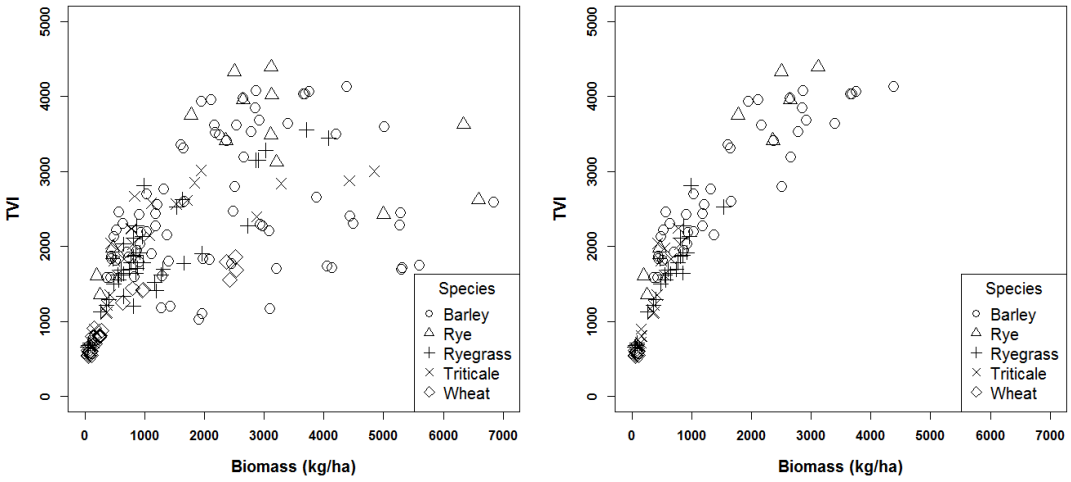


**Figure 10a-b:** TVI versus measured biomass (kg/ha) for all species and sampling dates (a). Plot B has been restricted to early sampling dates (before January 1, 2013) prior to the onset of yellowing or frost damage.

Unlike NDVI, which has an upper limit of 1.0, the Triangular Vegetation Index, TVI. does not reach an upper limit, thereby reducing the effects of asymptotic biomass saturation and making it better at estimating high biomass (Figure 10). However, the TVI is not as sensitive at low biomass, when crop reflectance is minimal relative to background soil reflectance, as was evidenced by the clustering of low biomass points in Figure 10b compared to the distinction of the same values in Figure 9b. TVI calculates the total area of a triangle with the three vertices in different parts of the electromagnetic spectrum. These areas include minimum red

reflection due to high absorption by chlorophyll, near-infrared, and variable reflection in the green portion of the spectrum (Haboudane et al., 2004). Increases in chlorophyll increase both absorption in the red portion of the spectrum and reflection approaching the near-infrared, increasing the size of the triangle while also decreasing the height of the triangle determined by reduced reflection in the green portion of the spectrum. TVI is less effective at differentiation at low biomass due to TVI's decreased sensitivity in this range. Removing low biomass points does improve $r^2$ values slightly, from 0.83 to 0.85 using TVI.

This analysis suggests that data should be restricted to early sampling dates to avoid the effects of frost damage and achieve accurate estimates of biomass using vegetation indices. Once dates are restricted, NDVI is most useful for estimates at low to medium vegetation levels (Broge and LeBlanc, 2000), and TVI is useful for higher canopy biomass (Chen et al., 2009).

2.3.7 Biomass and percent groundcover

The relationship between accumulated GDD and cover crop biomass can be used to help assess whether fields are reaching critical water quality goals, as more biomass leads to greater nutrient uptake and increased groundcover. Across all dates (Figure 10a), the relationship between aboveground biomass and percent groundcover was complicated by a number of factors, including saturation of percent groundcover with respect to biomass, and reduction in midwinter biomass resulting from leaf senescence.

a) b)

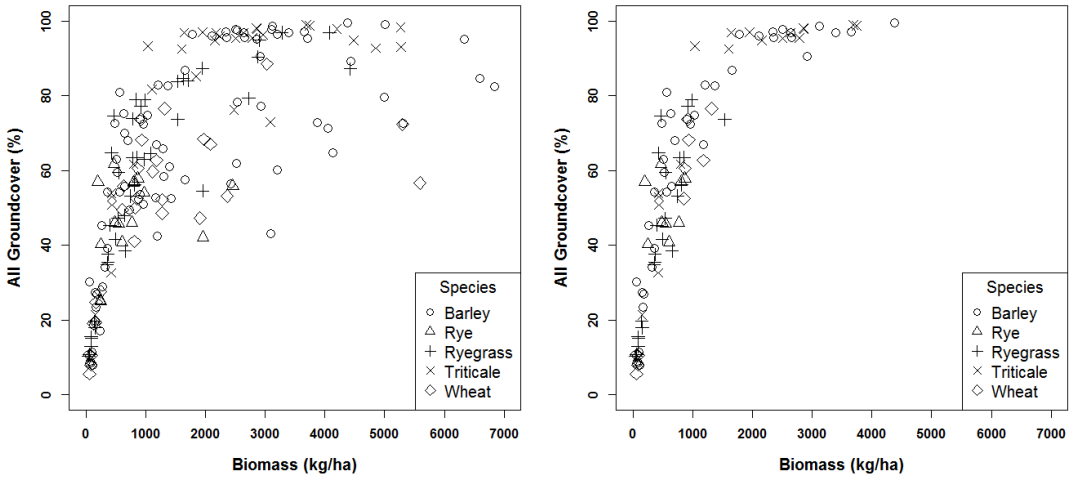


**Figure 11a-b.** Percent groundcover for all vegetation across all dates versus biomass (kg/ha) (a); b shows early dates, prior to January 1, 2013.

Restricting analysis to early sampling dates before January 1, 2013, tightened up the relationship between percent groundcover and biomass. As seen in Figure 11b, percent groundcover appears to reach 100 percent and saturate with respect to biomass saturation at roughly 1500 kg/ha of biomass. Eliminating the higher biomass measurements from analysis results in an $r^2$ value of 0.75 across all vegetation and has the same effect as eliminating percent groundcover values above 90 percent, when changes in percent biomass do not correlate to meaningful changes in groundcover. The biomass levels associated with critical groundcover thresholds are listed in Table 6.

**Table 6:** Estimates of biomass needed to reach percent groundcover thresholds

| Percent Groundcover | Biomass (kg/ha) |
|---|---|
| 30 | 200 |
| 60 | 825 |
| 100 | 1658 |

2.3.8 Percent groundcover and GDD

Establishing a relationship between accumulated GDD and cover crop percent groundcover is helpful to determine when fields are reaching critical water quality goals, as increased groundcover is associated with decreased soil erosion and sedimentation.

a) b)

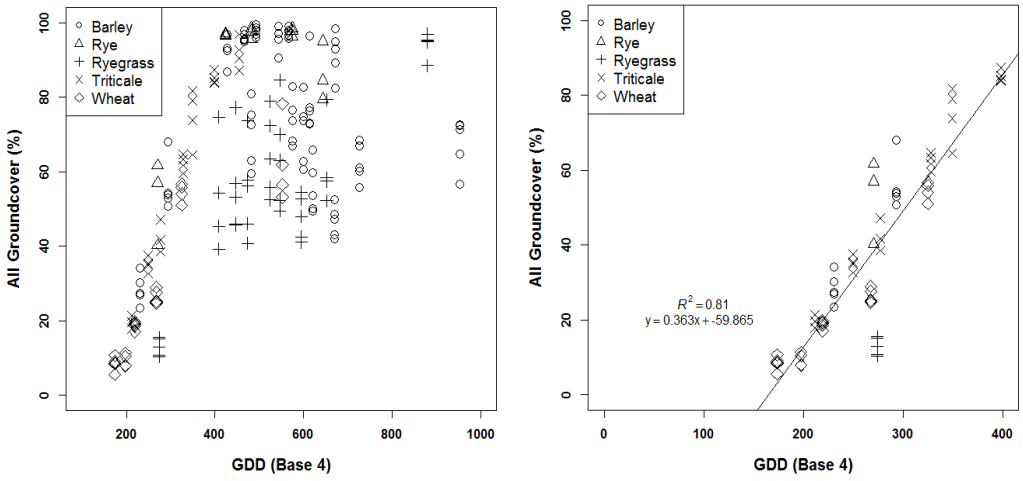


**Figure 12a-b:** Trends in groundcover as they relate to accumulated GDD following cover crop planting, including a) percent groundcover versus GDD for all dates, and b) percent groundcover versus GDD with GDD restricted to <400.

Figure 12b demonstrates that there is a strong linear relationship ($r^2 = 0.81$) between percent groundcover and growing degree days in the early part of the growing curve, below 400 GDD. Using the linear equation in Figure 12b, it is possible to estimate the number of accumulated growing degree days needed to reach critical groundcover thresholds (Table 7).

**Table 7:** Estimates of GDD needed to reach groundcover thresholds

| All Groundcover (%) | GDD Base 4 |
|---|---|
| 10 | 192 |
| 20 | 220 |
| 30 | 248 |
| 40 | 275 |
| 50 | 303 |
| 60 | 330 |
| 70 | 358 |
| 80 | 385 |

Table 7 provides estimates of the number of GDD needed to reach different groundcover thresholds, with analysis restricted to early growth (less than 400 accumulated growing degrees). The low number of days needed to achieve high groundcover shows that cover crops generally accumulate groundcover quickly during the early part of their growth cycle, before the onset of winter dormancy.

2.3.9 Biomass and GDD

The relationship between GDD and cover crop biomass is a useful indicator of how quickly fields accumulate biomass. Fields with higher accumulated biomass generally have higher nutrient uptake, reducing nutrient runoff into waterways.

a) b)

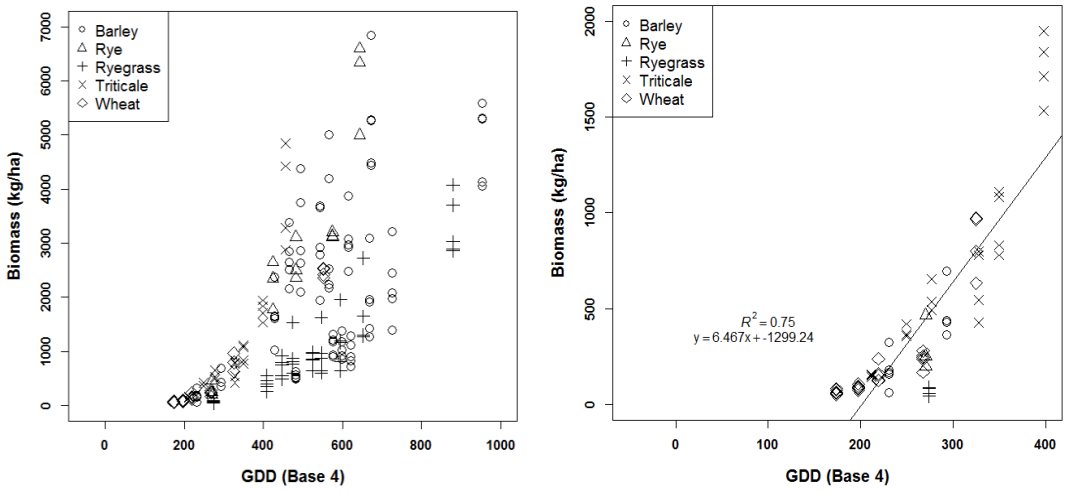


**Figure 13a-b:** Trends in biomass as they relate to accumulated GDD following cover crop planting, including a) biomass (kg/ha) versus GDD for all dates, and b) biomass (kg/ha) versus GDD with GDD restricted to <400.

Figure 13b demonstrates that there is a good relationship ($r^2 = 0.75$) between biomass and growing degree days in the early part of the growing curve, below 400 GDD. Estimates of the number of accumulated growing degree days needed to reach critical biomass thresholds are shown in Table 8. Average nitrogen content in cover crops can be estimated at roughly 2 percent (Hively et al., 2009), resulting in an associated sequestration of between 2-23 kg N.

**Table 8:** Estimates of growing degrees needed to reach biomass thresholds

| Biomass (kg/ha) | GDD Base 4 |
|---|---|
| 250 | 240 |
| 500 | 278 |
| 750 | 317 |
| 1000 | 356 |
| 1250 | 394 |

Similarly to percent groundcover, the relationship between aboveground biomass and GDD becomes more complex as GDD increases. Above 400 GDD some fields began to experience frost damage and yellowing of leaves, and over time there is far greater variation between GDD and biomass. Species that were planted early and experienced more yellowing of leaves may have a high number of accumulated GDD but a declining biomass through the winter. Conversely, triticale and wheat fields that were planted later and had fewer accumulated GDD had steadily rising biomass and were less affected by reduced leaf greenness over winter.

### *2.4 Conclusion*

This study employed a GPS-enabled CROPSCAN proximal sensor to collect surface reflectance data from cover cropped fields, over the winter of 2012-2013. Results compared the utility of 10 vegetation indices for measuring cover crop aboveground biomass, and percent vegetated groundcover. Remote sensing techniques were most successful for measuring both percent groundcover and biomass of winter cover crops prior to the onset of freezing weather. Throughout the winter cover crop season, accurate measurements were made as long as frost damage, leaf yellowing, and index saturation were handled properly.

In areas that experience cold temperatures during the winter season, adjusting remote sensing measurements to account for frost damage and leaf yellowing is critical to ensure accuracy in estimating both percent groundcover and biomass. Fortunately, the effects of leaf yellowing and frost damage result in underestimation, rather than over-estimation, of the water quality benefits (nutrient and sediment capture) associated with cover crops. When dates were restricted, the linear relationship between percent groundcover and NDVI improved from $r^2$ of 0.87 to $r^2$ of 0.93. In fact, restricting the date was as effective as separating out green groundcover from yellowed and frost-burned vegetation, which was a time- and data-intensive process.

The effects of index saturation at high biomass and clustering of points at low biomass should be considered when measuring cover crop biomass. Many indices cannot differentiate the amount of biomass when there is too much vegetation, and a clear proportional relationship between the index and biomass is lost. This study showed that choosing different indices for high and low biomass ranges can prevent both low and high index saturation and increase predictive capability when early dates are modeled. Once saturation was removed, using a natural log transformation further increased the correlation between biomass and spectral indices.

Of the 10 indices that were evaluated, G-R, GNDVI and SAVI performed similarly to NDVI, detecting differences at low biomass and saturating at high. SR, EVI, NGRD, VARI and NDREI were not as effective with low biomass and also experienced saturation. TVI was the best at estimating high biomass points. However, TVI was

not as good as NDVI at detecting low levels of biomass. NDVI was equal or superior to the other indices in predicting percent groundcover.

There was a good relationship between growing degree days and both percent groundcover and biomass for early in the growing season. When GDD was restricted to <400, or the early part of plant growth curves, there was a strong relationship between percent groundcover and GDD with an $r^2$ of 0.81; and similarly for biomass and GDD, with an $r^2$ or 0.75. Biomass and percent groundcover both increased rapidly during the beginning of growth. After 400 GDD, the increase in growing degree days was not well correlated with biomass due to a decreased groundcover and biomass in species that experienced wintertime leaf damage.

Although this study was conducted in Maryland, areas with comparable winter conditions planted with small grain winter cover crops could benefit from the information put forward here. Chosen fields were reflective of realistic winter cover crop scenarios, but future research could include controlled planting dates and field management to further analyze species-specific and treatment-specific differences in plant growth over the winter crop season. Additionally, although it is beyond the scope of this paper, extending these data and scaling up this study to make comparisons between satellite index measurements, especially from readily-available Landsat data, and proximal surface reflectance would allow for greater operational applications of remote sensing to map the water quality benefits associated with winter cover crops.

# Chapter 3: Comparability of same-day remote sensing data for measuring winter cover crops

## *3.1 Introduction*

Winter cover crops have proven to be an effective method to reduce nutrient runoff and sedimentation into waterways, and to increase environmental benefits for soil health and water quality (MDA, 2016). As they accumulate biomass, winter cover crops sequester residual nutrients that remain in the soil post-harvest, and also prevent wind and water erosion of soils by providing vegetative groundcover (Meisinger et al., 1991; Dabney, Delgado & Reeves, 2001). In ecologically sensitive estuaries, such as the Chesapeake Bay, they can reduce losses of nitrate and sediment from agricultural areas (Ator & Denver, 2015). The use of cover crops to mitigate nitrogen leaching and sedimentation play a vital role in reducing algal blooms, eutrophication, and threats to wildlife (Dauer et al., 2000). The United States Environmental Protection Agency (EPA) has identified winter cover crops as an effective practice to reduce agricultural pollutants in the Chesapeake Bay (Talberth et al., 2015). A number of states within the watershed provide economic incentives to plant winter cover. Maryland provides cost-share for farmers to plant winter cover crops, and a record 492,244200 acres were planted in Maryland in 2016 (MDA, 2016).

Remote sensing has been demonstrably successful as a tool to monitor winter cover crop growth and performance (Hively et al., 2009; Prabhakara et al., 2015). Remote sensing of the land surface in concert with technologies such as GIS and

GPS, allows for precision geospatial management of agricultural fields. Additionally, proximal reflectance sensors that are able to detect in-field variation are becoming more widely used (Gebbers & Adamchuk, 2010; Hedley, 2014; Mulla, 2013). Proximal sensors are held a short distance from the ground, recording reflectance measurements near the land surface with minimal adulteration from atmospheric conditions, theoretically allowing comparison with satellite imagery that has been corrected to surface reflectance. Unlike stationary proximal sensors that record single readings, the instruments used in this study were integrated with GPS technology that take measurements "on-the-go," as they are moved across the landscape. This method of data collection incorporates spatial variability within agricultural fields.

While proximal sensors offer high temporal and spatial resolution for crop monitoring, the instruments are often expensive and require training to operate, data collection is time intensive, and physical access to fields is requisite. Such limitations may necessitate the use of other types of remote sensing data. Satellite data are often publicly accessible, but there are tradeoffs between temporal and spatial resolution. For example, field sizes within the Chesapeake Bay watershed tend to be comparatively small. For example, in Talbot County, Maryland, fields average 20 hectares in size compared with 65 hectares in the Midwest. This smaller size disallows use of coarse-resolution satellites with high temporal resolution such as MODIS and AVHRR that image daily. Satellite imagery with fine to moderate spatial resolution (2 m to 30 m pixel size) minimize mixed pixels and are required for measuring small fields that are not discernible using coarser resolution platforms. However, platforms such as Landsat 7 (30 m), SPOT-5 (10 m), and WorldView-2 (2

m) have lower temporal resolution. Lower temporal frequency, in combination with clouds or snow on overpass days can potentially cause long breaks with no useable data. Such strengths and shortcomings may be overcome if several types of remote sensing data can be used, necessitating measurement comparisons among the different instruments. Exploring the relationship between high-resolution handheld sensor data and satellite-based measurements can allow for scaling up of difficult-to-acquire proximal data, resulting in greater operational efficiency when assessing the benefits of cover crops on water quality.

Although previous studies have explored the relationship between satellite reflectance measurements and surface reflectance measurements from ground-based instruments, this research compares ground-based "on-the-go" proximal sensor data with fine and moderate resolution sensor data that have been corrected to both top of atmosphere (TOA) and surface reflectance (SR).

### 3.1.1 Research Questions

Do surface reflectance products have better relationships with proximal sensor measurements compared to top-of-atmosphere for winter cover crop fields? Are same-day measurements among satellite platforms highly correlated with each other when spatial resolution differences are accounted for? Are surface reflectance measurements capable of predicting agronomic variables such as cover crop biomass and percent vegetative groundcover?

## *3.2 Materials and Methods*

### 3.2.1 Study site and experimental design

All data were collected on fields situated at the United States Department of Agriculture Beltsville Agricultural Research Center in Beltsville, Maryland, that were planted to winter cover crops common in the Mid-Atlantic region. The cover cropped fields included two barley (Hordeum vulgare L.) fields, one ryegrass (Lolium multiflorum Lam.) field, one triticale (Triticale hexaploide Lart.) field, one 'Aroostook' rye (Secale cereale) field, and one wheat (Triticum estivum L.) field. Planting dates and management methods are described in Prabhakara et al., (2015). Data were collected on two dates (December 6, 2012 and January 23, 2013) at a total of 35 sampling locations (Figure 14) using satellites and proximal sensors. Biomass and percent vegetative groundcover were collected at 23 of the sampling locations.

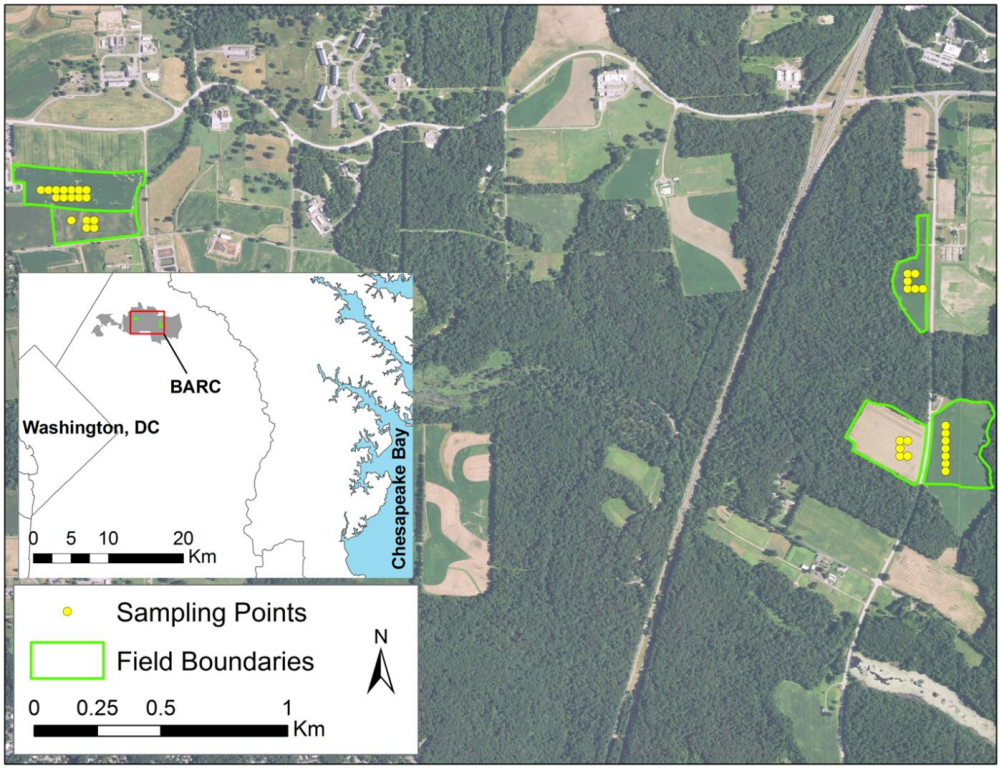


**Figure 14:** The study area consisted of five fields at the USDA-ARS Beltsville Agricultural Research Center shown as the gray polygon on inset map. Field locations and sampling points are shown on top of a 2015 true-color NAIP orthophoto.

### 3.2.2 Sensors

Five different sensors were used in this analysis between the two sampling dates. The three satellite sensors were Landsat-7, SPOT-5 and WorldView-2. The three satellite platforms have different temporal, radiometric and spatial resolutions as described in Table 9 and Figure 15. Two proximal sensors, CROPSCAN and Crop Circle, were also utilized. The handheld proximal sensors were GPS-enabled to collect measurements every two to three seconds as they moved across the landscape.

**Table 9:** Specifications for satellite platforms.

| | Landsat 7 | WorldView-2 | SPOT5 |
|---|---|---|---|
| **Swath Width (km)** | 185 | 16.4 | 60 - 80 |
| **Repeat Coverage (days)** | 16 | 1.1-3.7 | 2 - 3 |
| **Altitude (km)** | 705 | 770 | 822 |
| **Ground Resolution (m)** | 30 | 1.84-2.4 | 10 |

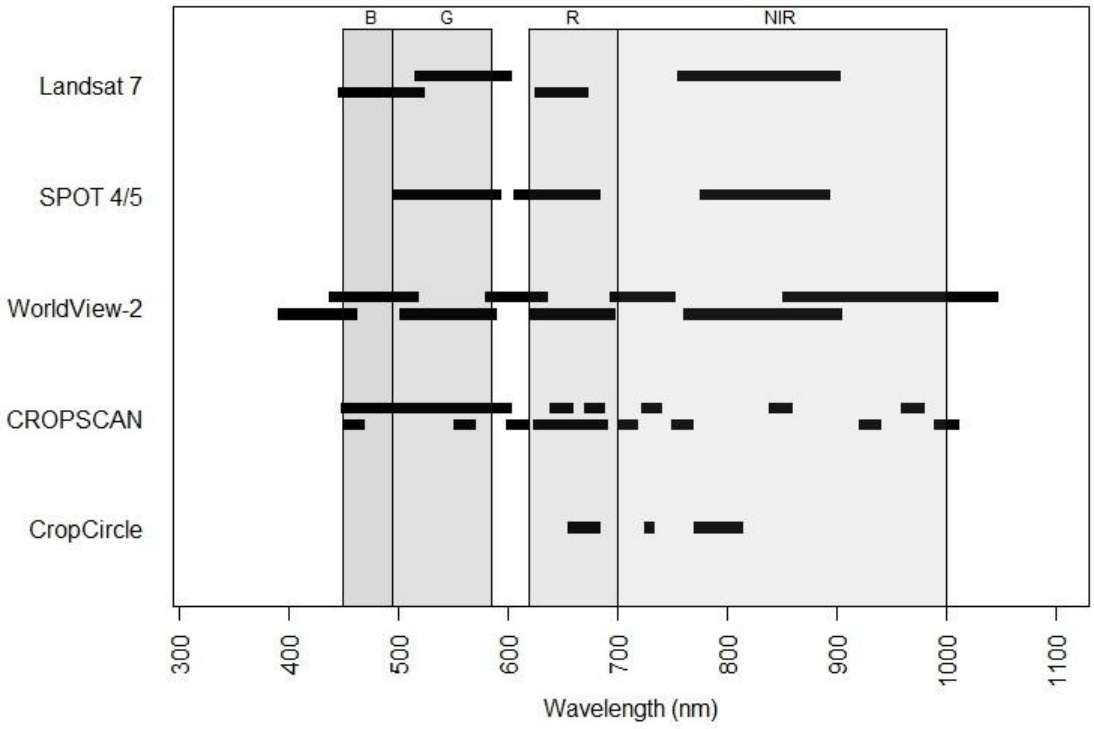


**Figure 15:** Bandwidths for satellite (Landsat 7, SPOT-5, and WorldView-2) and proximal (CROPSCAN, Crop Circle) sensors across the visible and near-infrared regions of the electromagnetic spectrum.

### 3.2.3 Landsat 7

Landsat 7 scenes from December 6, 2012, and January 23, 2013 (path 15/row 33) were downloaded in GeoTiff format from the USGS Earth Resources Observation

and Science (EROS) Center Science Processing Architecture (ESPA) (USGS, 2016) site as an unstacked image with separate tiff files for each band. When delivered, the files had already been preprocessed to top of atmosphere and surface reflectance. Visible bands 1-5 and 7 were layer stacked using ENVI version 4.8 (Exelis Visual Information Solutions, Boulder, Colorado) to create one multiband image. The ESPA file also contained an NDVI image that had been calculated from surface reflectance. Both surface and top of atmosphere images had a 30m spatial resolution and 6 optical bands (Figure 15). It should be noted that Landsat 7 scenes contain stripes of missing data due to a scan line corrector failure from 2003 (USGS, 2015). Fortunately, all of the sampling points used in this study fell on pixels in the center of the scene that were unaffected by striping and associated data loss.

### 3.2.4 SPOT-5

A SPOT-5 image for BARC (path 622/row 271) was tasked as part of the USGS North American Data Buy and was acquired from the USGS Earth Explorer site. The raw image was spatially shifted to match a field boundary polygon vector data file and ensure proper alignment by visual inspection in ENVI. Top of atmosphere reflectance was also calculated using ENVI. Surface reflectance was calculated from SPOT using coefficients derived from the MODTRAN 5.3.3.atmospheric radiative transfer model (MODTRAN5, 2012). Data for the required atmospheric correction include information about various aerosols, including water vapor and ozone. Air optical thickness data were downloaded using Aerosol Robotic Network (AERONET) data from the Goddard Space Flight Center site (Holben, B., 1993). Radiosonde data needed for temperature and relative humidity

measurements in the upper atmosphere were acquired for the Dulles Airport/IAD site as it was the closest station in an urban or suburban area (http://www.esrl.noaa.gov/raobs/). Total ozone data were estimated using Environment Canada daily ozone maps (Environment Canada, 2016). All other necessary data were found in the imagery metadata file. SPOT-5 data has a 10m spatial resolution and four bands (Figure 15). To allow for a more precise comparison against other sensors, the SPOT-5 pixels were smoothed using a low pass filter and a 3x3 kernel in order to more closely match Landsat's spatial resolution.

### 3.2.5 WorldView-2

WorldView-2 imagery was acquired on December 6, 2012. The WorldView-2 sensor has 8 spectral bands that overlap in various parts of the spectrum (Figure 15) with a 2-meter spatial resolution for visible and NIR bands. The WorldView-2 imagery was shifted to properly align with the other satellite imagery and ground truth data, using the same protocol as the shifting of SPOT-5 data. The WorldView-2 imagery was also converted to surface reflectance using MODTRAN with variable inputs from the same sources as those used to convert SPOT-5 data.

### 3.2.6 CROPSCAN

The CROPSCAN MSR16R handheld multispectral radiometer (CROPSCAN, Inc.) used in this study is unique in its ability to record "on-the-go" measurements every 3 seconds as it crosses the landscape. Geographic coordinates associated with each reflectance data point were recorded using a Trimble GeoXH GPS unit with sub-meter accuracy. CROPSCAN has a greater spectral resolution than either Landsat or SPOT, gathering data across 16 wavebands that are centered on a portion of the

electromagnetic spectrum (Figure 15). The CROPSCAN instrument was held approximately 1.8 meters above the vegetation canopy, creating a 1-$m^2$ field of view. The instrument employs a two-way sensor that measures incident solar irradiation as well as reflectance from the ground to calculate a calibrated percent surface reflectance. When skylight conditions are not optimal due to cloudy conditions or low sun angle, lack of radiation reaching the sensor can result in inaccurate measurements. Therefore, all data values with incident radiation below 300 $w/m^2$ were excluded from analysis. Landsat pixels were buffered in by 5-meters to avoid edge effects and CROPSCAN points falling within each buffered Landsat pixel were averaged for each waveband.

### 3.2.7 Crop Circle

A Crop Circle ACS-430 proximal sensor (Holland Scientific, Inc.) was deployed in concert with the CROPSCAN to gather spectral data. The Crop Circle, unlike the CROPSCAN, is an active sensor with its own light source, and therefore has fewer limitations than passive radiometric sensors which require specific skylight conditions. However, the light signal is not strong and can result in low reflectance readings. Active remote sensing signals can also be affected by plant canopy characteristics, distance from the plant canopy, and device temperature (Kipp et al., 2014). The spectral resolution of the Crop Circle is limited to three bands in the red and NIR portions of the electromagnetic spectrum (Figure 15). The sensor was held approximately 1-m above the soil surface and collected approximately one scan per second, associated with a GPS coordinate. The resulting data were converted into

shapefile format and loaded into ArcGIS. Crop Circle readings were averaged within the same buffered Landsat pixels as CROPSCAN.

3.2.8 Biomass sampling

Samples of aboveground biomass were collected for each field on December 14, 2012 and January 10, 2013. The barley1, barley2, and ryegrass fields were sampled in five locations, and the triticale field was sampled in four locations. Biomass samples were collected within 3 m of each Landsat pixel centroid using destructive sampling, by cutting a 1-m length of 3 adjacent rows of cover crop at ground height ($0.5m^2$ surface area). Samples were dried for 48 hours at 60 °C and weighed. The sampling area and dry weights were extrapolated to estimate biomass at the field scale (kg/ha). Although biomass samples were not measured on the same day as sensor data collection, they were collected within two weeks of the sensor dates, and it was assumed that biomass, percent vegetative groundcover, and composition of the samples would remain relatively static due to negligible cover crop growth during the cold weather conditions (Figure 17).

3.2.9 Percent vegetative groundcover

Three shoulder-height (1.5 m) RGB photos of the soil surface were taken using a Nikon D3100 DSLR camera at each sampling location during sensor data collection. The photos were processed using SamplePoint software (Booth et al., 2006) in order to determine the amount of the following types of vegetative groundcover: green vegetation, yellow vegetation, bare soil, and residue. The software randomly placed 200 points at various locations within each image and the

vegetative groundcover under the point was recorded. Only green vegetation was used to estimate percent vegetative groundcover.

3.2.10 Growing degree days

GDD predict the timing of phenological milestones in plants (McMaster and Wilhelm, 1997). The base temperature is set to a point where plants are unable to grow, and although this base temperature varies based on species, for winter small grains it is often calculated with base temperatures of 4° Celsius. GDD were calculated using the formula:

$$GDD = [Tmax + Tmin)/2]-Tbase$$

where Tmax and Tmin are daily maximum and minimum temperatures, and Tbase is 4° Celsius (McMaster and Wilhelm, 1997). Mean temperatures below Tbase were set to Tbase, and then base temperature was subtracted from this value.

3.2.11 Statistical Analysis

Linear regression for sensor-to-sensor comparisons across spectral bands was performed using the R Statistical Package (R Core Team, 2016). Reflectance measurements were regressed against each other within-date for the red, near-infrared, and green wavelengths. The NDVI is a measure of plant vigor (Tucker, 1979). To reduce the dimensionality of the data set by eliminating differences in NDVI due to large biomass variability between fields, an absolute value of the difference between CROPSCAN measurements and every other sensor were calculated for each sampling point. Sensors with larger variation had mean values that were different than zero and further from other means.

## *3.3 Results*

### 3.3.1 General Conditions

This study analyzed the comparability of reflectance values among several remote sensing measurements taken on the same day. On December 6, 2012, WorldView-2 and Landsat satellite imagery were acquired and radiometrically corrected to both top-of-atmosphere and surface reflectance. On January 23, 2013, SPOT and Landsat overpasses took place and both images were also converted to top of atmosphere and surface reflectance. Proximal sensor measurements from CROPSCAN and Crop Circle were collected at all sampling locations on both December 6, 2012 and January 23, 2013.

### 3.3.2 Atmospheric conditions

The atmospheric conditions on both days were evaluated using AERONET data from the Goddard Space Flight Center in Greenbelt, Maryland. Both days were relatively clear, but December 6, 2012 (300 km visibility) was clearer than January 23, 2013 (157 km visibility) (B. Holben, 2013). On January 23, there were popcorn clouds scattered throughout the image (Figure 18). No clouds or shadows were present on December 6. The high visibility levels indicate clear conditions, which were purposefully chosen to provide adequate irradiance to handheld sensors, and cloud free satellite imagery, conditions that were the most conducive to data gathering for this study.

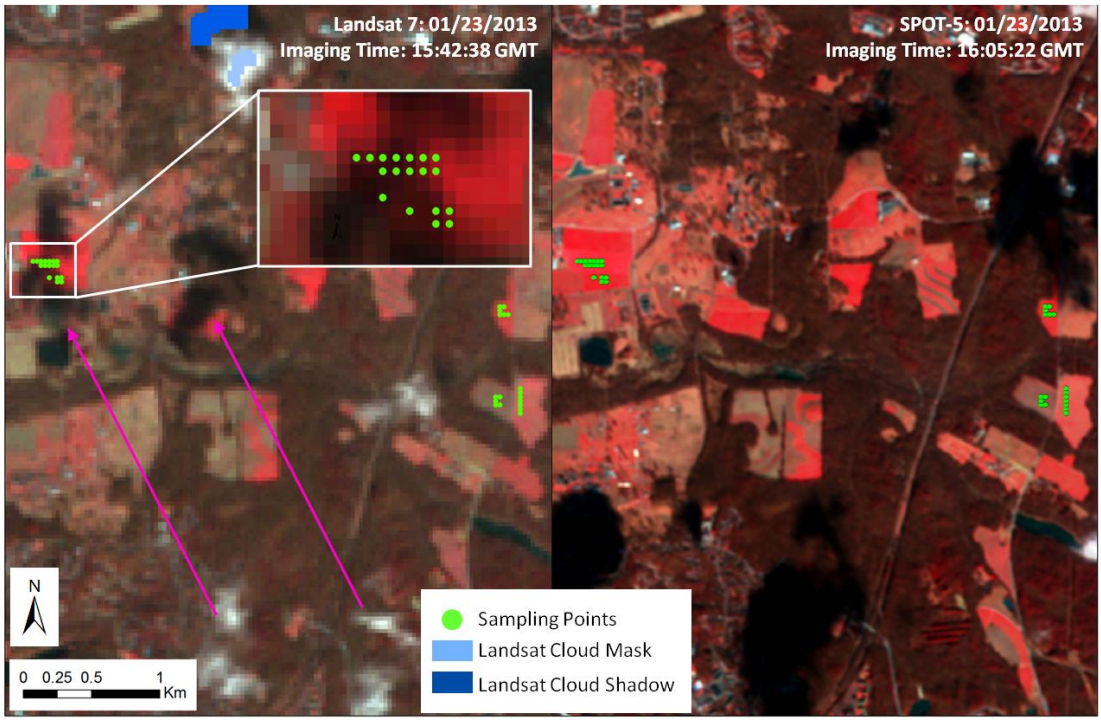


**Figure 16.** The study area is shown with January 23, 2013 Landsat 7 imagery on the left and SPOT-5 imagery of the same extent on the right. The Landsat 7 inset shows sampling points obscured by cloud shadow. The pink arrows point out the location of clouds and their associated shadows. These areas were not detected using the cloud shadow and clouds mask that was included with the Landsat Level-1 data product. The dark and light blue areas indicated in the legend are cloud and cloud shadows that were present in the Landsat mask products.

### 3.3.3 Climate conditions

The temperature during the sampling period was in line with climate normals for the area (Figure 17). There was no snow on the ground during either sampling date. In the 48 days between the sampling dates, mild freezing occurred, and a total of 70 GDD were accumulated.

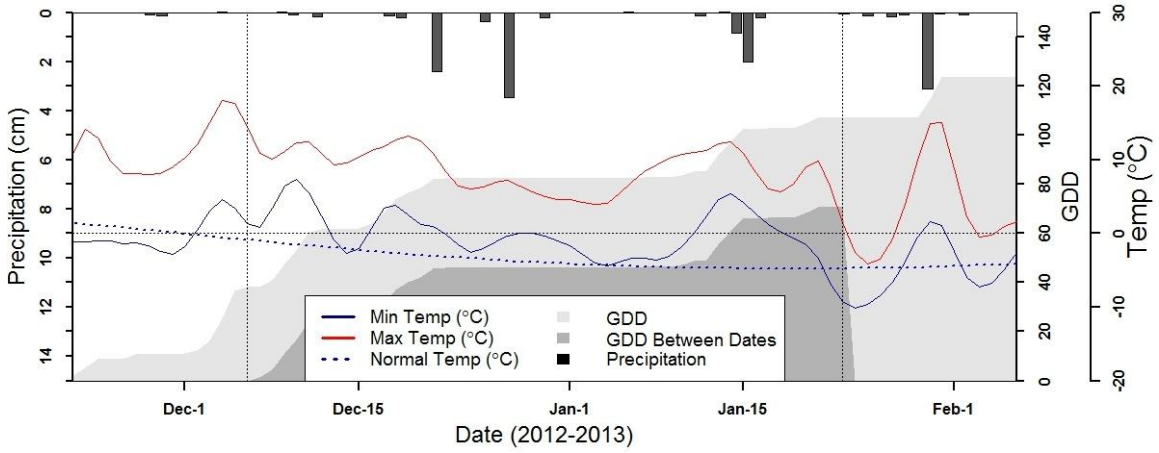


**Figure 17:** Climatic data for the study period shows that there were approximately 70 accumulated growing degree days (dark gray) between the two satellite acquisition dates (vertical dotted lines), implying minimal cover crop growth. The lighter gray is accumulated growing degree days over the study period. The minimum temperatures (solid dark blue line) were in line with climate normals (blue dotted line).

3.3.4 Winter cover crop growth

On December 6, cover crop percent vegetative groundcover varied between 8 and 99 percent, and on January 23, varied between 18 and 98 percent. Biomass on December 6 had a range of between 75 and 3700 kg/ha and on January 23 between 150 and 4200 kg/ha. This wide range of biomass and vegetative groundcover provided a suitable basis for evaluation of sensor performance.

3.3.5 Comparisons of Satellite and Proximal Sensors

Comparing satellite surface reflectance data to proximal sensor data

CROPSCAN was selected as the "gold standard" surface reflectance method due to its high spatial resolution, on-the-go measurements, and ability to correct its reflectance based on the amount of incoming solar radiation.

### 3.3.6 December 6, 2012

Goodness of fit measures (r-squared, RMSE) of the correlation between satellite and proximal sensors were high for all bands. When the green bands of Landsat and Worldview images from December 6, 2012 were regressed against CROPSCAN, the r-squared values were 0.85 and 0.89 respectively, for both TOA and SR imagery (Figure 18). However, the SR imagery resulted in correlations closer to a 1:1 relationship with CROPSCAN surface reflectance. The satellite measurements were highly correlated to each other, with goodness of fit values between Landsat and Worldview of 0.92 for both TOA and SR imagery (Figure 18).

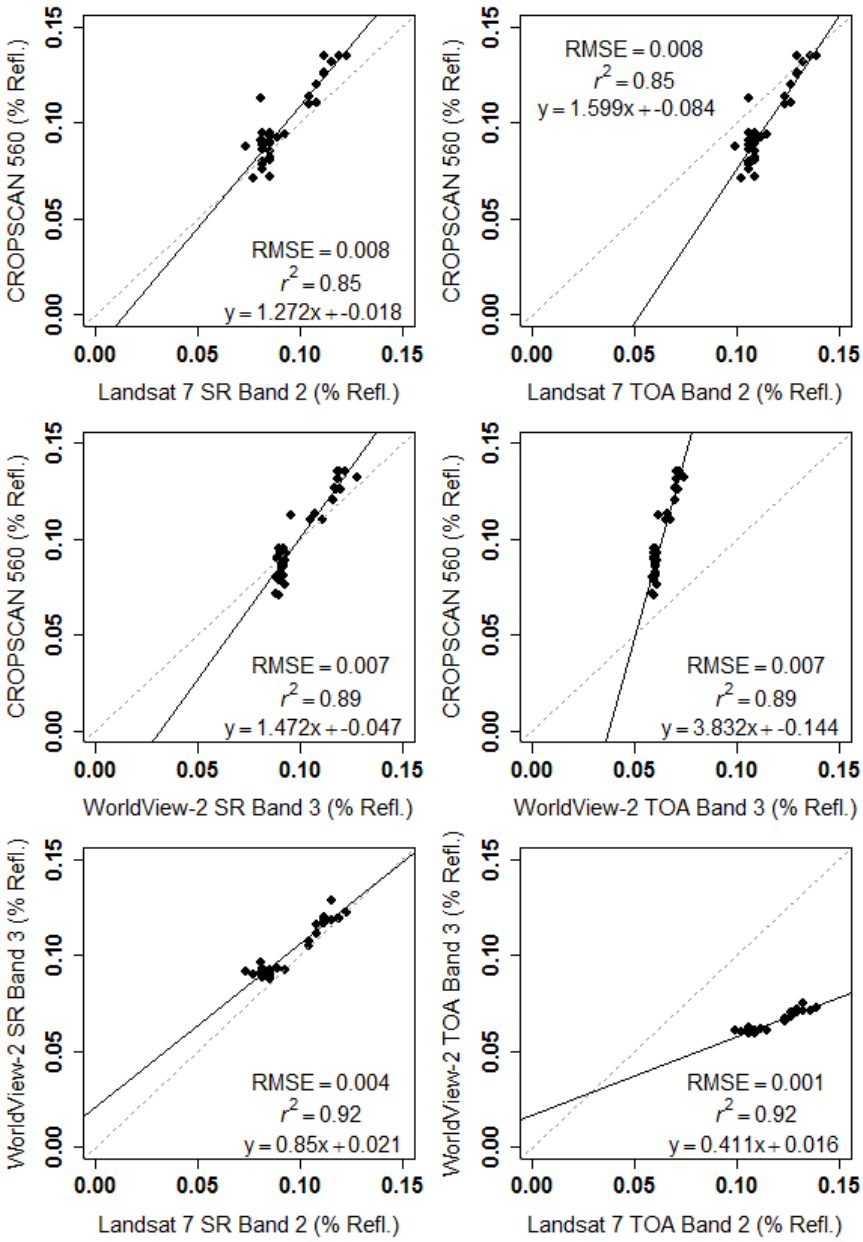


**Figure 18:** Linear regression of green bands of sensors on December 6, 2012. The dashed line represents a 1 to 1 relationship with an intercept of zero.

The same trend held true in the red region of the spectrum. Correlation between satellites and CROPSCAN proximal reflectance resulted in r-squared values of 0.85 (Landsat) and 0.89 (Worldview) for both TOA and SR imagery, with the SR imagery falling closer to a 1:1 relationship with CROPSCAN surface reflectance

(Figure 19). The satellite measurements were highly correlated to each other, with goodness of fit values between Landsat and Worldview of 0.92 for both TOA and SR imagery (Figure 19)

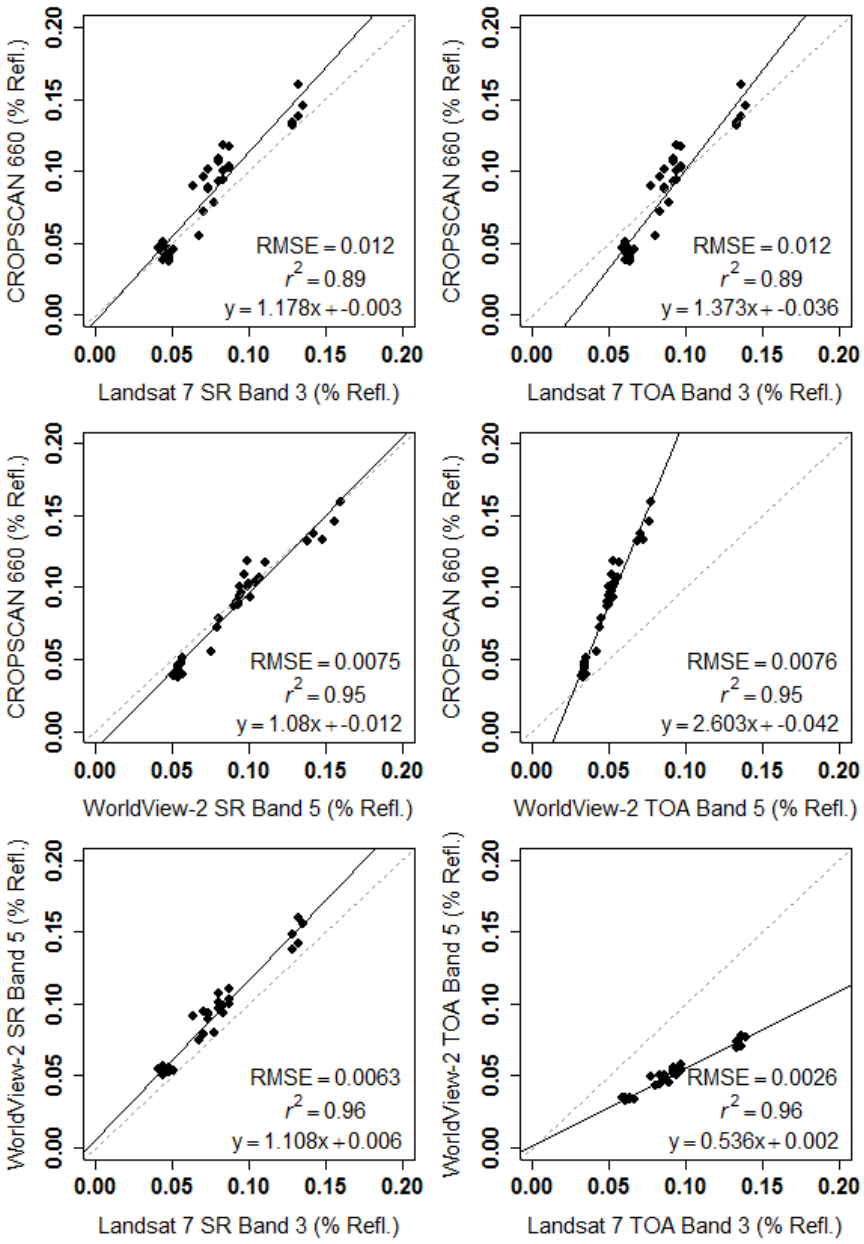


**Figure 19:** Linear regression of red bands of sensors on December 6, 2012. The dashed line represents a 1 to 1 relationship with an intercept of zero.

In the near infra-red wavelengths, correlation between satellites and CROPSCAN proximal reflectance was quite strong, with r-squared values of 0.94 (Landsat) and 0.95 (Worldview) for both TOA and SR imagery, with the SR imagery falling closer to a 1:1 relationship with CROPSCAN surface reflectance (Figure 20). The satellite measurements were highly correlated to each other, with goodness of fit values between Landsat and Worldview of 0.97 for both TOA and SR imagery (Figure 20).

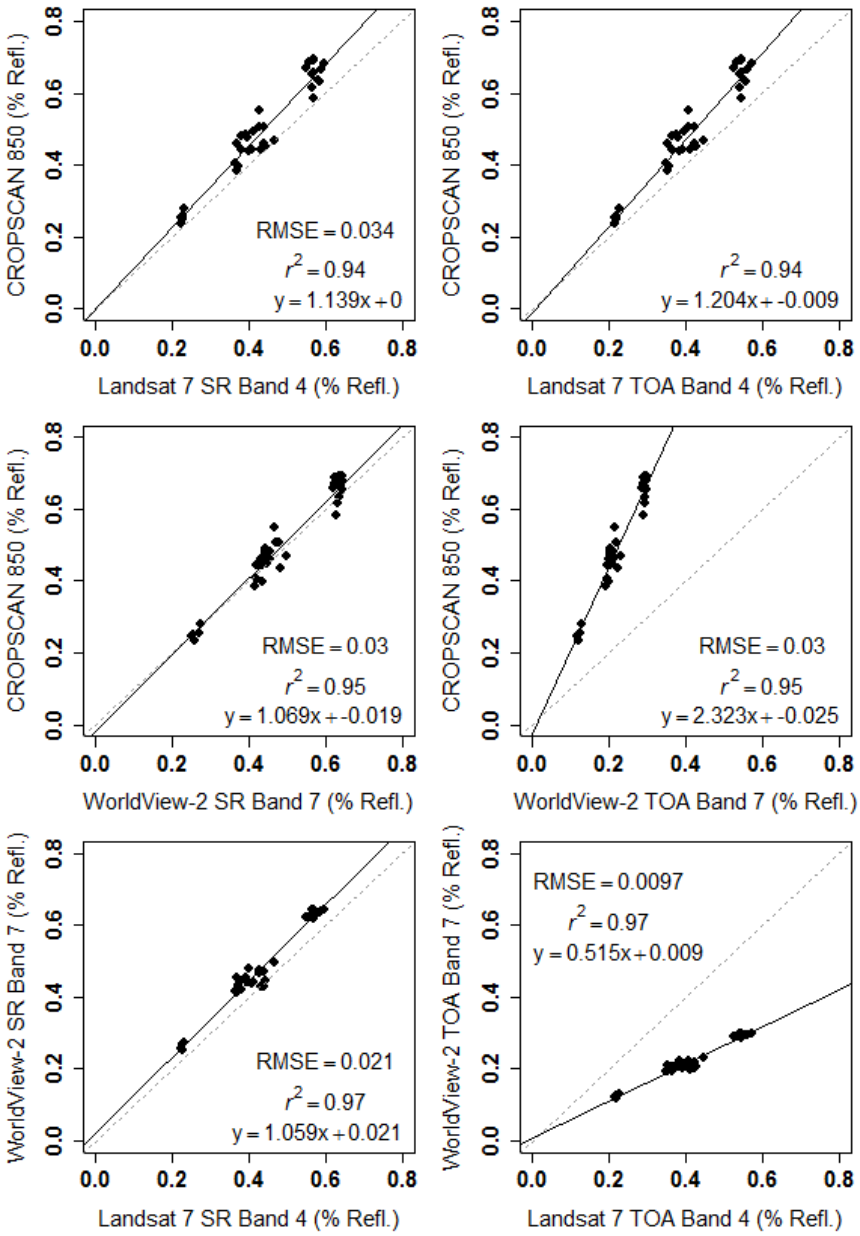


**Figure 20:** Linear regression of near-infrared bands of sensors on December 6, 2012. The dashed line represents a 1 to 1 relationship with an intercept of zero.

Overall, for the December 6, 2012 sampling, goodness of fit measurements for the correlation between satellite reflectance and CROPSCAN proximal surface reflectance were strong ($r^2$ 0.85 to 0.95), with slightly stronger correlation in the longer wavelengths, and Worldview showing slightly stronger correlation than Landsat. While conversion from TOA to SR did not improve the goodness of fit, it

did result in more accurate correlation, moving the y-intercepts closer to zero and slopes closer to one. Robust vegetation will have higher reflectance values in the near-infrared and higher absorption in the red region of the spectrum, yielding higher NDVI values. Satellite TOA and surface NDVI measurements were measured against one another and against proximal sensors.

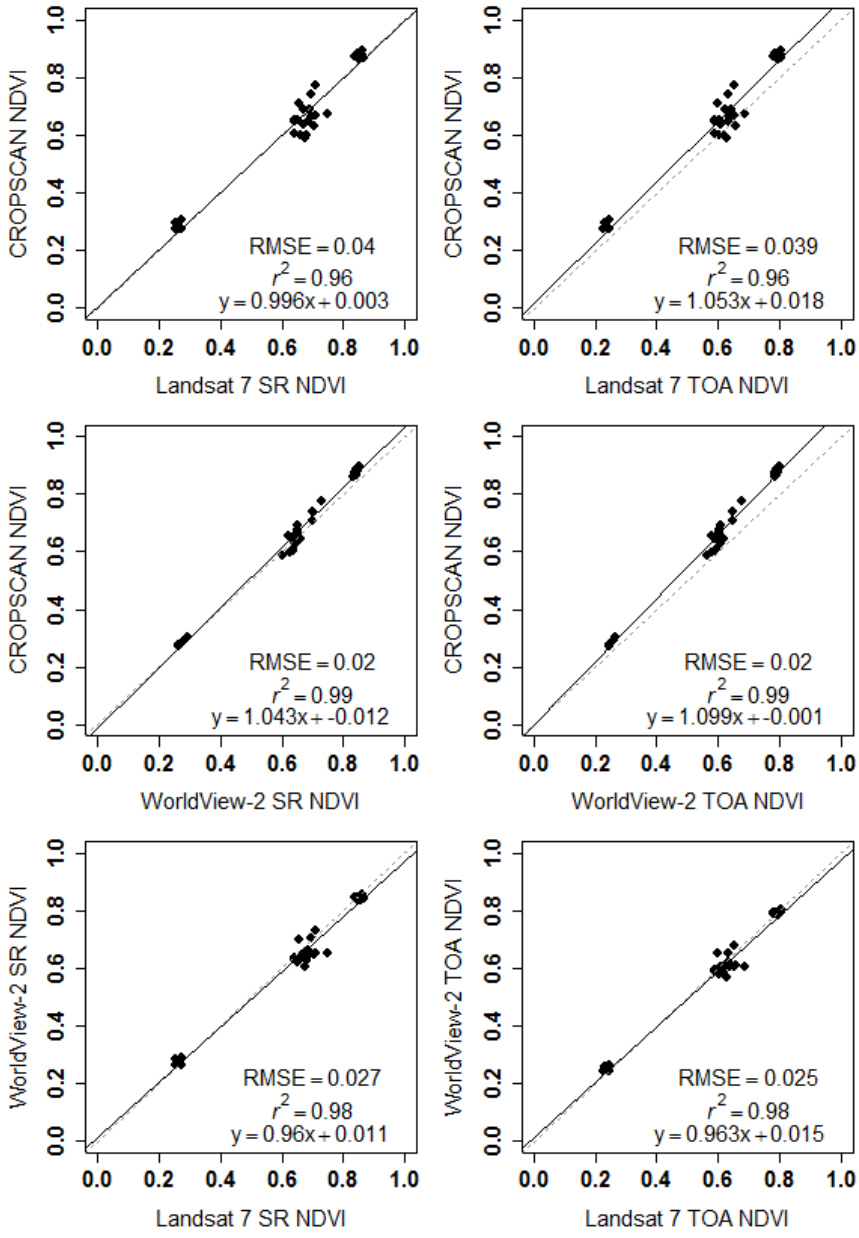


**Figure 21:** Linear regression of NDVI measurements among sensors on December 6, 2012. The dashed line represents a 1 to 1 relationship with an intercept of zero.

Landsat and WorldView NDVI had high r-squared values with CROPSCAN of 0.96 and 0.99 respectively (Figure 21). In both of these cases, although the relationship wasn't one-to-one, the slope of line deviates only slightly and y-intercept is close to zero. The relationship between NDVI calculations from satellites on this date was especially strong. Landsat and WorldView values were highly correlated with an r-square of 0.98. The slope of the regression line was extremely close to 1 with a value of 0.96 and the y-intercept was nearly zero, with a value of 0.011 (Figure 21). As with individual band correlations in the visible and near-infrared, r-squared values for NDVI were exactly the same between satellite top of atmosphere and surface reflectance.

3.3.7 January 23, 2013

The January 23 Landsat image contained cloud shadows covering 18 sampling points within the triticale and barley1 fields (Figure 16). Cloud shadows over the study sites were only present in the Landsat image due to differences in imaging times (the Landsat image was acquired at 15:52:38 GMT and the SPOT image at 16:05:22 GMT). The proximal reflectance measurements were collected without overhead cloud cover. Because the cloud shadows affected reflectance, Landsat correlations were calculated with the shadowed sampling points removed. Goodness of fit measures of the correlation between satellite and proximal sensors were also high for all bands on January 23. When the green bands of Landsat and SPOT images from January 23, 2013 were regressed against CROPSCAN, the r-squared values were 0.84 and 0.85 respectively, for both TOA and SR imagery (Figure 22). Surface reflectance satellite imagery resulted in correlations closer to a

1:1 relationship with CROPSCAN surface reflectance. The satellite measurements were highly correlated to each other, with goodness of fit values between Landsat and SPOT of 0.92 for both TOA and SR imagery (Figure 22).

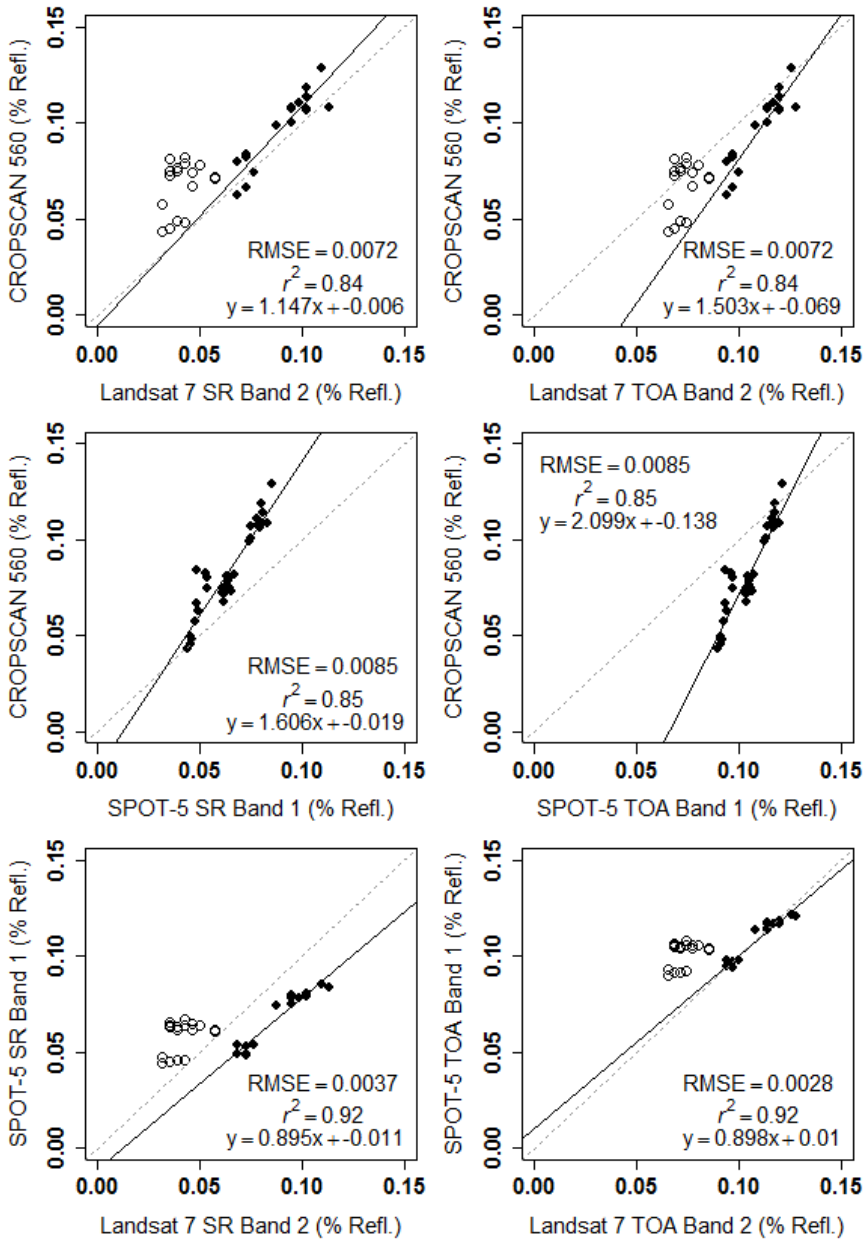


**Figure 22:** Linear regression of green bands of sensors on January 23, 2013. The dashed line represents a 1 to 1 relationship with an intercept of zero. The solid circles are data points that were free of clouds. The hollow circles represent areas that are covered by cloud shadow and were excluded from the linear regression analysis.

As was the case on December 6, the same trend held true in the red region of the spectrum on January 23. Correlation between satellites and CROPSCAN proximal reflectance resulted in r-squared values of 0.88 (Landsat) and 0.92 (SPOT) for both TOA and SR imagery, with the SR imagery falling closer to a 1:1 relationship with CROPSCAN surface reflectance (Figure 23). The satellite measurements were highly correlated to each other, with goodness of fit values between Landsat and Worldview of 0.96 for both TOA and SR imagery (Figure 23)

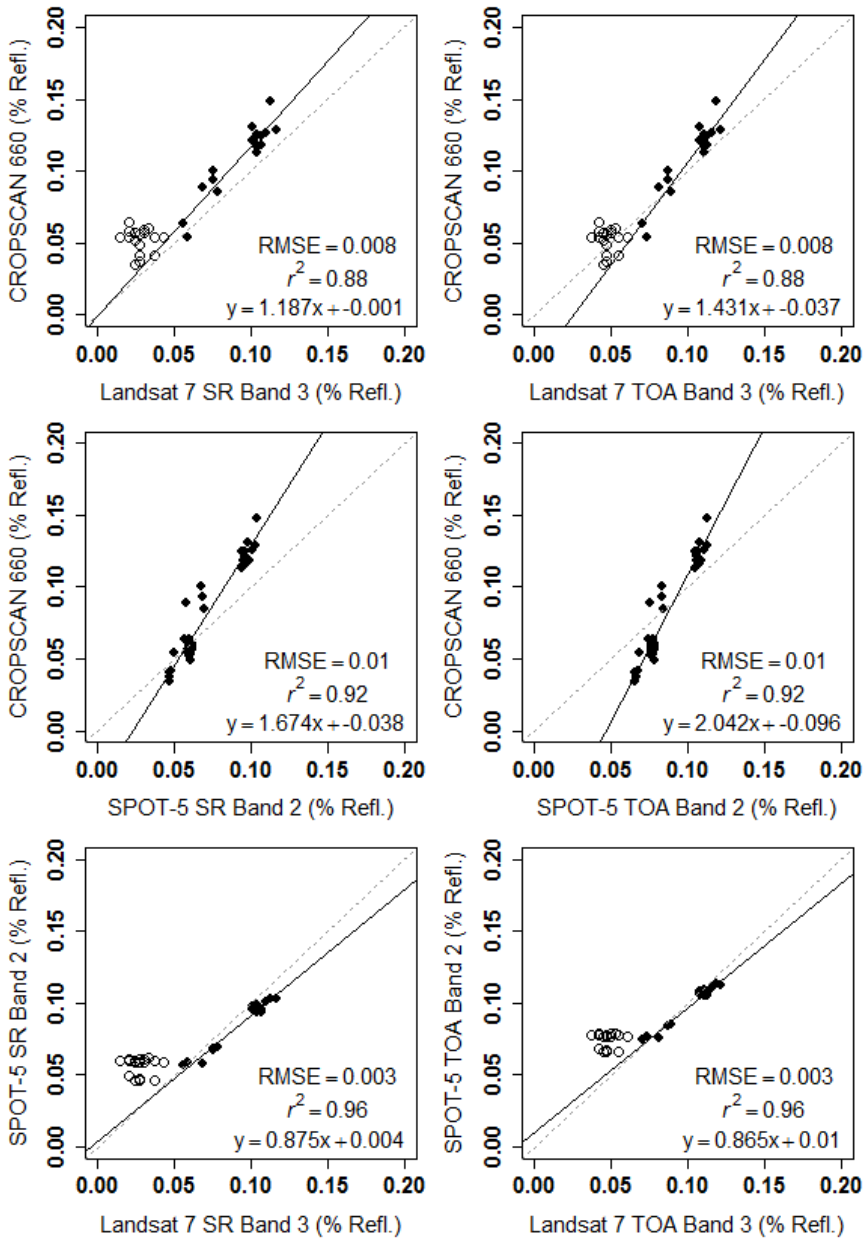


**Figure 23:** Linear regression of red bands of sensors on January 23, 2013. The dashed line represents a 1 to 1 relationship with an intercept of zero. The solid circles are data points that were free of clouds. The hollow circles represent areas that are covered by cloud shadow and were excluded from the linear regression analysis.

In the near infra-red wavelengths, correlation between satellites and CROPSCAN proximal reflectance were more variable, with r-squared values of 0.79 (Landsat) and 0.93 (SPOT) for both TOA and SR imagery, with the SR imagery

falling closer to a 1:1 relationship with CROPSCAN surface reflectance (Figure 24). Several points were eliminated in the Landsat analysis due to cloud shadows, reducing the overall number of sampling points available for comparison. The satellite measurements were highly correlated to each other, with goodness of fit values between Landsat and SPOT of 0.99 for both TOA and SR imagery (Figure 24).

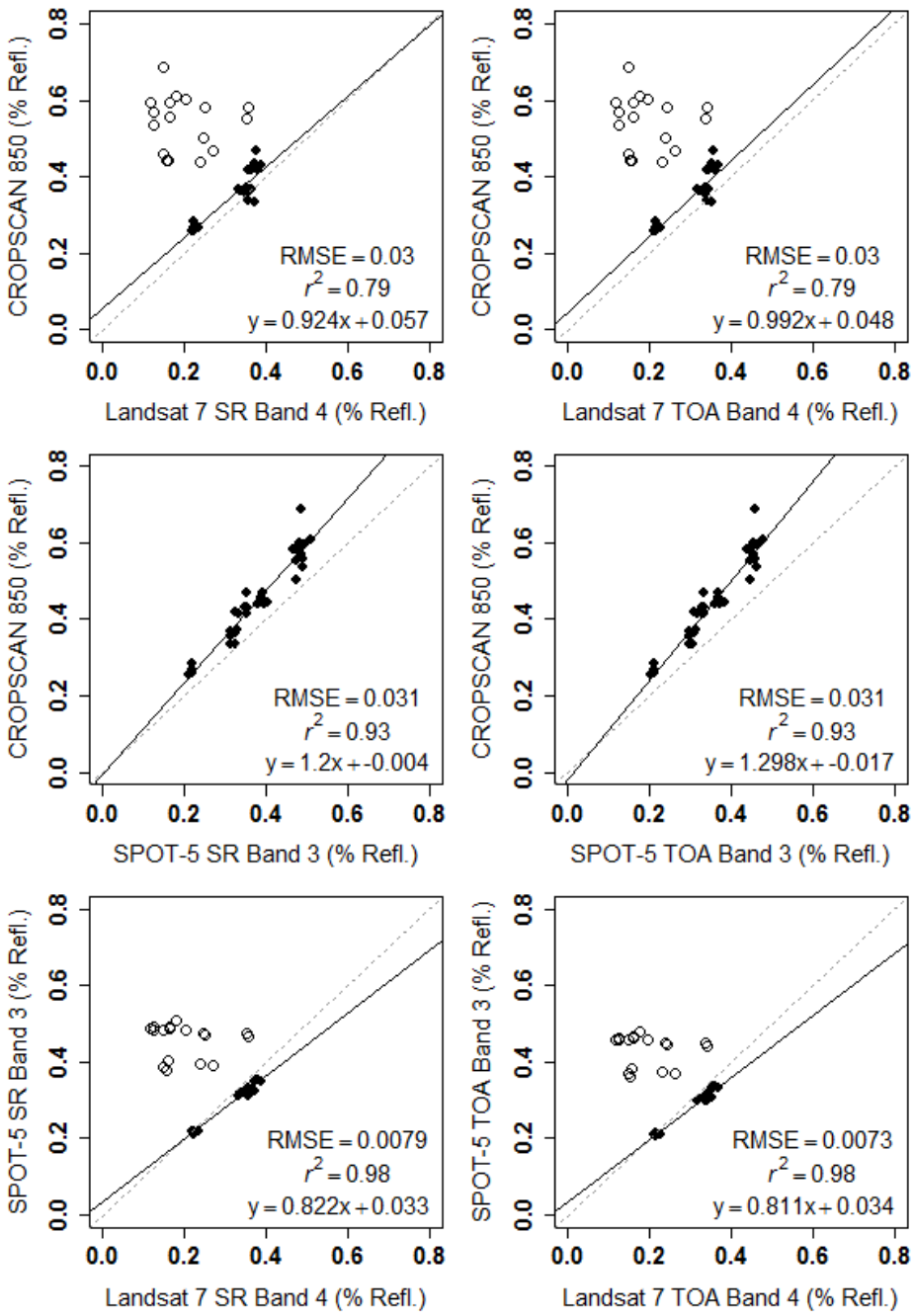


**Figure 24:** Linear regression of near-infrared bands of sensors on January 23, 2013. The dashed line represents a 1 to 1 relationship with an intercept of zero. The solid circles are data points that were free of clouds. The hollow circles represent areas that are covered by cloud shadow and were excluded from the linear regression analysis.

Conversion to surface reflectance reveals the same pattern between satellite and proximal sensors that was present on December 6. Although all slopes are different than the one-to-one line, conversion to surface reflectance moves the y-intercepts closer to zero and reduces the steepness of slopes slightly on this date.

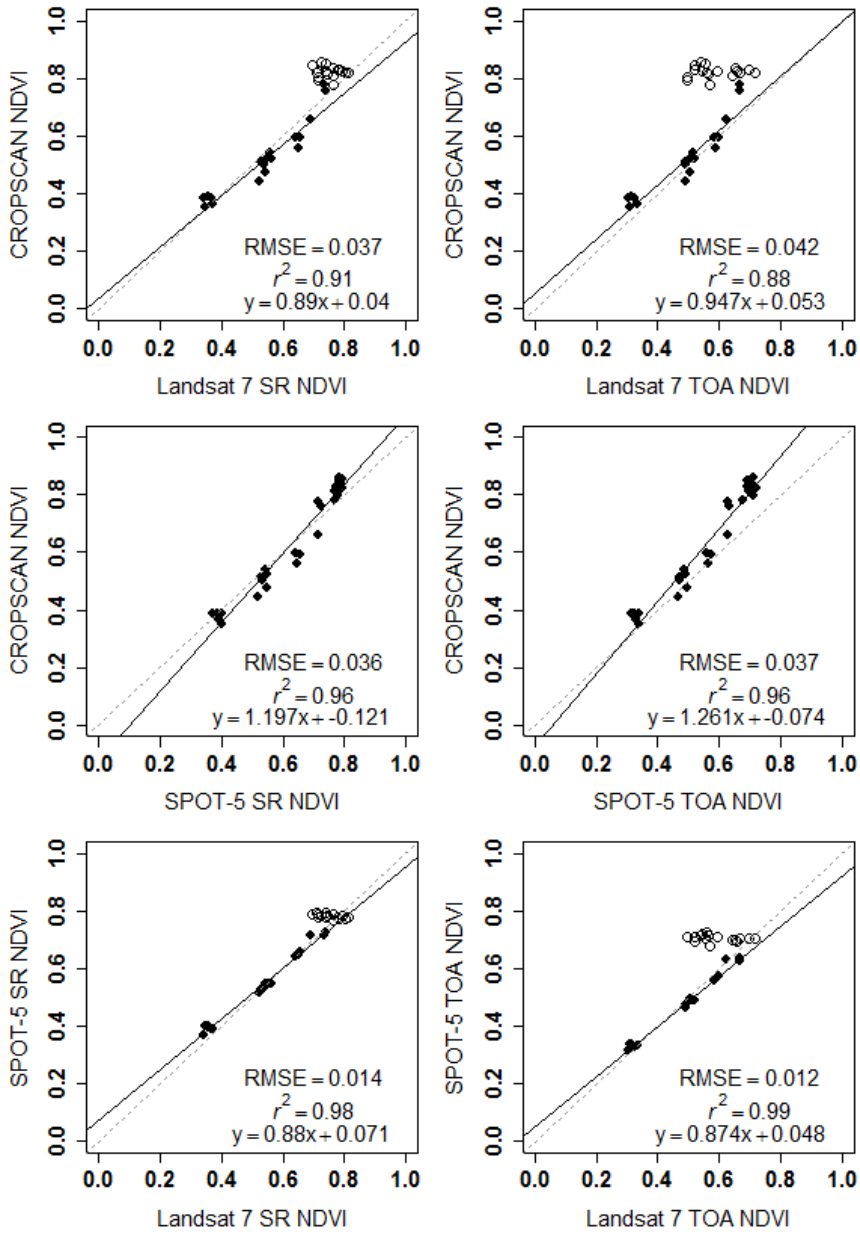


**Figure 25:** Linear regression of NDVI measurements among sensors on January 23, 2013. The dashed line represents a 1 to 1 relationship with an intercept of zero. The solid circles are data points that were free of clouds. The hollow circles represent areas that are covered by cloud shadow and were excluded from the linear regression analysis.

SPOT surface reflectance and top of atmosphere NDVI had high correlations with CROPSCAN of 0.96 (Figure 25). When Landsat is analyzed with no points under cloud pixels, regression results against CROPSCAN are similar, with Landsat

surface reflectance and top of atmosphere having r-squared results of 0.91 and 0.88 (Figure 25). Unlike SPOT, there wasn't a shift toward the one to one line with the conversion to Landsat surface reflectance. Correlation between satellites was also high, with r-squared values of 0.98 between Landsat and SPOT (Figure 25).
For January 23 NDVI values with points under cloud shadow removed, the r-squares values differed by only one percent. Keeping points under cloud shadow in the analysis resulted in more significant differences in goodness of fit values between NDVI values calculated from Landsat surface reflectance and top of atmosphere. NDVI values of Landsat surface reflectance regressed against CROPSCAN had an r-squared value of 0.89, compared with an r-squared value of 0.56 for top of atmosphere. The same pattern held true for between-satellite comparisons, as comparisons to SPOT surface reflectance were 0.95 for Landsat surface reflectance and only 0.64 for Landsat top of atmosphere.

These results indicate that the conversion to surface reflectance before transforming data to NDVI slightly increases correlation between sensors. However, NDVI may also be compensating for the effects of cloud shadows. In cloud shadows, reflectance drops due to little near-infrared radiation reaching the ground due to blocking and absorbing near-infrared radiation. Although scattering in the visible increases, very little red radiation is reflected from vegetation and a reduction in red reflectance also occurs.

When sampling points under cloud shadows were not eliminated from analysis, relationships between Landsat and CROPSCAN surface reflectance degraded considerably, with goodness of fit ($r^2$) falling from 0.84 to 0.74 (green),

0.88 to 0.52 (green) and 0.79 to 0.00 (NIR). Similarly, the correlation between Landsat and SPOT fell from 0.92 to 0.12 (green), 0.92 to 0.85 (red), and 0.98 to 0.26 (NIR).

The observed effects of cloud shadows can be explained due to differences in atmospheric scattering at various wavelengths. Clouds block and absorb nearly all near-infrared light. Therefore, there is a strong darkening of the signal within shadow areas because very little near-infrared light is getting through, and there is minimal scattering from the atmosphere and the ground. In the shorter green and red wavelengths, increased atmospheric scattering of photons, both from the haze in the atmosphere and diffuse radiation from the surface, can result in a fairly strong signal as scattered light fills in shadowed areas (Zhu and Woodcock, 2012), explaining the lesser degree of degradation of the green and red shadowed reflectance relative to the NIR shadowed reflectance. This is in accordance with research by Simpson and Sitt (1998) demonstrating that cloud shadows exert a greater influence on near-infrared bands than visible bands.

For the December 6 values and January 23 without cloud shadow points, slopes decreased and intercepts moved closer to zero after satellite imagery were converted to surface reflectance. However, when points under cloud shadow were left in the analysis for January 23, this effect also disappears. In fact, intercepts move further away from zero with the conversion to surface reflectance.

Cloud shadows are typically removed as "contaminated" pixels that are not useful for derivation of surface characteristics (Huang et al., 2010). These results show that when there is not contamination by cloud shadow, there is high correlation not only

among ground-based proximal sensors and moderate to fine spatial resolution satellite platforms, and also high correlation between such satellites. In practical terms, this indicates that a variety of satellites and proximal instruments give comparable results and can be used for measuring small fields and winter cover crops. However, the automated cloud and cloud shadow masks delivered with Landsat surface reflectance products did not detect many of the popcorn clouds and shadows they cast (Figure 16), indicating that caution should be used to visually identify cloud shadows prior to analysis of cover crop surface vegetation.

### 3.3.8 Comparison of NDVI measurements among sensors

Although there was generally good correlation of NDVI values between sensors and the predictive capability is high based on linear regression, the closeness of sensor measurements become important for some applications. For instance, categorizing cover crops by amount of biomass or percent vegetative groundcover is useful on a landscape scale, with "higher" biomass crops having more water quality benefits compared to "low" or "medium" biomass categories (Hively, 2009). Through the thresholds demarcating these groups may vary based on user specifications, they rely on consistent NDVI measurements between sensors.

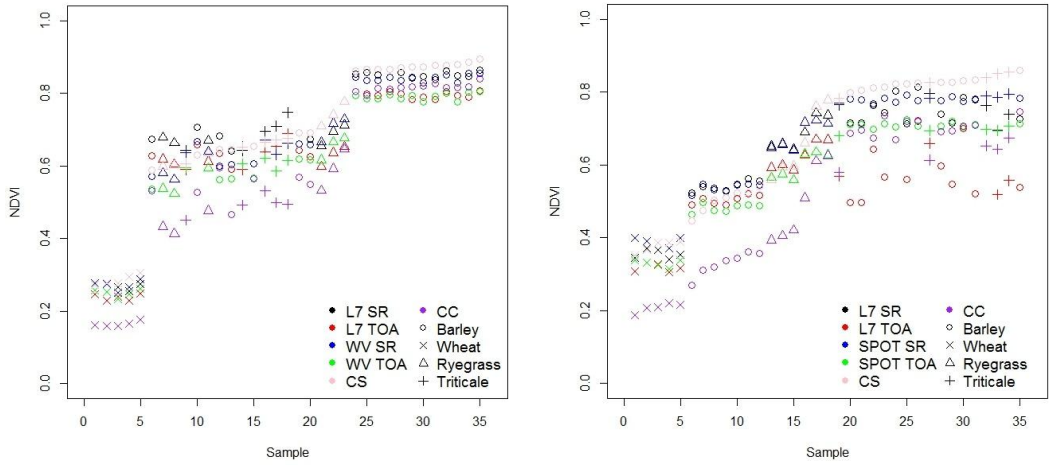


**Figure 26:** Shows NDVI measurements on December 6 (left) and January 23 (right) for each sensor and each sampling point.

NDVI measurements calculated from surface reflectance are higher than top of atmosphere due to increased reflectance in the NIR and smaller reflectance measurements in the red band (Trishchenko et al., 2002). Satellite surface reflectance measurements are more tightly clustered with CROPSCAN, and less tightly with Crop Circle and top of atmosphere NDVI. The low NDVI values returned from Crop Circle, similar to other examples, are likely due to lower signal returns compared with sunlight for the passive sensors. Crop Circle may be appropriate for isolated analysis but in this study did not have comparable surface reflectance measurements.

For each date, an analysis was run on these data to show within-sampling point variation in sensor measurements. NDVI values for top of atmosphere and surface reflectance were subtracted from the CROPSCAN measurements for each of the sampling locations. Boxplots were constructed (Figure 27) from the NDVI difference data to show the mean estimates of the differences between instrument measurements.

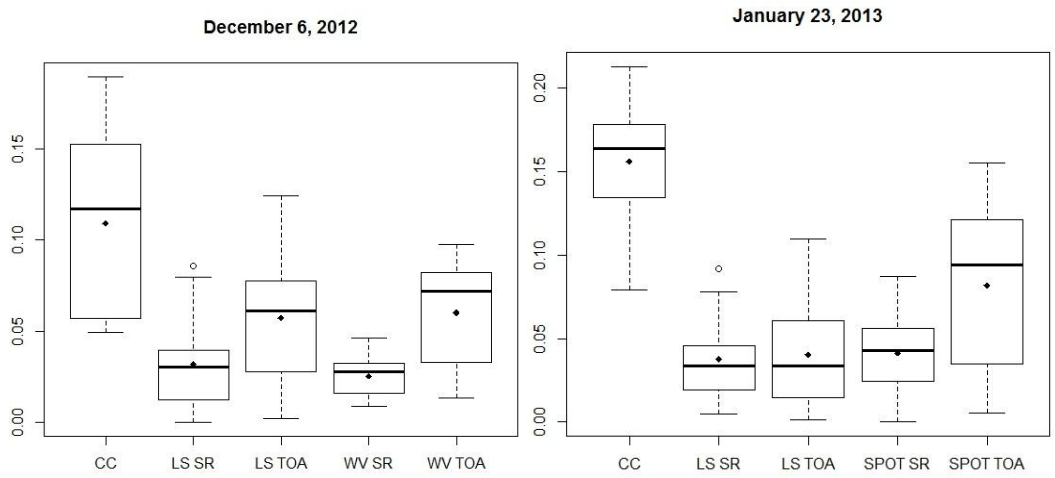


**Figure 27:** Boxplots showing the deviation from 0 (CROPSCAN), range of values, and standard error for each sensor on both dates. Mean values of the differences are represented by the black dot.

Each box represents the range of values of differences from CROPSCAN (Figure 27). On both dates, the mean values for the satellite surface reflectance products are closer to the CROPSCAN measurements and to each other. The boxplots shown for January 23 leave all NDVI values in the analysis. When Landsat NDVI values under cloud shadow are eliminated, the trend is the same for SPOT and Crop Circle, but the differences between mean values is significantly smaller between Landsat surface reflectance and Landsat top of atmosphere. This tighter clustering could be due to fewer sampling points compared with the SPOT. However, in both cases, the boxplots show that there less variance in the surface reflectance products across sampling points. Both the mean values and the variance indicate that satellite surface reflectance products more closely mirror CROPSCAN.

3.3.9 Surface Reflectance and Cover Crop Performance

When comparing percent green vegetative groundcover to NDVI, r-squared values for the surface reflectance and top of atmosphere variables are exactly the

same in most cases, despite the slope and intercepts of regression lines varying between the two. For the sampling points used in our study, the differences between surface reflectance and top of atmosphere pixel values were proportional in all cases. While pixel values between imagery corrected to surface reflectance and top of atmosphere were not proportional across the entire image, though they were less than 0.03%. For December 6, r-squared values ranged between 0.94 and 0.98 (Figure 28).

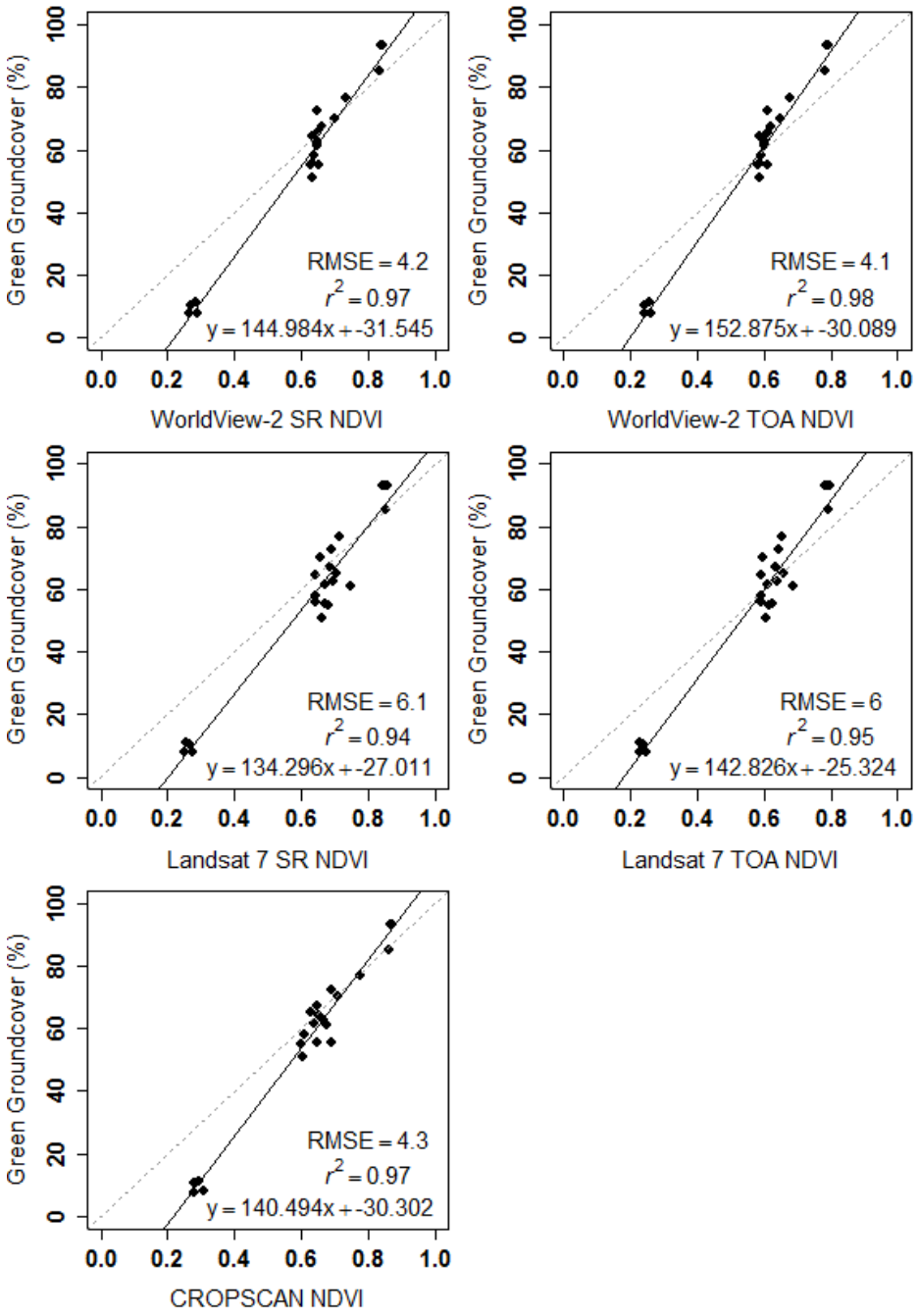


**Figure 28:** Linear regression of NDVI measurements for each sensor against percent green vegetative groundcover on December 6, 2012. The dashed line represents a 1 to 1 relationship with an intercept of zero.

For January 23 with cloud shadow points removed, r-squared values were between 0.86 and 0.95 (Figure 29), with the top-of-atmosphere values having slightly lower correlations compared with surface reflectance or proximal sensors.

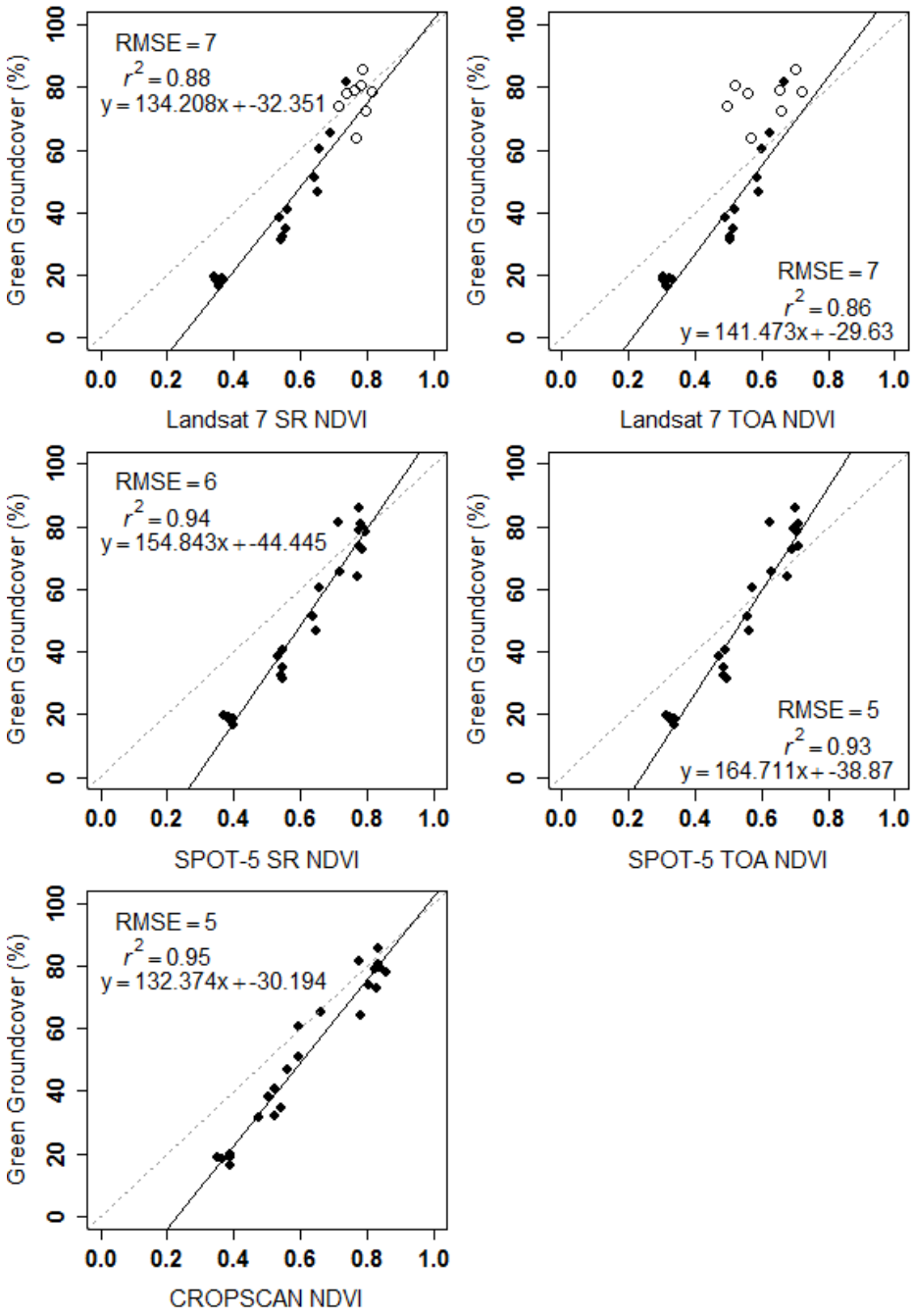


**Figure 29:** Linear regression of NDVI measurements for each sensor against percent green vegetative groundcover on January 23, 2013. The dashed line represents a 1 to 1 relationship with an intercept of zero. The solid circles are data points that were free of clouds. The hollow circles represent areas that are covered by cloud shadow and were excluded from the linear regression analysis.

For the two study dates, all sensors and processing levels were highly correlated with percent vegetative groundcover, NDVI derived from surface reflectance did not create a stronger relationship with cover crop performance variables. However, coefficients of correlation were lower when comparing NDVI to biomass with little to no difference between surface reflectance and top of atmosphere. On December 6, r-squared values ranged between 0.58 and 0.76. However, biomass values in general have a greater spread between the fields due to differences in planting dates and the amount of accumulated biomass at time of sampling. Biomass values are not bounded on the upper end like percent vegetative groundcover (Prabhakara, 2015). Low biomass values for wheat, which was planted late and exhibited little growth by December 6, may contribute to low r-squared values.

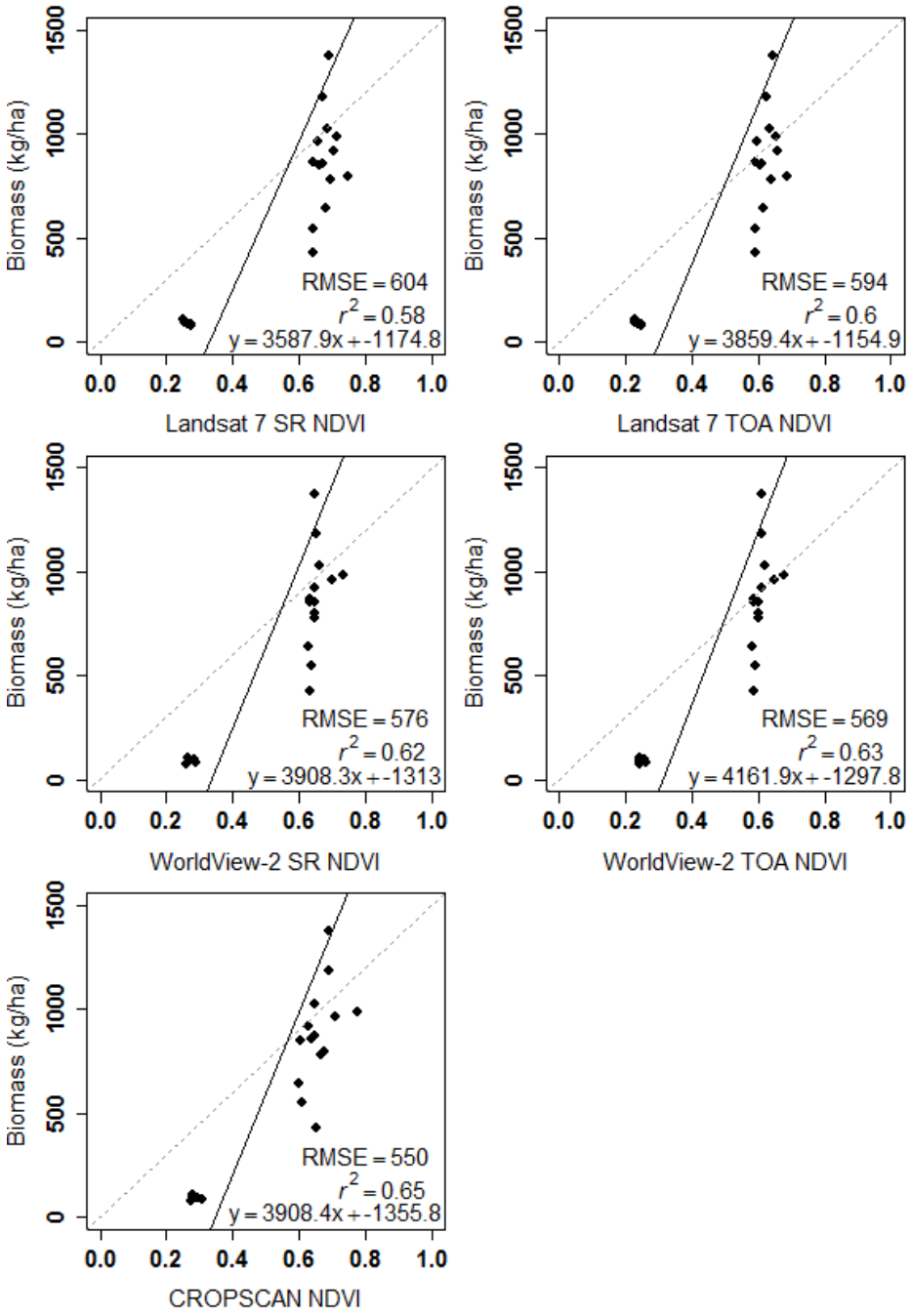


**Figure 30:** Linear regression of NDVI measurements for each sensor against measured biomass on December 6, 2012. The dashed line represents a 1 to 1 relationship with an intercept of zero.

January 23 had lower correlation than December 6, with r-squared values ranging between 0.41 and 0.66.

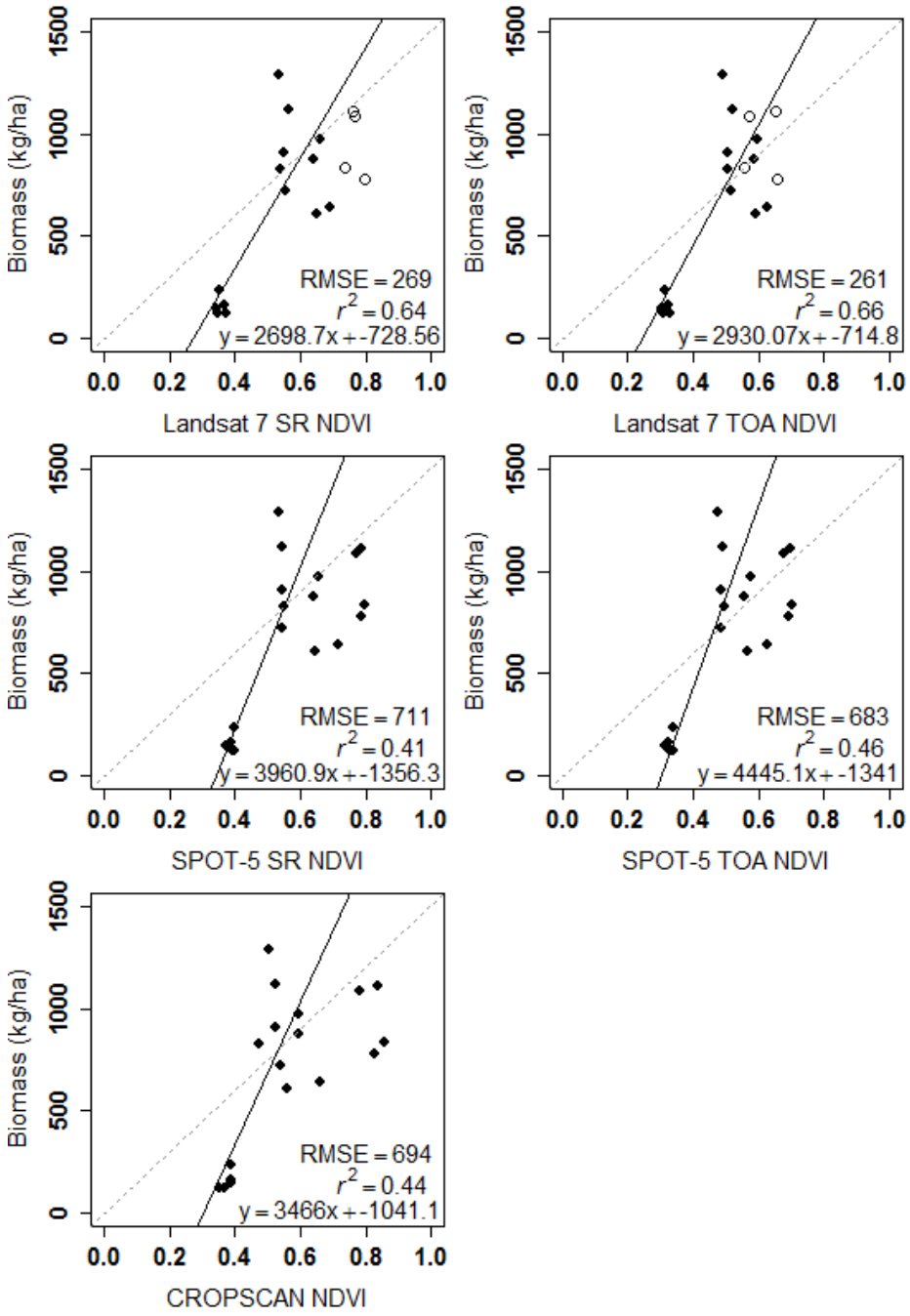


**Figure 31:** Linear regression of NDVI measurements for each sensor against measured biomass on January 23, 2013. The dashed line represents a 1 to 1 relationship with an intercept of zero. The solid circles are data points that were free of clouds. The hollow circles represent areas that are covered by cloud shadow and were excluded from the linear regression analysis.

Similarly to December 6, processing to surface reflectance did not increase predictive ability. Between December 6 and January 23, barley and ryegrass experienced yellowing that dropped NDVI values while still retaining high biomass (Prabhakara, 2015). This led to higher variance in r-squared and NDVI values, and lower correlations.

### *3.4 Conclusions*

The results of this study show that all sensors were highly correlated with each other for both visible and near-infrared bands. When satellite imagery was converted to surface reflectance and compared with proximal data, y-intercepts were closer to zero and slopes were closer to the one-to-one line than when top of atmosphere imagery was used. The exceptions were sampling points covered by cloud shadow as in the January 23 Landsat image. When these points were left in for analysis, near-infrared measurements showed a poor relationship between satellite and proximal sensors and between both satellite images. When the cloud shadow points were removed, correlation increased significantly.

NDVI between satellites and proximal sensors also displayed high correlation among sensors on both dates. For the January 23 Landsat imagery, conversion to surface reflectance followed by calculation of NDVI resulted in a better match between satellite and proximal sensors, eliminating the some of the effect from cloud shadow. This effect was clearly visible in this study, and merits further observation in the future.

Conversion of satellite data to surface reflectance resulted in reflectance values that were closer to proximal surface reflectance than were top of atmosphere

data. This is important for categorizing cover crops based on their NDVI values. There was high correlation between percent vegetative groundcover and NDVI values for all proximal sensor and satellite measurements. However, conversion to surface reflectance did not improve correlation to percent vegetative groundcover compared to TOA. NDVI was less useful for prediction of biomass on both sampling dates. Data were gathered for this study under relatively clear sky conditions to ensure that adequate irradiance reached the sensors. In order to acquire clear satellite imagery and be able to capture ground conditions with proximal sensors, mostly clear conditions are necessary. Surface reflectance data from satellites might be more important under hazy conditions where there is increased atmospheric interference and calibration to ground-based sensors is more challenging. The results of this study would likely change in extremely cloudy or hazy conditions. However, this research shows that surface reflectance products calculated from satellite sensors and on-the-go proximal sensors are highly correlated with each other during measurement of winter cover crops.

# Chapter 4: Modeling the influence of winter factors on cover crops using SAIL

## *4.1 Introduction*

The performance of winter cover crops implemented within the Chesapeake Bay for the purpose of water quality protection has been shown to be variable, with many fields exhibiting relatively low biomass over the wintertime. Factors affecting winter cover crop performance include planting date, planting method, residual nitrate, cropping system, landscape position, and climate. Remote sensing provides useful tools for measuring and mapping cover crop performance, biomass, nutrient accumulation, and fractional vegetative groundcover (Hively et al., 2009; Prabhakara et al., 2015). Previous research has shown that early planted cover crops (prior to October 1) were able to accumulate more biomass and sequester more nutrients compared with those that were planted later (after October 15) (Hively et al., 2009). Although there is evidence that crops with higher biomass and percent groundcover are more ecologically efficient and provide greater environmental benefits, a variety of practical agricultural management factors result in some cover crops being planted later, with less available growing days before the onset of cold temperatures. Late-planted cover crops generally do not have adequate growing weather available before the onset of cold temperatures to accumulate significant biomass, typically have fewer leaves, reduced biomass, and a lower LAI compared with those that were planted earlier.

Agricultural groundcover, as might be represented by a nadir photograph of the field surface, is typically composed of three physical components (green vegetation, crop residue, and bare soil), each with distinct spectral reflectance characteristics, along with a fourth spectral component: shadows. Crop residues are an important contributor to background reflectance and are often left on cover crop fields for conservation tillage (Daughtry et al., 2005). Relative to vegetation, the combination of soil and residue forms the background component of average field reflectance. Background reflectance is particularly important for remote sensing of winter cover crops, because there is a diverse mix of soil and residue throughout the agricultural landscape, and under wintertime conditions limited cover crop growth often results in low fractional vegetative groundcover and LAI has not reached high enough levels to mask background effects. Under wintertime conditions vegetative growth provides fractional groundcover that is responsive to indices such as NDVI, and the remainder of the field reflectance signal is provided by partial groundcover contributions of soil and crop residue, which can vary between bare soil (plow till) to complete residue cover (long-term no-till management), with many intermediate stages of residue cover depending on management (disking, turbo till, chisel plow, etcetera).

When there is less ground area covered by leaves, background reflectance, especially by soils, is increased. Soils vary in reflectance across wavelengths based on a variety of factors including color, texture, amount of organic matter and composition. Soils of all types increase in reflectivity as a function of wavelength over the range of the electromagnetic spectrum, with low reflectance due to

absorption bands in portions of the mid-infrared. Large amounts of organic matter can greatly impact the reflectivity of soils, as can moisture levels and color.

Additionally, finer particle sizes, such as clays, will tend to have higher reflectivity, though they also are capable of holding more moisture, which could reduce their reflectivity (Jacquemoud et al., 1992). Crop residues are left on fields post-tillage to prevent soil erosion and protect soil quality, but create a unique problem from a remote sensing perspective. Although crop residues and soils are measurably different than green vegetation, they may vary from each other only in terms of amplitude of reflectance, while following generally the same reflectance curve over all wavelengths (Daughtry et al.,1996). Therefore, understanding the in situ characteristics of the soil is vital in low LAI and agricultural areas as there is, again, diffuse flux from the soil surface (Suits, 1972). Varying LAI and soil reflectance interfere with the ability of vegetation indices, such as NDVI, to properly quantify the amount of green vegetation on the ground. In fact, studies have shown that LAI is not linearly related to NDVI (Goward & Huemmrich, 1992). Although NDVI does saturate at high LAI, it also may be inaccurate at low LAI if background reflectance factors are not accounted for.

The SAIL (Scattering by Arbitrarily Inclined Leaves) model was developed to characterize three radiative fluxes through a plant canopy: downward flux of direct solar radiation, upward flux of diffuse radiation from the surface, and a downward flux of diffuse radiation (Goward & Huemmrich, 1992). The SAIL model assumes that the crop canopy consists of multiple uniform layers, which is fairly accurate for winter cover crops as they have very few components. Although in a cover crop

vegetation canopy, fields have generally homogenous cover and management across individual fields is the same, there is spatial variability in cover crop performance due to topographic differences (Muñoz & Kravchenko, 2012). Factors such as soil moisture, and the effects of management practices (tire tracks, combine width) can also contribute to variability. SAIL, similar to moderate-resolution satellite imagery, will simulate an average affect and this type of variability will not be a consideration. Additionally, winter cover crops consist of very few components compared with forest or more complex canopies.

The goals of this research are look specifically at the interplay of fractional cover by vegetation, soil, shadow, and residue, at varying soil moisture content, utilizing a specific field calibration data set collected during the winter of 2012-13. These goals have important real-world implications to the remote sensing of cover crops, especially at low LAI.

#### 4.1.1 Research Questions

Do differences in soil moisture affect field reflectance measurements at the low LAIs often seen in winter cover crops? Does reflectance of residues at different moisture levels change proportionately to reflectance of soils and vegetation at various moisture levels? How do low sun angles in the winter, as represented by increasing shadow, affect cover crop reflectance measurements?

## *4.2 Materials and Methods*

This study utilized cover crop vegetation samples collected from five fields in April of the 2012-2013 winter cover crop season (Prabhakara et al., 2015). The crops

planted on the fields were triticale, barley, wheat, and ryegrass. Data sets were developed to parameterize the SAIL model to simulate field reflectance. Several basic input parameters were held constant, while other parameters were varied based on measurement of plant and soil characteristics specific to the cover cropped environment (Table 10).

**Table 10:** Description of varied and constant parameters to the SAIL model. The manner in which varied parameters were measured is also listed.

| Varied Parameters | | Constant Parameters | |
|---|---|---|---|
| Soil Moisture | Measured RWC | Leaf Angle Dist. | Spherical |
| Soil Reflectance | ASD Spectra | Latitude | 39.03 (GPS Samples) |
| Residue Moisture | Measured RWC | Solar Declination | -23.4? |
| Residue Reflectance | ASD Spectra | Time of Day | 12:00 p.m. |
| Leaf Reflectance | ASD Spectra | Fraction Direct Solar | Default |
| Leaf Transmittance | ASD Spectra | View Azimuth Angle | Default |
| LAI | Li-Cor Area Meter | View Zentih Angle | Default |

Parameters held constant included fraction of direct solar radiation, view azimuth angle, and view zenith angle. Additional site- and date-specific variables were calculated: solar declination in degrees, time of day, latitude of sampling sites, and leaf area distribution. The input parameters developed from field and laboratory measurements included surface reflectance of soils under varying water content, and species specific measurements of leaf reflectance, leaf transmittance, leaf area index, and canopy composition, as well as residue reflectance spectra at varying moisture content provided by Quemada & Daughtry, (2016).

### 4.2.1 Soil Gravimetric Water Content

Soil samples were collected at 25 locations on January 10, 2013. Three 12-inch (30-cm) soil cores were combined from each sampling location, air dried for 48 hours, and ground to pass a 2-mm screen. The soil samples were then loaded into 4-cm

diameter rings of 1cm depth, with the bottom covered by a fine stainless steel mesh screen in preparation for measurement of gravimetric water content and spectral reflectance. Soil holders were weighed empty, filled to the top and leveled with soils from each sampling location, and reweighed. Subtracting the weight of the soil and the holder minus the holder alone resulted in soil weight. The soils were dried overnight at 60 degrees Celsius and weighed. This measurement was the dry weight of each sample. The samples were then brought to saturation by putting the samples in a tray, filling it with water, and waiting until the top of each sample was wet. Samples were weighed and this measurement was wet weight at 100% saturation.

Samples were then systematically dried by fanning for half an hour, rotating the trays, and fanning for another half an hour. After fanning, the tray of samples was covered with a plastic bag to minimize water loss into the atmosphere and left overnight, allowing water to re-equilibrate within the samples. The next day the samples were weighed to measure moisture content, and were then measured for reflectance. This procedure was repeated 7 to 8 times over two weeks resulting in reflectance measurements throughout the soil drying curve.

### 4.2.2 Soil Reflectance

To be able to vary soil reflectance values in SAIL using realistic estimates, it was essential to collect a variety of soil spectra across different fields and moisture levels. Soil reflectance measurements were made on soils from each sampling point and at varying degrees of moisture using an Analytic Spectral Devices (FieldSpec Pro, Boulder, CO, USA) spectroradiometer with a spectral resolution between 350-2500 nm. The height of the sensor was approximately 25-cm, and an 8-degree foreoptic

was used, resulting in a circular field of view with a diameter of 11.5-cm. Soil holders were placed in middle in the field of view and illuminated by six 100-W lamps that were placed 50 cm over the sample at a 45°zenith angle (Figure 32).

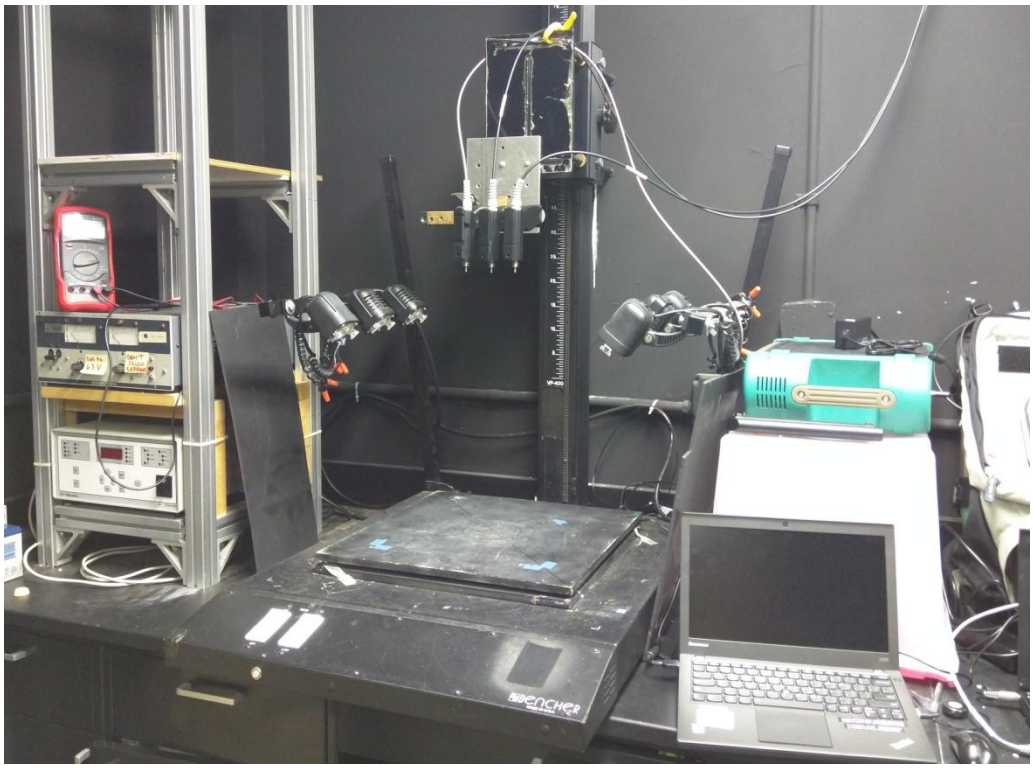

**Figure 32.** Set up used to measure soil reflectance in laboratory conditions, including six lamps for illumination, and sensors linked to ASD instruments through fiber-optic cables.

Calibration to reflectance was achieved using a Spectralon panel immediately prior to measurement of each batch of samples. Four readings were taken per sample, rotating 90 degrees between readings to account for variations in soil roughness relative to illumination angle. Each reading was the average of 50 measurements by the ASD instrument. If cracks were present in the surface of the soil, attempts were made to fill them in to reduce sensor readings of dark areas.

### 4.2.3 Residue Reflectance

Reflectance data for maize residue were provided by colleagues, who had collected the dataset using the identical ASD instrument used to scan our soil samples. The maize residue was approximately seven months old at measurement, and samples were processed as outlined in Quemada and Daughtry (2016) using the identical ASD instrument (Figure 32).

### 4.2.4 Leaf Reflectance and Transmittance

Leaf reflectance and transmittance were both measured using an LI-COR 1800-12 Integrating Sphere (LI-COR, Inc., 1998) and an ASD spectroradiometer with a spectral resolution of 350-2500 nm. Samples are limited to the early and late spring, after March 2013, because cover crop leaves were not large enough to cover the light source of the integrating sphere prior to that date and therefore could not be accurately measured. The samples were analyzed using an illuminating light source of 10 watts. This instrument measured all of the radiation reflected from or transmitted through a leaf surface. Measurements included, for each sample, stray radiation, white reference, and reflectance and transmittance for both the adaxial and abaxial leaf surfaces

### 4.2.5 Leaf Area Index

Plant samples were measured LAI using the Li-Cor LI-3100C Area Meter (Li-Cor Environmental). Representative plants from each biomass sample were measured from early fall to late spring of 2012-2013. Leaves were separated from stems for each individual sample until the total weight of the leaves was 10-g. For samples where was little aboveground biomass, total weight of the leaves was limited to 5-g.

The stems were weighed separately, and both stem weight and leaf weight were recorded. Separated leaves were run through the LI-3100C Area Meter, which measures the area of leaves to a 0.1 $mm^2$ resolution, and the values were recorded. Stems and leaves were dried in an oven at 60 degrees C overnight, along with the whole sample, and reweighed to calculate their dry weight. LAI calculations were made using the following formula:

LAI = (LA/DWL) * (DWL/(DWL + DWS)) * ((DWbulk + DWS + DWL)/SA)

where LA is the area measured by the LI-3100C Area Meter, DWL is the dry weight of leaves, DWS is the dry weight of stems, DWbulk is the total dry weight of the sample, and SA is the total sample area. The resulting value is the leaf area index of the sample.

4.2.6 Additional Input Parameters

Several input parameters needed for the model were held constant. The fraction direct solar radiation parameters were kept as a constant at 1, which indicates no diffuse light from the sun and minimal atmospheric attenuation as minimal hazy and cloud cover is ideal for cover crop sampling. The SAIL model calculates solar zenith angle as a function of latitude, time of day, and solar declination angle. Latitude of all sampling points was averaged and will be held constant at 39.03 as locations ranged only 0.01 degrees in latitude. For the purposes of this study, time of day will be held constant at noon, which is fairly close to 10:30 satellite overpass times and similar to times of reflectance data collected over the winter in Prabhakara et al., 2015. The solar declination angle was set to -23.4 degrees, equivalent to a December 23$^{rd}$ timeframe representative of mid-winter conditions, View zenith angle

was set at nadir, representative of proximal reflectance data collection described in Prabhakara et al., 2105. In future analysis, it could be varied up to 20° off nadir, to account for satellite view angle, but that was not within the scope of this study. Sample leaf area distributions are supplied by the SAIL program and inputs include spherical, uniform, planophile, erectophile, and plagiophile. The leaf angle used in this study was spherical.

### 4.2.7 Canopy Composition at Field Sampling Locations

Shoulder-height photos (2 m) on each field and run through SamplePoint software (Booth, Cox & Berryman, 2006; Prabhakara, 2015). This program allows the user to select which groundcover underlies the crosshairs of 200 points that are randomly placed on the image. SamplePoint results are equivalent to highly accurate in-field methods for measuring groundcover (Booth, Cox & Berryman, 2006). The categories chosen for this experiment included dark frost, bright frost, frost, dark vegetation, bright vegetation, vegetation, dark residue, bright residue, residue, dark bare, bright bare, and bare. These categories were then combined into more basic categories: frost, vegetation, residue, and bare. The percent of shadow were estimated by summing groundcover percentages for dark frost, dark vegetation, dark residue, and dark bare. These data were used to estimate fractional cover of vegetation, soils, and residue under winter cover crop conditions, for comparison to SAIL model output.

*4.3 Results*

Individual leaf reflectance and transmittance measurements by the ASD were processed using ViewSpec Pro software and output to a single comma separated file (ASD Inc., 2008). Choosing appropriate spectrum for input into the SAIL model was a subtractive process. Leaf reflectance and transmittance readings were taken on multiple samples for each species. Samples were not measured prior to early spring as they were not wide enough to cover the lamp in the integrating sphere. Because cover crops do not grow to maturity, and leaves were small and thin throughout the winter cover crop season. When the leaf reflectance and transmittance spectra were input into SAIL and run for LAI ranging from 0.01 to 7.0 with a dry soil background, results showed little variability among species below an LAI of 2.0 which corresponded to an NDVI of 0.8 (Figure 33). Based on the results, the spectra for all species of leaves were averaged into one for input to SAIL.

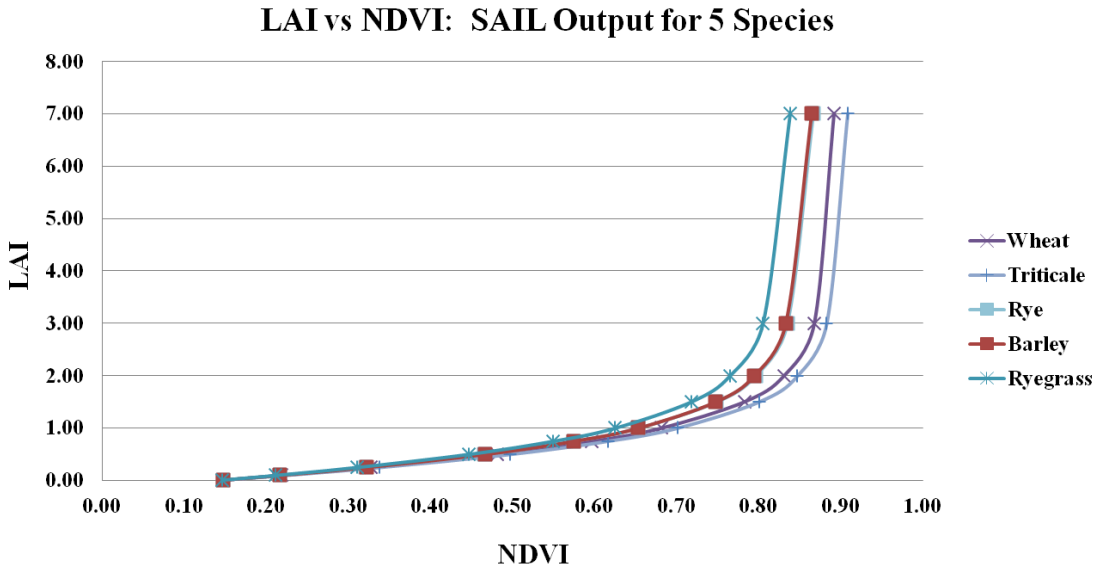


**Figure 33:** Reflectance and transmittance spectra for green leaves from 5 species of cover crop run through SAIL using a dry soil background.

Soil reflectance spectra for each sampling point were selected at air dry levels (0.1-0.2 RWC), a mid-point (0.35-0.45 RWC), and field capacity (FC) (0.7-0.85 RWC). When plotted within field, the spectra for Wheat, Barley2 and Ryegrass exhibited similar curves and values (Figure 34). The same was true for Triticale and Barley1. The differences in reflectance spectra between these fields can likely be explained by geographic proximity. Results showed similarity in three fields (Wheat, Ryegrass, and Barley2) located near each other on the East side of the research station, and similarity in two fields (Triticale and Barley1) located on the west side of the research station (Figure 34).

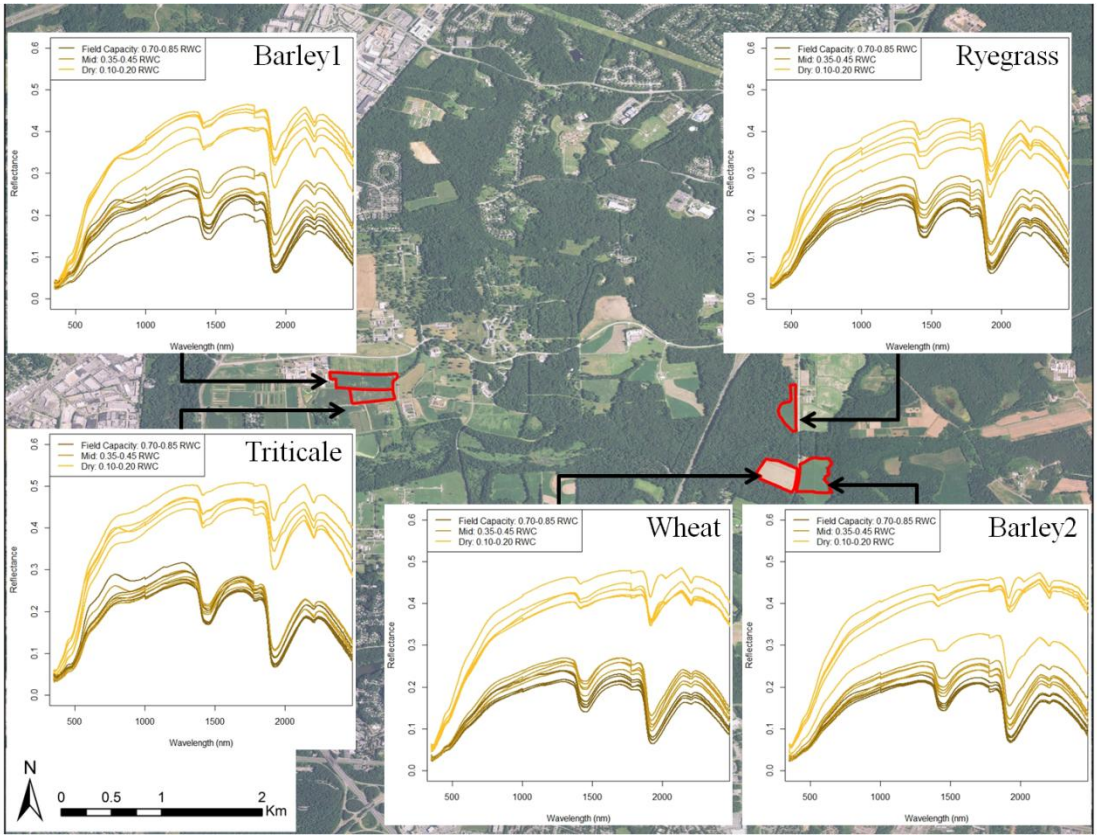


**Figure 34:** Reflectance curves for soils within each field. The fields to the west are barley1 and triticale and the fields to the east are barley2, ryegrass, and wheat.

For purposes of SAIL modeling, we calculated average spectra for the three eastern fields at each of three water contents (wet: field capacity, mid: 40% RWC, and dry: 10% RWC) and used those spectra as the soil component of background reflectance. Soil reflectance spectra associated with each field sampling point were selected at air dry levels (0.1-0.2 RWC), a mid-point (0.35-0.45 RWC), and field capacity (FC) (0.7-0.85 RWC).

4.3.1 Background Spectra Characteristics

The moisture contents of the three input soil spectra were similar to moisture contents of maize residue spectra that had been supplied by colleagues. The residue had a dry RWC of 0.02, a midpoint at approximately 0.4, and wet level at approximately 0.8 RWC. Soil RWCs were chosen to mirror residue water contents as closely as possible. Linear mixing was used to calculate background reflectance between soil and residue for the three RWC levels at 0 percent soil, 25 percent soil, 50 percent soil, 75 percent soil, and 100 percent soil.

4.3.2. Shadow Characteristics

Low sun angles under wintertime conditions were simulating by adding 20% shadow (zero reflectance across all wavelengths) to the background reflectance, resulting in an additional 15 shadowed background reflectance spectra. Shadow was equated to zero reflectance in all wavebands.

4.3.3 SAIL Model Output

The SAIL model was run 30 times, incorporating 3 moisture contents at 5 residue levels, with and without shadow. Results will be shown for three levels of LAI,

representing minimal, medium, and high amounts of cover crop biomass. These levels were selected based on the minimum LAI found on fields (0.01), a medium LAI (0.75), and a nearly full-coverage value (2.0). These values correspond to NDVI, biomass, vegetative cover as outlined in previous research (Hively et al., 2009; Prabhakara, et al., 2015) (Table 11).

**Table 11:** Values of leaf area index (LAI), Normalized Difference Vegetation Index (NDVI), biomass, and vegetative groundcover associated with low, medium, and high amounts of winter cover crop vegetation.

| | Biomass level | | |
|---|---|---|---|
| | Low | Medium | High |
| LAI | 0.01 | 0.75 | 2 |
| NDVI | 0.2 | 0.45 | 0.8 |
| Biomass kg/Ha | 0 | 500 | 1000 |
| % Vegetative Cover | 0 | 25 | 75 |

Spectra were run through the SAIL model and were graphed at the dry, midpoint and field capacity soil and residue levels at three LAI levels, as outlined in Figurers 35-37 and Table 12. The NDVI associated with the various treatments were calculated, with results shown in Table 12.

The SAIL model output was run for each water content under two scenarios, with shadow and without shadow. Figure 35 shows the model run for dry soils and residues and no shadow. The various three LAI levels are differentiated visually and it is apparent that at 0.75 and 2.0 LAI, as there is less interference from background, the spectra are tightly grouped for dry soil. The difference at low LAI is the background spectrum, which in this case has a clear inflection point in the near-infrared and a cellulose absorption features in the short-wave infrared (Quemada & Daughtry, 2016).

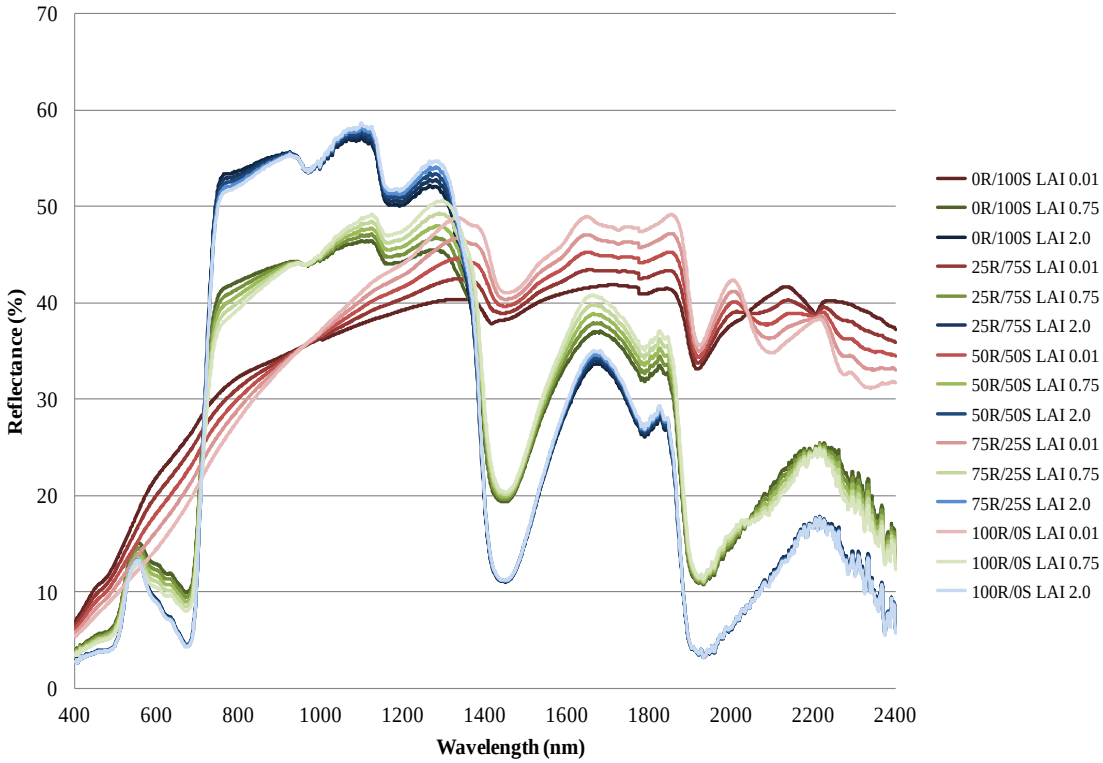


**Figure 35:** SAIL output for dry soils and residues at 3 LAIs (0.01, 0.75, and 2.0) and a variety of soil/residue mixtures

Figure 36 shows the model run for midpoint moisture for soils and residues and no shadow. Unlike dry soils and residues, as moisture increases, the difference between LAI levels becomes less pronounced in the near-infrared and spectra are not as tightly clustered. There is less differentiation in the longer wavelengths between different LAI levels as well compared with the dry soils and residues.

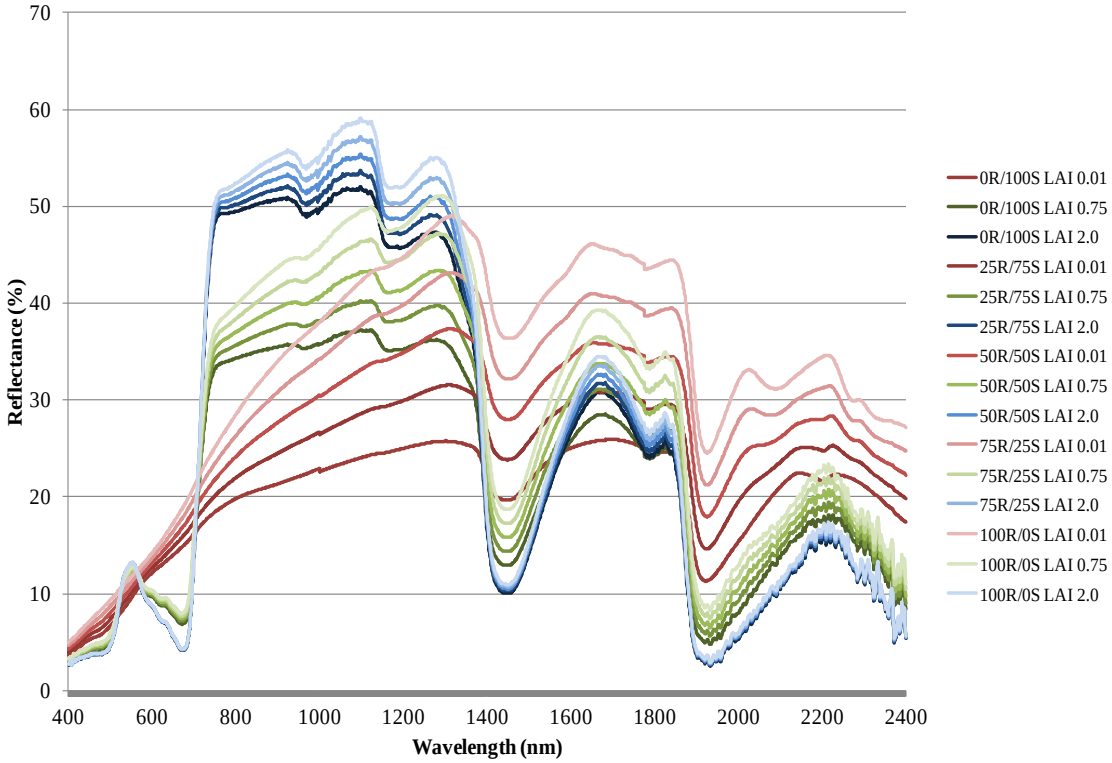


**Figure 36:** SAIL output for midpoint soils and residues at 3 LAIs (0.01, 0.75, and 2.0) and a variety of soil/residue mixtures

Figure 37 shows the model run for midpoint moisture for soils and residues and no shadow. The spectra show similar characteristics to the midpoint soils and residues.

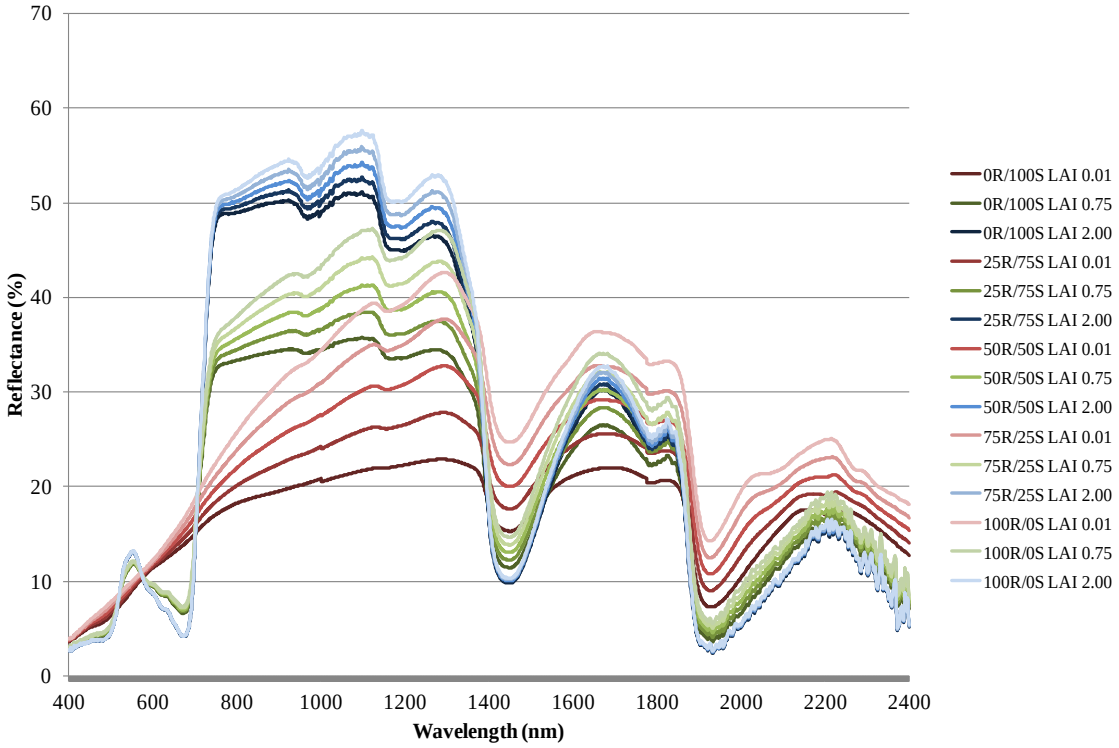


**Figure 37:** SAIL output for field capacity soils and residues at 3 LAIs (0.01, 0.75, and 2.0) and a variety of soil/residue mixtures

Figures 38, 39 and 40 show the model run for dry, midpoint, and field capacity soils and residues with shadow. The spectra show similar characteristics to non-shadowed figures at the same moisture level, with slightly less reflectance across the spectrum.

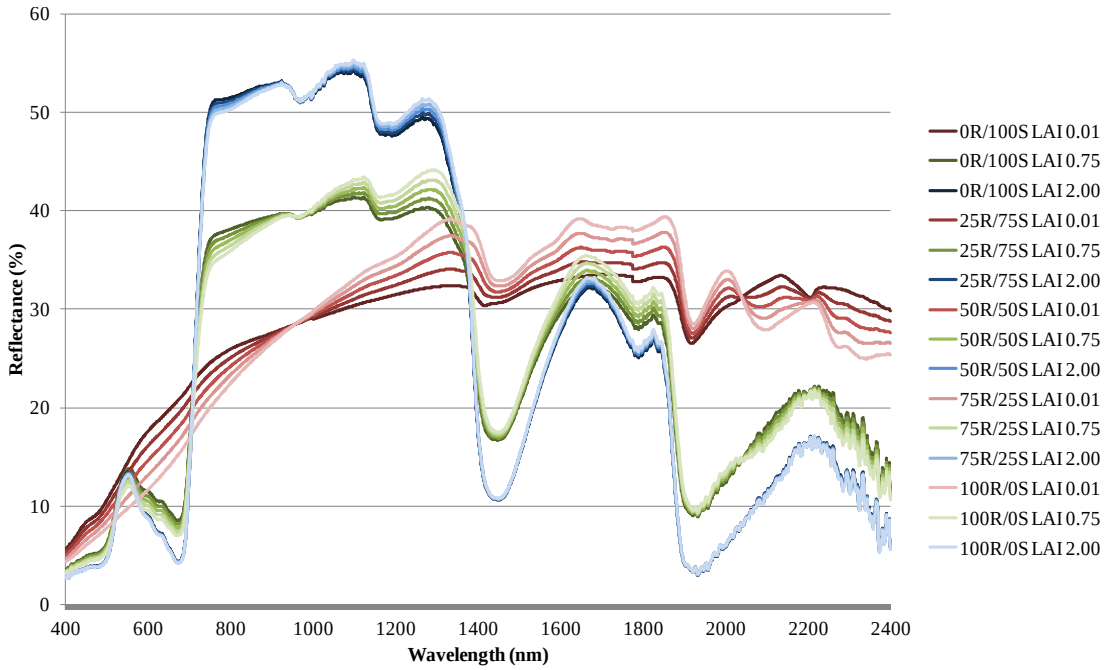


**Figure 38:** SAIL output for dry soils and residues at 3 LAIs (0.01, 0.75, and 2.0) and a variety of soil/residue mixtures with 20 percent shadow

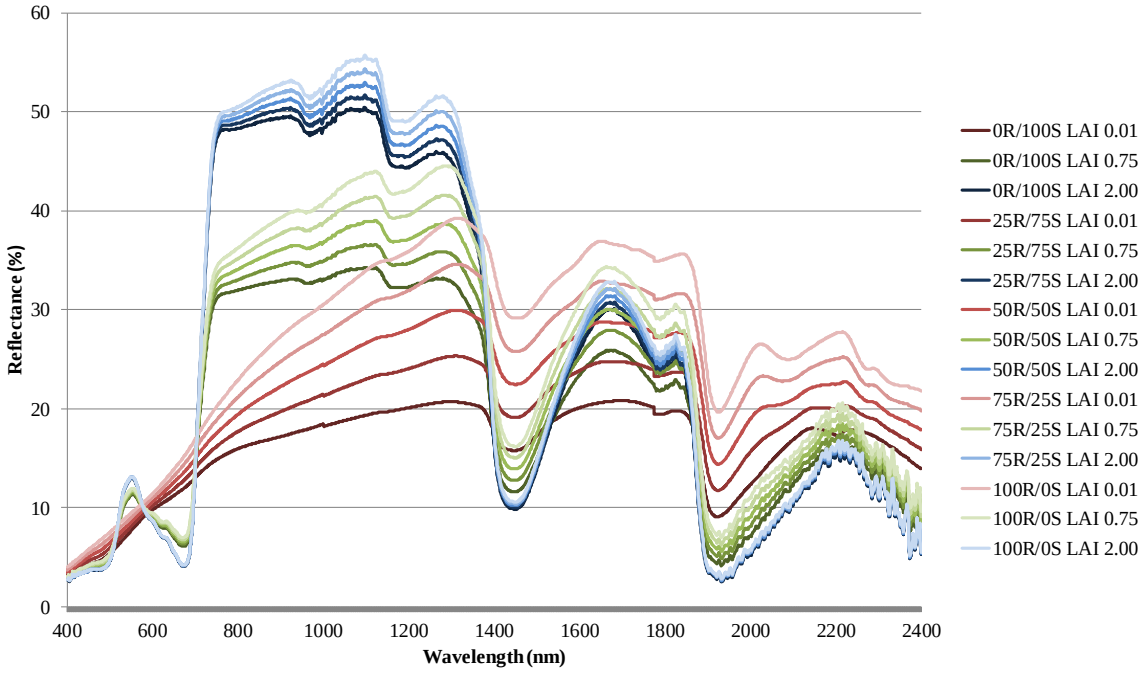


**Figure 39:** SAIL output for midpoint soils and residues at 3 LAIs (0.01, 0.75, and 2.0) and a variety of soil/residue mixtures with 20 percent shadow

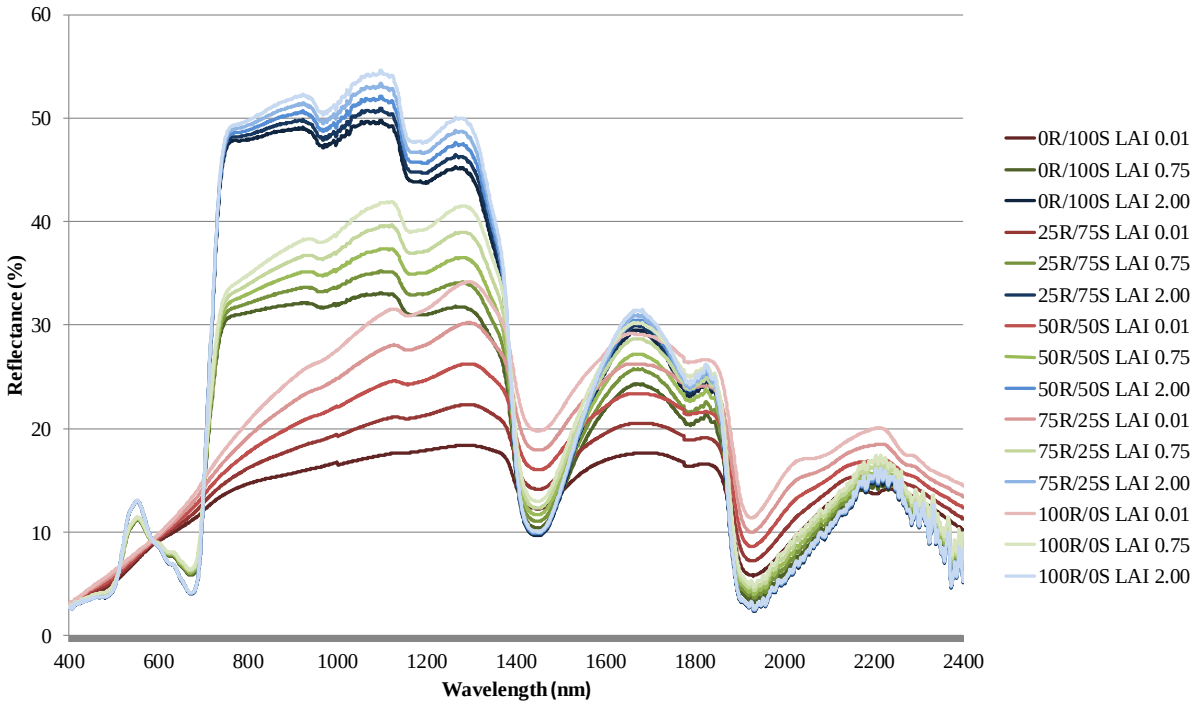


**Figure 40:** SAIL output for field capacity soils and residues at 3 LAIs (0.01, 0.75, and 2.0) and a variety of soil/residue mixtures with 20 percent shadow

**Table 12:** Values of the NDVI calculated from SAIL model output for three levels of LAI, three moisture contents (dry, midpoint, wet) and five levels of residue cover.

| a. unshadowed | | Proportion residue | | | | |
|---|---|---|---|---|---|---|
| | | 0 | 25 | 50 | 75 | 100 |
| Dry | LAI = 0.01 | 0.15 | 0.18 | 0.21 | 0.24 | 0.28 |
| | LAI = 0.75 | 0.60 | 0.61 | 0.62 | 0.64 | 0.65 |
| | LAI = 2.0 | 0.80 | 0.81 | 0.81 | 0.81 | 0.81 |
| Midpoint | LAI = 0.01 | 0.19 | 0.22 | 0.25 | 0.27 | 0.29 |
| | LAI = 0.75 | 0.64 | 0.64 | 0.65 | 0.65 | 0.65 |
| | LAI = 2.0 | 0.80 | 0.80 | 0.81 | 0.81 | 0.81 |
| Wet | LAI = 0.01 | 0.19 | 0.22 | 0.26 | 0.28 | 0.31 |
| | LAI = 0.75 | 0.64 | 0.64 | 0.65 | 0.66 | 0.66 |
| | LAI = 2.0 | 0.80 | 0.80 | 0.80 | 0.81 | 0.81 |
| b. 20% shadow | | Proportion residue | | | | |
| | | 0 | 25 | 50 | 75 | 100 |
| Dry | LAI = 0.01 | 0.15 | 0.18 | 0.21 | 0.24 | 0.28 |
| | LAI = 0.75 | 0.61 | 0.62 | 0.63 | 0.64 | 0.66 |
| | LAI = 2.0 | 0.80 | 0.80 | 0.80 | 0.80 | 0.81 |
| Midpoint | LAI = 0.01 | 0.19 | 0.23 | 0.25 | 0.27 | 0.29 |
| | LAI = 0.75 | 0.65 | 0.65 | 0.65 | 0.66 | 0.66 |
| | LAI = 2.0 | 0.80 | 0.80 | 0.80 | 0.80 | 0.81 |
| Wet | LAI = 0.01 | 0.19 | 0.23 | 0.26 | 0.29 | 0.31 |
| | LAI = 0.75 | 0.65 | 0.65 | 0.66 | 0.66 | 0.67 |
| | LAI = 2.0 | 0.80 | 0.80 | 0.80 | 0.80 | 0.81 |

*4.4 Discussion*

NDVI was calculated using the 650 wavelength for red and the 850 wavelength for this study. However, because the ASD instruments records in wavelengths from 400-2400, it is possible to use instrument-specific spectral reflectance curves to calculate NDVI for a variety of sensors. As shown in Table 12, as soil becomes moist (transition from dry to medium water content) the NDVI

associated with background soils increases by approximately 0.04. However, NDVI associated with 100% residue increases by only 0.01 because the wetting curves for residue versus soils behave differently and the behavior of such moisture curves is not yet well understood and can depend on the amount of decomposition and previous leaching (Quemada & Cabrera, 2002). The effect is fairly consistent until 80% groundcover. As LAI and moisture increase, NDVI is less able to differentiate between levels of residue cover, showing that NDVI is not good at measuring residue for winter cover crops at low LAI. The proportion of residue to bare soil in the background does not significantly affect NDVI and its use for measuring winter cover crop vegetation. Under non-vegetated conditions NDVI increased by approximately 0.1 as proportion of residue increased, regardless of soil moisture conditions. Due to inadequate growing weather, cover crop fields may have NDVI values below 0.3. Based on the results of this study, it would be impossible to tell under midpoint moisture levels whether NDVI values below 0.3 are for a bare soil with approximately 200 kg/ha vegetation or if these fields are actually devoid of vegetation and have a high residue content.

The addition of shadow into the spectrum results in an overall lowering of reflectance and could have consequences if non-ratio vegetation indices are used. However, under this scenario, NDVI masks the effect of shadowing and produces similar values to non-shadows areas. The effect of the bidirectional reflectance distribution factor (BRDF) is also unknown in this set of data, but the time of year the data was collected may contribute to a pronounced effect from BRDF and can be included using SAIL as an extension of this study.

*4.5 Conclusion*

Residue affects NDVI under low biomass conditions; therefore, accuracy of vegetation measurement under low biomass conditions could be improved by first using a SWIR index to map percent residue (Quemada & Daughtry, 2016), and then adjusting the calibration between NDVI and vegetation according to known residue. Further work will look for percent vegetative cover change points where effects of soil moisture move from significant to non-significant, and develop applications in remote sensing of winter cover crop performance. From this study, it can be concluded that if synoptic measurement of cover crops from satellite data is desired and NDVI is being used to measure cover crop performance, the effect of soil moisture and residue mixing is most pronounced during dry field conditions. Therefore, particular attention should be paid to climatic data and whether such conditions are feasible on the sampling date. In general, for moderate to wet conditions, background reflectance will not affect NDVI. However, at low LAI, the effect of residue reflectance may increase NDVI when there is no vegetation present.

# Chapter 5: Summary of Research and Conclusions

## *5.1 Summary of Main Research Findings*

Ensuring high water quality as agricultural demand increases will necessitate the use of winter cover crops and the need for understanding and monitoring their growth and effectiveness using the available technologies. This research has illuminated factors that need to be considered to accurately measure winter cover crops at the field scale. The two main benefits of winter cover crops include reduced soil erosion with higher percent groundcover; and reduced runoff from nutrients as cover crop biomass increases. These two variables can be accurately measured using remote sensing data if certain considerations are taken into account. Unlike typical harvest crops, winter cover crops are planted during a time when weather is not conducive to crop growth, and are often killed before they reach maturity. As cover crops are intended to scavenge residual soil nutrients that are left over after the main crops are harvested in the fall, they are often subject to nutrient deficiencies that can cause leaf chlorosis. Additionally, leaves may undergo senescence or leaf damage due to cold temperatures over the winter.

The second chapter of this dissertation outlined a temporal issue that comes about while measuring cover crops and revealed that remote sensing can be successful for measuring both percent groundcover and biomass when reduction in leaf greenness and index saturation are properly handled. A major conclusion of this chapter was that remote sensing indices can be used to accurately estimate both percent groundcover and biomass when measurements are adjusted to account for

frost damage and yellowing. When dates were restricted to before the onset of freezing weather, the linear relationship between percent groundcover and NDVI had an $r^2$ value of 0.95. When doing field research, restricting data to sampling dates before the onset of cold weather was effective as a method to separate green groundcover from yellow and frost burned vegetation. Results were comparable to estimates of green-only vegetation derived from shoulder-height photos.

Measuring cover crop biomass using optical remote sensing presents a difficult problem as many indices cannot differentiate variable levels of biomass when there is too little chlorophyll, or when during saturated at high biomass levels. This chapter revealed that different indices can be utilized for high and low biomass ranges to avoid saturation and increase model strength. The Triangular vegetation index (TVI) was much better at estimating high biomass due to the fact that it doesn't have an upper value boundary, and had an $r^2$ of 0.86. However, TVI was not as good as NDVI at detecting low levels of biomass. There was a strong relationship between GDD and both percent groundcover and biomass for early in the growing season, when GDD were restricted to 400. With this restriction in place, there was a strong relationship between percent groundcover and GDD with an $r^2$ of 0.81; and similarly for biomass and GDD, with an $r^2$ or 0.75. After 400 GDD, the increase in growing degree days wasn't well correlated due to a decrease in percent groundcover and biomass in species that experienced wintertime leaf damage and dormancy. Although the accuracy of estimates increased significantly when restricted to early dates regardless of which variables were being compared, an unrestricted date analysis would result in an underestimation of plant biomass or percent groundcover

across the landscape. This would occur due to yellowing or damaged leaves that do not have a signal typical of healthy vegetation, but still have provided nutrient sequestration or groundcover benefits.

The third chapter of this dissertation focused on the instruments that can be used to monitor winter cover crops and whether or not their measurements are comparable. When field sizes are small (average field size in this study was 8 hectares), the use of coarse resolution satellites with daily overpasses is not feasible. Coarse resolution pixels (25m – 1km) can be composed of mixed landscape types and result in impure and inaccurate measurements for index calculation used to estimate biomass and percent groundcover on small fields. The moderate- to fine-resolution satellites used in the study – Landsat 7 (30m), SPOT-5 (10m), and WorldView-2 (2m) – have adequate spatial resolution but less frequent overpass times. Ground-based proximal sensors can collect data at a fine spatial resolution (several readings per second) as they cross the landscape, recording small variations in reflectance, and even passive sensors can be operated at any time as long as there is adequate solar irradiance. They are also unadulterated by atmospheric effects as they are close to the ground and radiation back to the sensor follows a short path. Unfortunately, the sensors can be expensive, require training to operate, require physical access to fields, and data gathering is physically-intensive and impractical over large areas.

In addition to temporal factors that contribute to usability of different sensors, satellite data can be processed to both top of atmosphere and surface reflectance. Landsat data is delivered as a surface reflectance product. SPOT and WorldView can be processed using MODTRAN. Although this process is complicated, this study

revealed that surface reflectance data from satellites across the green, red and near-infrared bands in this study have intercepts closer to zero and slopes closer to one when regressed against proximal sensor data and each other. The differences in NDVI were less noticeable than for individual bands when comparing top of atmosphere and surface reflectance. This is understandable as the NDVI is the ratio of two bands. However, the NDVI measurements from satellite surface reflectance were closer to values from proximal sensors. Importantly, the presence of small clouds and cloud shadows need to be accounted for. In this study, they only revealed themselves when looking at near infrared measurements. NDVI seems to "compensate" for these effects because it's a ratio, but the reflectance measurements themselves are inaccurate under patchy cloud cover and need to be eliminated for accurate analysis. Converting clear satellite imagery to surface reflectance results in more stable calibration between satellite and ground-based sensors and also more comparable measurements.

The fourth chapter of this dissertation utilized the Scattering by Arbitrarily Inclined Leaves (SAIL) model to evaluate factors unique to winter cover crops that could be influencing reflectance measurements. Winter cover crops often have lower LAI measurements than traditional crops that have a full canopy. As seen with the wheat field in these studies, winter cover crop fields that are planted late in the fall may never reach full vegetative cover, and even early planted fields lack full canopies early in the year. Fields with low LAI are more impacted by background reflectance. This background can be composed of soils that can have widely varying reflectance based on their type and relative water content. Additionally, winter cover crops are

often planted as a part of conservation tillage systems where crop residue is left on the field, providing a matrix of bare soil and residue plant material. This residue can cover much of the ground surface, and reflectance characteristics of both need to be included to ensure more characteristic background spectra. Residue during the beginning of winter is neither fresh nor almost entirely decomposed. The moisture content of the residue can also affect overall reflectance. The results of this chapter show that NDVI varies very little, even in the presence of low winter solar declination angles and associated increased shadowing. However, NDVI is not capable of differentiating between residue and vegetation at low LAI. This finding is particularly relevant for the study of winter cover crops as there may be residue cover present on fields and not vegetation.

### *5.2 Uncertainty and error quantification*

There are some possible sources of uncertainty that may have presented themselves in the data, although great care was taken to reduce or account for such factors. In using ground-based sensors, there may be slight differences between users as they are hand-held. Other fieldwork, such as biomass sampling, may have slight variation due to differences between individuals doing field sampling, though all were carried out per the guidelines laid out in standard operating procedures. A single user did all SamplePoint analysis to reduce differences between users in analyzing groundcover. Laboratory analysis of transmittance and reflectance properties of leaves and soils were done using standard operating procedures, and factors such as room ambient lighting were accounted for during data collection. Instruments used

for measurements, including sensors and scales, were not changed throughout the data collection and analysis process to eliminate slight differences in instrumentation.

### *5.3 Implications from the Research*

There are important implications for using remote sensing to measure cover crop growth. Due to yellowing and leaf damage, care needs to be taken when cover crops are measured. Because there is little growth during extremely cold weather, restricting cover crop measurements to dates before these conditions can result in more accurate calibration between satellite and ground conditions. Additionally, using indices with no upper bound, such as TVI, can lead to better measurements at extremely high biomass where NDVI might saturate. Beyond an NDVI of 0.8, biomass differences are impossible to meaningfully detect, whereas percent groundcover continues to have strong relationships with sensor measurements.

In general, the results of this study show that although top of atmosphere products have strong relationships with proximal sensor measurements across bands, conversion to surface reflectance moves intercepts closer to zero and slopes closer to one, regardless of satellite platform or date. Individual data values among proximal sensors and satellite measurements were closer to each other compared with top of atmosphere measurements. On an operational level, this implies that surface reflectance from satellite products are comparable to proximal ground-based sensors.

### *5.4 Directions for Future Research*

There are several avenues for future research based on the results of the studies contained herein. First, the fields used for this dissertation study were chosen

based on real-world conditions and what had been planted after the fall harvest. To further understand the role of nutrient limitation in chlorosis of leaves during wintertime, a randomized block study could be undertaken with known and controlled nutrient management. Although previous research has shown that early planted winter cover crops are more efficient at nutrient sequestration and generally provide more groundcover, the nutrient conditions in the soil that contribute to growth beyond planting date are not well understood.

For this particular research, clear-sky conditions are always needed for data collection and hazy or cloudy conditions are avoided. However, seeing whether or not there would be larger differences between surface reflectance and proximal sensors could be useful for other types of agricultural monitoring work, or in cases where clear days are limited or those where there is a greater amount of particulate pollution, especially near large cities. Although fields were chosen for this study were representative of realistic winter cover crop scenarios, future research could include controlled planting dates and field management to further analyze species-specific and treatment-specific differences in plant growth over the winter crop season.

The interplay between soils, residues and background reflectance is complex. A major area of current study that will continue into the future is detection of residue on agricultural fields. From this, further research on how vegetation affects detection of residue and vice versa should be carried out to truly understand the background spectrum and their environmental importance. A combination of NDVI and residue indices using longer wavelengths could be used to detect residue on fields where

visible and near infrared cannot. The issue of cloud shadow has been extensively studied, and many cloud masks exist. However, they may not always be able to fully capture the full extent of cloud shadows. If bands in the near-infrared spectrum have low reflectance over known vegetated surfaces, such as cover cropped locations, it could be another way to eliminate pixels under cloud shadow during analysis. This is especially important as this study showed that conversion to NDVI can falsely "compensate" for areas under cloud shadow despite contaminated pixels.

Importantly, data and equipment availability played a large role in this research. Without the use of complex and sometimes expensive laboratory and field equipment, satellite data products, and personnel, there would be limited opportunities for further research. This brings to light the important of freely available data in regions across the globe. Especially in the content of large-scale operational monitoring of cover crops, there is a need for freely available, usable data. Although some satellite data, such as Landsat, are already made available as surface reflectance products, processing of top of atmosphere data is complex, time-consuming, and requires a large number of data inputs. Automating this process for all satellite data and making surface reflectance products more readily available would improve accessibility and accuracy, allowing for myriad different types of sensor data to be utilized and increasing operability.

Future research is already being planned to measure winter cover crops on an operational scale. There are considerations from this research that could be incorporated into such a system. For instance, the most accurate measurements should be taken before the onset of cold weather and can be based on flattening GDD

accumulation, where cold weather reduces growing weather and increases the possibility for yellowing of cover crops. Previous research has used surface temperature measurements from MODIS to make automated GDD maps at the 1-km scale, and this data could prove useful for remotely restricting the timing of cover crop data collection.

### *5.5 Towards an Operational Cover Crop Monitoring System*

The results of this research will contribute to the development of operational satellite-based cover crop monitoring systems. Remote sensing can contribute to the timely and accurate assessment of cover crop growth on a regional basis, and provide information to cover crop implementation programs in order to improve environmental outcomes. Given the need for state-level information on cover crop location and extent, large area coverage will be needed. The location of cover crops can be known for states like Maryland that collect such data, but a method to locate cover cropped fields using only remote sensing would be helpful in areas where such information is not available. Satellite-based systems can provide the necessary synoptic view and moderate resolution sensors (10-30m) enable the mapping of all but the smallest fields. The cost of finer spatial resolution data, which could be used for mapping such fields remain prohibitive. The presence of cover crops can be identified and crop cover and biomass can be monitored if there are sufficiently frequent observations. However, the satellite data will need to be atmospherically corrected and made available in a timely fashion after acquisition as correct individual scenes manually to surface reflectance is a time- and labor-intensive process. Atmospherically corrected Landsat data are now being made available

routinely by the EROS Data Center, though these products are still provisional and subject to improvements and changes (USGS, 2016). The Landsat system has long been promoted as a tool for agricultural monitoring but has traditionally had limited utility due to its 16-day overpass, which when one considers cloud cover can result in even less frequent observations (Whitcraft et al. 2015). At the time of the field data collection for this study, Landsat 7 provided the U.S. moderate resolution data. Fortuitously the fields measured in this study were unaffected by the Landsat 7 SLC-off striping which severely limited its operational use in 2003. Landsat 8 is now operating with the necessary visible and near-infrared bands, and with a 30-m pixel size and could provide a major element of such a monitoring system. Satellite imagery from ESA's Sentinel-2a and b, with a 10-m spatial resolution and visible and near-infrared channels (similar to SPOT) can be used to improve the frequency of observations. The combination of the 5-day overpass for Sentinel-2 instruments and the 16-day overpass frequency of Landsat 8 make a combined 3-day temporal resolution for data collection feasible. Although surface reflectance products are not currently provided for Sentinel-2, a tool-box is available from the ESA which includes an atmospheric correction tool (https://sentinel.esa.int/web/sentinel/toolboxes/sentinel-2). NASA is in the process of developing combined atmospherically corrected products from Landsat and Sentinel-2 (Jeff Masek, GSFC Personal Communication).

Such a cover crop monitoring system would enable identification of areas where use of cover crops are less successful and could potentially be used to target interventions by extension agents or incentives for farmers to participate in the

subsidy programs. Monitoring when combined with land ownership data, would also enable verification of claims for state subsidies. When combined in a geographic information system with a hydrologic model, priority areas for cover crops could be identified in terms of their potential impact on water quality. Repeated annual mapping of cover crop extent would enable the tracking of trends in uptake and use.

### *5.6 Concluding Thoughts*

Although cover crops have been used for centuries, their relevance is increasing in the United States as a scientific proven way to reduce nitrate and sediment pollution into sensitive waterways. As global population increases and water bodies become more stressed, this type of pollution prevention is a necessary goal. Just as pressing is the need to preserve soil fertility. Although cover crops can help to preserve soil fertility and are a major part of sustainable crop rotations, cover crop potential has not been fully realized (Dunn et al., 2016). Based on research about their benefits, scaling-up remote sensing systems to measure and monitor cover crops in this country and around the globe is a worthwhile endeavor and one that should continue to be researched and funded.

# Bibliography

Anderson, D.M., Glibert, P.M., Burkholder, J.M. 2002. Harmful Algal Blooms and Eutrophication: Nutrient Sources, Composition, and Consequences. Estuaries 25(4b), 704-726.

Andrews, C.J. 1987. Low-Temperature Stress in Field and Forage Crop Production – An Overview. Canadian Journal of Plant Science 67, 1121-1133.

Arnold, J.G., Harmel, R.D., Johnson, M.V., Bingner, R., Strickland, T.C., Walbridge, M., Santhi, C., DiLuzio, M., Wang, X. 2014. Impact of the Agricultural Research Service Water Assessment Studies on the Conservation Effects Assessment Project Cropland National Assessment. Journal of soil and water conservation 69(5), 137A-144A.

ASAE. 2005. Terminology and Definitions for Soil Tillage and Soil-Tool Relationships. St. Joseph, MI. http://www.nrcs.usda.gov/Internet/FSE_DOCUMENTS/nrcs144p2_053410.pdf

Ashford, D.L., Reeves, D.W. 2003. Use of a mechanical roller-crimper as an alternative kill method for cover crops. American Journal of Alternative Agriculture 18(1), 37-45.

Ator, S. W., & Denver, J. M. 2015. Understanding Nutrients in the Chesapeake Bay Watershed and Implications for Management and Restoration—The Eastern Shore. U.S. Geological Survey Circular 1406, Version 1.2.

Baret, F., Guyot, G. 1991. Potentials and Limits of Vegetation Indices for LAI and APAR Assessment. Remote Sensing of Environment 35(2-3), 161-173.

Batiuk, R.A., Linker, L.C., Cerco, C.F. 2013. Featured Collection Introduction: Chesapeake Bay Total Maximum Daily Load Development and Application. Journal of the American Water Resources Association (JAWRA) 1-5.

Berman, J.M., Arrigo, K.R., Matson, P.A. 2005. Agricultural runoff fuels large phytoplankton blooms in vulnerable areas of the ocean. Nature 434, 211-214.

Boesch, D.F., Brinsfield, R.B., Magnien, R.E. 2001. Chesapeake Bay Eutrophication: Scientific Understanding, Ecosystem Restoration, and Challenges for Agriculture. Journal of Environmental Quality 30(2), 303-320.

Booth, D.T., Cox, S.E., Berryman, R.D. 2006. Point sampling digital imagery with 'SamplePoint.' Environmental Monitoring and Assessment 123, 97-108.

Broge, N.H., Leblanc, E. 2000. Comparing prediction power and stability of broadband and hyperspectral vegetation indices for estimation of green leaf area index and canopy chlorophyll density. Remote Sensing of Environment 76, 156-172.

Broge, N.H., Mortensen, J.V. 2002. Deriving green crop area index and canopy chlorophyll density of winter wheat from spectral reflectance data. Remote Sensing of Environment 81, 45-57.

Chen, J., Song, G., Miagen, S., Tang, Y. 2009. Estimating aboveground biomass of grassland
having a high canopy cover: an exploratory analysis of in situ hyperspectral data. International Journal of Remote Sensing 30(24), 6497-6517.

Chesapeake Bay Program. 1983. The Chesapeake Bay Agreement of 1983.

Chesapeake Bay Program. 2013. Continuous High Residue, Minimum Soil Disturbance BMP. Annapolis, MD.
http://www.chesapeakebay.net/documents/AgWG_100313_Hi_RES_MSD_Report_4_FINAL.pdf

Cooper, S.R. 1995. Chesapeake Bay Watershed Historical Land Use: Impact on Water Quality and Diatom Communities. Ecological Applications 5(3), 703-723.

CROPSCAN, Inc., 2013. Rochester, MN. http://www.cropscan.com/

Dabney, S.M., 1998. Cover crop impacts on watershed hydrology. Journal of Soil and Water Conservation 53(3), 207-213.

Dabney, S.M., Delgado, J.A., Reeves, D.W. 2001. Using winter cover crops to improve soil and water quality. Communications in Soil Science and Plant Analysis 32, 7-8, 1221-1250.

Daniel, J.B., Abaye, A.O., Alley, M.M., Adcock, C.W., Maitland, J.C. 1999. Winter Annual Cover Crops in a Virginia No-till Cotton Production System: 1. Biomass production, Ground cover, and Nitrogen Assimilation. Journal of Cotton Science 3, 74-83.

Dauer, D.M., Ranasinghe, J.A., Weisberg, S.B. 2000. Relationships Between Benthic Community Condition, Water Quality, Sediment Quality, Nutrient Loads, and Land Use Patterns in Chesapeake Bay. Estuaries 23(1), 80-96.
De Baets, S., Poesen, J., Merrsmans, J., Serlet, L., 2011. Cover crops and their erosion-reducing effects during concentrated flow erosion. Catena 85(3), 237-244.

Daughtry, C.S.T., Hunt, E.R., Doraiswamy, P.C., McMurtry III, J.E. 2005. Remote Sensing the Spatial Distribution of Crop Residues. Agronomy Journal 97, 864-871.

Deery, D., Jiminez-Berni, J., Jones, H., Sirault, X., Furbank, R. 2014. Proximal Remote Sensing Buggies and Potential Applications for Field-Based Phenotyping. Agronomy 5, 349-379.

Delgado, J.A., Dillon, M. A., Sparks, R.T., Essah, S.Y.C. 2007. A decade of advances in cover crops. Journal of Soil and Water Conservation 62(5), 110A-117A.

Doran, J.W. 2002. Soil health and global sustainability: translating science into practice. Agriculture, Ecosystems and Environment 88, 119-127.

Dunn, M., Ulrich-Schad, J.D., Prokopy, L.S., Myers, R.L., Watts, C.R., Scanlon, K. 2016. Perceptions and use of cover crops among early adopters: Findings from a national survey. Journal of Soil and Water Quality 71(1), 29-40.

ENVI: Release 4.8. Boulder, Colorado. Exelis Visual Information Solutions.

Executive Order 13508—Chesapeake Bay Protection and Restoration, 3 C.F.R. 2009.

Environment Canada. Ozone Map Archive, 2016. http://exp-studies.tor.ec.gc.ca/cgi-bin/clf2/selectMap?lang=e&printerversion=false&printfullpage=false&accessible=off / Accessed 16.03.23.

Esri, 2013. ArcGIS Desktop: Release 10. Redlands, CA: Environmental Systems Research Institute.

Feng, M., Sexton, J.O., Huang, C., Masek, J.G., Vermote, E.F., Gao, F., Narasimhan, R., Channan, S., Wolfe, R.E., Townshend, J.R. 2013. Global surface reflectance products from Landsat: Assessment sing coincident MODIS observations.

Fisher, K. A., Momen, B., Kratochvil, R.J. 2011. Is broadcasting seed an effective winter cover crop planting method? Agronomy Journal 103(2), 472-478.

Fisher, T.R., Hagy, J.D., Boynton, W.R., Williams, M.R. 2006. Cultural eutrophication in the Choptank and Patuxent estuaries of Chesapeake Bay. Limnology and Oceanography 51(1, part 2), 435-447.

Foley, J.A., DeFries, R., Asner, G.P., Barford, C., Bonan, G., Carpenter, S.R., Chapin, F.S., Coe, M.T., Daily, G.C., Gibbs, H.K., Helkowski, J.H., Holloway, T., Howard, E.A., Kucharik, C.J., Monfreda, C., Patz, J.A., Prentice, I.C., Ramankutty, N., Snyder, P.K. 2005. Global Consequences of Land Use. Science 309, 570-574.

Fraser, R.S., Kaufman, Y.J. 1985. The Relative Importance of Aerosol Scattering and Absorption in Remote Sensing. IEEE Transactions on Geoscience and Remote Sensing GE-23(5), 625-633.

Gan, S., Amasino, R.M. 1997. Making Sense of Senescence. Plant Physiology 113, 313-319.

Gebbers, R., & Adamchuk, V. I. 2010. Precision Agriculture and Food Security. Science 327, 828–831.

Gitelson, A.A., Merzlyak, M.N. 1994, Quantitative estimation of chlorophyll-a using reflectance spectra: experiments with autumn chestnut and maple leaves, Journal of Photochemistry and Photobiology 22, 247-252.

Gitelson, A.A., Kaufman, Y.J., Stark, R., Rundquist, D. 2002. Novel algorithms for remote estimation of vegetation fraction. Remote Sensing of Environment 80, 76-87.

Gitelson, A.A. 2004. Wide dynamic range vegetation index for remote quantification of biophysical characteristics of vegetation. Journal of Plant Physiology 161(2), 165-173.

Godwin, R.J., Miller, P.C.H. 2003. A Review of the Technologies for Mapping Within-Field Variability. Biosystems Engineering 84(4), 393-407.

Goetz, S.J., Jantz, C.A., Prince, S.D., Smith, A.J., Varlyguin, D., Wright, R.K. 2004. Integrated Analysis of Ecosystem Interactions With Land Use Change: The Chesapeake Bay Watershed, in: Defries, R.S., Asner, G.P., Houghton, R.A. (Eds.), Ecosystem and Land Use Change. American Geophysical Union, Washington DC, pp. 263-275.

Goward, S.N., Huemmrich, K.F. 1992. Vegetation Canopy PAR Absorptance and the Normalized Difference Vegetation Index: An Assessment Using the SAIL Model. Remote Sensing of Environment 39, 119-140.

Gregersen, P.L., Holm, P.B., Krupinska, K. 2009. Leaf senescence and nutrient remobilisation in barley and wheat. Plant Biology 10, 37-49.

Haboudane, D., Miller, J.R., Pattey, E., Zarco-Tejada, P.J., Strachan, I.B. 2004. Hyperspectral vegetation indices and novel algorithms for predicting green LAI of crop canopies: Modeling and validation in the context of precision agriculture. Remote sensing of environment 90(3): 337-352.

Hagy, J.D., Boynton, W.R., Keefe, C.W., Wood, K.V. 2004. Hypoxia in Chesapeake Bay, 1950-2001: Long-term Change in Relation to Nutrient Loading and River Flow. Estuaries 27(4), 634-658.

Hedley, C. 2014. The role of precision agriculture for improved nutrient management on farms. Journal of the Science of Food and Agriculture 95, 12-19.

Hively, W.D., Lang, M., McCarty, G.W., Keppler, J., Sadeghi, A., McConnell, L.L. 2009. Using satellite remote sensing to estimate winter cover crop nutrient uptake efficiency. Journal of Soil and Water Quality 64(5), 303-313.

Holben. B. 1993. AERONET, Greenbelt, MD. http://aeronet.gsfc.nasa.gov/

Holland Scientific. 2011. Crop Circle ACS-470 Multi-Spectral Crop Canopy Sensor. http://hollandscientific.com/crop-circle-acs-470-multi-spectral-crop-canopy-sensor/

Hmimina, G., Dufrêne, E., Pontailler, J.-Y., Delpierre, N., Aubinet, M., Caquet, B., de Grandcourt, A., Burban, B., Flechard, C., Granier, A., Gross, P., Heinesch, B., Longdoz, B., Moureaux, C., Ourcivil, J.-M., Rambal, S., Saint André, L., Soudani, K. 2013. Evaluation of the potential of MODIS satellite data to predict vegetation phenology in different biomes: An investigation using ground-based NDVI measurements. Remote Sensing of Environment 132, 145-158.

Huete, A.R. 1988. A Soil-Adjusted Vegetation Index (SAVI). Remote Sensing of Environment 25, 295-309.

Huete, A., Didan, K., Miura, T., Rodriguez, E.P., Gao, X., Ferreira, L.G. 2002. Overview of the radiometric and biophysical performance of the MODIS vegetation indices. Remote Sensing of Environment 83, 195-213.
Jacquemoud, S., Baret, F., Hanocq, J.F. 1992. Modeling Spectral and Bidirectional Soil Reflectance. Remote Sensing of Environment 41: 123-132.

Jacquemoud, S., Bacour, C., Poilvé, H., Frangi, J.-P. 2000. Comparison of Four Radiative Transfer Models to Simulate Plant Canopies Reflectance: Direct and Inverse Mode. Remote Sensing of Environment 74, 471-781.

Jordan, T.E., Correll, D.L., Weller, D.E., 1997. Effects of Agriculture on Discharges of Nutrients from Coastal Plain Watersheds of Chesapeake Bay. Journal of Environmental Quality 26, 836-848.

Kipp, S., Mistele, B., Schmidhalter, U. 2014. The performance of active spectral reflectance sensors as influenced by measuring distance, device temperature and light intensity. Computers and Electronics in Agriculture, 24-33.

Kling, C.L., Panagopoulos, Y., Rabotyagov, S.S., Valcu, A.M., Gassman, P.W., Campbell, T., White, M.J., Arnold, J.G., Srinivasan, R., Jha, M.K., Richardson, J.J., Moskal, L.M., Turner, R.E., Rabalais, N.N. 2014. LUMINATE: linking agricultural land use, local water quality and Gulf of Mexico hypoxia. European Review of Agricultural Economics 41(3), 431-459.

Li, W., Weiss, M., Waldner, F., Defourny, P., Demarez, V., Morin, D., Hagolle, O. Baret, F. 2015. A Generic Algorithm to Estimate LAI, FAPAR and FCOVER

Variables from SPOT4_HRVIR and Landsat Sensors: Evaluation of the Consistency and Comparison with Ground Measurements. Remote Sensing 7, 15494-15516.

Li, X. Strahler, A.H. 1992. Geometric-Optical Bidirectional Reflectance Modeling on the Discrete Crown Vegetation Canopy: Effect of Crown Shape and Mutual Shadowing. IEEE Transactions on Geoscience and Remote Sensings 30(2), 276-292.

LI-COR, Inc. 1998. 1800-12 Integrating Sphere Instruction Manual. Lincoln, NE.

Linker, L.C., Dennis, R., Shenk, G.W., Batiuk, R.A., Grimm, J., Wang, P. 2013. Computing Atmospheric Nutrient Loads to the Chesapeake Bay Watershed and Tidal Waters. Journal of the American Water Resources Association (JAWRA) 49(5), 1025-1041.

Maiersperger, T.K., Scaramuzza, P.L., Leigh, L. Shrestha, S., Gallo, K.P. 2014. Characterizing LEDAPS surface reflectance products by comparisons with AERONET, field spectrometer and MODIS data. Remote Sensing of Environment 136, 1-13.

Maryland Department of Agriculture (MDA). 2015. Maryland's 2015-2016 Cover Crop Sign-Up. http://mda.maryland.gov/resource_conservation/counties/2015CoverCropProgram.pdf

Maryland Department of Agriculture (MDA). 2016. Maryland Department of Agriculture Announces Record Cover Crop Sign-up. http://news.maryland.gov/mda/press-release/2016/08/17/maryland-department-of-agriculture-announces-record-cover-crop-sign-up/

McMaster, G.S., Wilhelm, W. Growing degree-days: one equation, two interpretations. Agricultural and Forest Meteorology 87, 291-300.

Meisinger, J.J., Hargrove, W.L., Mikkelsen, R.L., Williams, J.R., Benson, V.W. 1991. Effects of cover crops on groundwater quality. Cover Crops for Clean Water. Soil and Water Conservation Society 266, 57-84.

Mirsky, S.B., Curran, W.S., Mortensen, D.A., Ryan, M.R., Shumway, D.L. 2009. Control of cereal rye with a roller/crimper as influenced by cover crop phenology. Agronomy journal 101(6), 1589-1596.

MODTRAN5, 2012. http://modtran5.com/ Accessed 16.03.23.

Moges, S.M., Raun, W.R., Mullen, R.W., Freeman, K.W., Johnson, G.V., Solie, J.B. 2004. Evaluation of Green, Red, and Near Infrared Bands for Predicting Winter Wheat Biomass, Nitrogen Uptake, and Final Grain Yield. Journal of Plant Nutrition 27(8), 1431-1441.

Moran, M.S., Inoue, Y., Barnes, E.M. 1997. Opportunities and Limitations for Image-Based Remote Sensing in Precision Crop Management. Remote Sensing of Environment 61, 319-346.

Mueller, N.D., Gerber, J.S., Johnston, M., Ray, D.K., Ramankutty, N., Foley, J.A. 2012. Closing yield gaps through nutrient and water management. Nature 490(7419), 254-257.

Mulla, D. J. 2013. Twenty five years of remote sensing in precision agriculture: Key advances and remaining knowledge gaps. Biosystems Engineering 114, 358-371.
Mutanga, O., Skidmore, A.K., 2004. Narrow band vegetation indices overcome the saturation problem in biomass estimation. International Journal of Remote Sensing 25(19), 3999-4014.

Muñoz, J.D, Kravchenko, A. 2012. Deriving the optimal scale for relating topographic attributes and cover crop plant biomass. Geomorphology 179: 197-207.

Myneni, R.B., Williams, D.L. 1994. On the relationship between FAPAR and NDVI. Remote Sensing of Environment 49, 200-211.

NASA. 2011. Landsat 7 Science Data User's Handbook. http://landsat.gsfc.nasa.gov/wp-content/uploads/2016/08/Landsat7_Handbook.pdf

Nixon, S.W. 1987. Chesapeake Bay nutrient budgets—a reassessment. Biogeochemistry 4, 77-90.

NOAA/ESRL. Radiosonde Database, 2016. http://www.esrl.noaa.gov/raobs/ Accessed 16.03.23.

Panagos, P., Borrelli, P., Meusburger, K., Alewell, C., Lugato, E., Montanarella, L. 2015. Estimating the soil erosion cover-management factor at the European scale. Land Use Policy 48, 38-50.

Pimentel, D., Harvey, C., Resosudarmo, P., Sinclair, K., Kurz, D., McNair, M., Crist, S., Shpritz, L., Fitton, L., Saffouri, R., Blair, R. 1995. Environmental and Economic costs of Soil Reosion and Conservation Benefits. Science 267(5201), 1117-1123.

Prabhakara, K., Hively, W. D., McCarty, G.W. 2015. Evaluating the relationship between biomass, percent groundcover and remote sensing indices across six winter cover crop fields in Maryland, United States. International Journal of Applied Earth Observation and Geoinformation 39, 88-102.

Purevdorj, T.S., Tateishi, R., Ishiyama, T., Honda, Y. 1998. Relationships between percent vegetation cover and vegetation indices. International Journal of Remote Sensing 19(18), 3519-3535.

Quemada, M., Cabrera, M.L. 2002. Characteristic moisture curves and maximum water content of two crop residues. Plant and Soil 238, 295-299.

Quemada, M., Daughtry, C.S.T. 2016. Spectral Indices to Improve Crop Residue Cover Estimation under Varying Moisture Conditions. Remote Sensing 8(660), 1-20.

R Core Team. 2016. R: A language and environment for statistical computing. R Foundation for Statistical Computing. Vienna, Austria. https://www.R-project.org/

Reicosky, D.C., Forcella, F. 1998. Cover crops and soil quality interactions in agroecosystems. Journal of Soil and Water Conservation 53, 224-229.

Richard, I.R., Wallace, P.A., Turner, I.D.S. 1996. A comparison of six cover crop types in terms of nitrogen uptake and effect on response to nitrogen by a subsequent spring barley crop. Journal of Agricultural Science 127, 441-449.

Roy, D.P., Zhang, H.K., Gomez-Dans, J.L., Lewis, P.E., Schaaf, C.B., Sun, Q., Li, J., Huang, H., Kovalskyy, V. 2016. A general method to normalize Landsat reflectance data to nadir BRDF adjusted reflectance. Remote Sensing of Environment 176, 255-271.

Shenk, G.W., Linker, L.C. 2013. Development and Application of the 2010 Chesapeake Bay Watershed Total Maximum Daily Load Model. Journal of the American Water Resources Association, 1-15.

Simpson, J.J., Stitt, J.R. 1998. A Procedure for the Detection and Removal of Cloud Shadow from AVHRR Data over Land. IEEE Transactions on Geoscience and Remote Sensing 36 (3), 880-897.

Smith, P., House, J.I., Bustamante, M., Sobocká, J., Harper, R., Pan, G., West, P., Clark, J., Adhya, T., Rumpel, C., Paustian, K., Kuikman, P., Cotrufo, M.F., Elliott, J.A., McDowell, R., Griffiths, R.I., Asakawa, S., Bondeau, A., Jain, A.K., Meersmans, J., Pugh, T.A.M. 2015. Global Change Pressures on Soils from Land Use and Management. Global Change Biology 22(3), 1008-1028.

Snapp, S.S., Swinton, S.M., Labarta, R., Mutch, D., Black, J.R., Leep, R., Nyiraneza, J., O'Neil, K. 2005. Review and Interpretation: Evaluating Cover Crops for Benefits, Cost and Performance within Cropping System Niches. Agronomy Journal 97, 322-332.

Stafford, J.V. 2000. Implementing Precision Agriculture in the 21st Century. Journal of Agricultural Engineering Research 76: 267-275.

Staver, K.W., Brinsfield, R.B. 2001. Agriculture and Water Quality on the Maryland Eastern Shore: Where Do We Go from Here? Bioscience 51(10), 859-868.

Talberth, J., Selman, M., Walker, S., Gray, E. 2015. Pay for Performance: Optimizing public investments in agricultural best management practices in the Chesapeake Bay Watershed. Ecological Economics 118, 252–261.

Taylor, J.C., Wood, G.A., Earl, R., Godwin, R.J. 2003. Soil Factors and their Influence on Within-Field Crop Variability II: Spatial Analysis and Determination of Management Zones. Biosystems Engineering 84(4), 441-453.

Teasdale, J.R. 1996. Contribution of Cover Crops to Weed Management in Sustainable Agricultural Systems. Journal of Production Agriculture 9 (4), 475-479.

Thenkabail, P.S., Smith, R.B., and De Pauw, E. 2000. Hyperspectral vegetation indices and their relationships with agricultural crop characteristics. Remote sensing of Environment 71(2), 158-182.

Tilman, D., Cassman, K.G., Matson, P.A., Naylor, R., Polasky, S. 2002. Agricultural sustainability and intensive production practices. Nature 418, 671-677.

Tong, S.T.Y., Chen, W. 2002. Modeling the relationship between land use and surface water quality. Journal of Environmental Management 66, 377-393.

Trishchenko, A.P., Cihlar, J., Li, Z. 2002. Effects of spectral response function on surface reflectance and NDVI measured with moderate resolution satellite sensors. Remote Sensing of Environment 81, 1-18.

Tucker, C.J. 1979. Red and Photographic Infrared Linear Combinations for Monitoring Vegetation. Remote Sensing of Environment 8, 127-150.

Tucker, C.J., Sellers, P.J. 1986. Satellite remote sensing of primary production. International Journal of Remote Sensing 7(11), 1395-1416.

Unger, P.W., Vigil, M.F. 1998. Cover crop effects on soil water relationships. Journal of Soil and Water Conservation 53(3), 200-207.

USGS, 2016. http://landsat.usgs.gov/CDR_LSR.php Accessed. 16.10.12.

USGS, ESPA, 2016. http://espa.cr.usgs.gov/ Accessed 16.03.23.

USGS, SLC-off Products: Background**.** 2015. http://landsat.usgs.gov/products_slcoffbackground.php. Accessed 16.04.20.

Verhoef, W. 1984. Light scattering by leaf layers with application to canopy reflectance modeling: The SAIL model. Remote Sensing of Environment 16(2), 125-141.

Verhoef, W., Jia, L., Xiao, Q., Su, Z. 2007. Unified Optical-Thermal Four-Stream Radiative Transfer Theory for Homogenous Vegetation Canopies. IEEE Transactions on Geoscience and Remote Sensing 45(6), 1808-1822.

Verhoeven, J.T.A., Arheimer, B., Yin, C., Hefting, M.M. 2006. Regional and global concerns over wetlands and water quality. Trends in Ecology and Evolution 21(2), 96-103.

Vermote, E.F., Tanré, D., Deuzé, J.L., Herman, M., Morcrette, J. 1997. Second Simulation of the Satellite Signal in the Solar Spectrum, 6S: An Overview. IEEE Transactions in Geoscience and Remote Sensing 35(5), 675-686.

Wagner, P., Hank, K. 2013. Suitability of aerial and satellite data for calculation of site-specific nitrogen fertilisation compared to ground based sensor data. Precision Agriculture 14, 135-150.

Whitcraft, A.K., Vermote, E.F., Becker-Reshef, I., Justice, C.O. 2015. Cloud cover throughout the agricultural growing season: Impacts on passive optical earth observations. Remote Sensing of Environment 156: 438-447.

Wiedemuth, K., Müller, J., Kahlau, A., Amme, S., Mock, H., Grzan, A., Hell, R., Egle, K., Beschow, H., Humbeck, K. 2005. Successive maturation and senescence of individual leaves during barley whole plant ontogeny reveals temporal and spatial regulation of photosynthetic function in conjunction with C and N metabolism. Journal of Plant Physiology 162(11), 1226-1236.

Wiegand, C.L., Richardson, A.J., Escobar, D.E., Gerbermann, A.H. 1991. Vegetation indices in crop assessments. Remote Sensing of Environment 35(2), 105-119.

Yao, Xinfeng, Yao, Xia, Jia, W., Tian, Y., Ni, J., Cao, W., Zhu, Y. 2013. Comparison and Intercalibration of Vegetation Indices from Different Sensors for Monitoring Above-Ground Plant Nitrogen Uptake in Winter Wheat. Sensors 13, 3109-3130.

Yu, K. Tsai, L., Chen, S., Ho, S. 2001. Chemical Binding of Heavy Metals in Anoxic River Sediments. Water Resources 35(17), 4086-4094.

Zhu, Z., Woodcock, C.E. 2012. Object-based cloud and cloud shadow detection in Landsat imagery. Remote Sensing of Environment 118, 83-94.